FOSSIL ENERGY

KINETICS AND MECHANISM OF DESULFURIZATION AND DENITROGENATION OF COAL-DERIVED LIQUIDS

Fourth Quarterly Report, March 20—June 20, 1976

J. R. Katzer
B. C. Gates
J. H. Olson
H. Kwart
A. B. Stiles

July 15, 1976

Work performed under Contract No. E(49-18)-2028

University of Delaware
Newark, Delaware

ENERGY RESEARCH AND DEVELOPMENT ADMINISTRATION

DISCLAIMER

NOTICE

FE-2028-T5

~~FE-2028-5~~

Distribution Category UC-90d

KINETICS AND MECHANISM OF DESULFURIZATION AND DENITROGENATION OF COAL-DERIVED LIQUIDS

Fourth Quarterly Report for Period
March 20, 1976 to June 20, 1976

Prepared by:

James R. Katzer, Bruce C. Gates,
Jon H. Olson, Harold Kwart and Alvin B. Stiles

Departments of Chemical Engineering and Chemistry
University of Delaware
Newark, Delaware 19711

Date Published
July 15, 1976

Prepared for
Fossil Energy
Energy Research and Development Administration
Washington, D.C.

Under Contract No. E(49-18)-2028

I. ABSTRACT

The high-pressure liquid-phase flow microreactors are operating satisfactorily in both hydrodesulfurization and hydrodenitrogenation studies after minor modifications to allow in situ sulfiding. The hydrodesulfurization of dibenzothiophene occurs by a simple network giving only H_2S and biphenyl as primary reaction products. The reaction network for quinoline hydrodenitrogenation has been determined, and a kinetic model developed to allow quantitative determination of the first-order kinetic constants for each of the steps in the reaction network. The effect of H_2S concentration, hydrogen pressure, quinoline concentration, and catalyst type on the rate of the various steps in the reaction network has been determined. Aged catalyst from the 1.1 in ID Synthoil reactor showed considerable amounts of mineral matter on it, but not as much FeS_x as on the catalyst from the 5/16 in. ID unit. Moment analysis for the evaluation of pulse microreactor data has been completed.

TABLE OF CONTENTS

LIST OF TABLES

LIST OF FIGURES

II. OBJECTIVES AND SCOPE

The major objectives of this research are:

i) to develop a high-pressure liquid-phase microreactor for operation in pulse and steady-state modes of operation for the determination of quantitative reaction kinetics and catalytic activities on small quantities of reactants and catalyst.

ii) to determine reaction networks, reaction kinetics and relative reactivities for catalytic hydrodesulfurization of multi-ring aromatic sulfur-containing compounds found in coal-derived liquids,

iii) to determine reaction networks, reaction kinetics and relative reactivities for catalytic hydrodenitrogenation of multi-ring aromatic nitrogen-containing compounds found in coal-derived liquids,

iv) to develop quantitative data on the chemical and physical properties of aged hydroprocessing catalysts used in coal liquefaction processes and to establish the mechanisms of deactivation of these hydroprocessing catalysts,

v) to develop the reaction engineering models required to predict the behavior of coal-to-oil processing and of catalytic hydroprocessing of coal-derived liquids and to suggest effective methods for improved operation of hydrodesulfurization and hydrodenitrogenation processes, and

vi) to recommend based on the sum of the above work improvements for the catalytic hydroprocessing of coal-derived liquids.

A unique high-pressure, liquid-phase microreactor is being developed for pulse (transient) and steady-state modes of operation for kinetic measurements to achieve objectives ii) through iv). The relative reactivities of the important types of multi-ring aromatic compounds containing sulfur and nitrogen are being measured under industrially important conditions (300-450°C and 500-4000 psi). The reaction networks and kinetics of several of the least-reactive multi-ring aromatic sulfur-containing and nitrogen-containing compounds commonly present in coal-derived liquids will be determined. Catalyst deactivation is an important aspect of the commercial scale upgrading of coal-derived liquids. Accordingly, the chemical and physical properties of commercially aged coal-processing catalysts are being determined to provide an understanding of catalyst deactivation; these efforts can lead to improved catalysts or procedures to minimize the problem. To make the results of this and related research most useful to ERDA, reaction engineering models of coal-to-oil processing in trickle-bed and slurry-bed catalytic reactors including deactivation will be developed to predict conditions for optimum operation of these processes. Based on the integrated result of all of the above work, recommendations will be made to ERDA for improved catalytic hydrodesulfurization and hydrodenitrogenation processing.

III. SUMMARY OF PROGRESS TO DATE

This summary is organized to parallel the task statements of the contract. A milestone chart is provided at the end of this section (Table I).

Microreactor Development

During this quarter the first microreactor was modified to incorporate some of the successful features of the second unit including valves for *in situ* sulfiding and a high-pressure liquid chromatography sampling valve for easy sample taking. The unit is now much easier to operat . The catalysts being used in Tasks 2 and 3 appear to require about 50 hours of continuous operation before the reaction kinetics become stabilized. Consequently there is an urgent need to construct a third microreactor, and a revised budget has been submitted to accomplish this goal. Task 1 has been completed in excess of the contractual specifications.

Hydrodesulfurization

The literature for the reaction pathways and kinetics of hydrodesulfurization of dibenzothiophene has been reviewed carefully; there is no agreement upon either the reaction products or the reaction kinetics. This study shall resolve some of this discrepancy.

The flow microreactor was operated at 300 to 1050 psig hydrogen saturation pressure and at 300 and 350°C reaction temperature. The disappearance of dibenzothiophene follows first-order kinetics with respect to dibenzothiophene and apparent 0.9 order kinetics with respect to hydrogen concentration. The reaction on a Co-Mo/Al_2O_3 (HDS-16A) catalyst is 70 to 90 percent selective to biphenyl indicating that biphenyl may be the only primary product formed; the remaining reaction products have not been identified. The catalyst activity for hydrodesulfurization of dibenzothiophene is at least 50 times greater than expected. The current experimental program is investigating the effect of H_2 and H_2S concentration at higher saturation pressures.

Hydrodenitrogenation

The reaction network for the hydrodenitrogenation of quinoline on a Ni-Mo/Al_2O_3 (HDS-16A) catalyst was determined, and it involves equilibrium hydrogenation to 1,2,3,4-tetrahydroquinoline; other ring hydrogenation steps are much slower and do not reach equilibrium. The saturated nitrogen-containing ring is then cracked forming o-propylaniline and γ-phenyl-n-propylamine which then undergoes denitrogenation. A reaction model has been developed which allows the first-order rate constants for each of the steps in the reaction network to be quantitatively determined. The first-order rate constants for the more important steps in the reaction network have been evaluated as a function of H_2 and H_2S concentration, initial quinoline concentration and catalyst type. These studies show that the relative behavior of each of the steps in the reaction network can be rationalized in great part by analysis of nitrogen-carbon bond reactivity. The batch experiments are being extended to acridine and carbazole. As an extension of the batch experiments quinoline is being examined in the flow microreactor.

Catalyst Deactivation

The deactivation of Synthoil pilot plant catalyst was investigated further during this quarter. A small sample of catalyst, removed from the front of the 1.1 in. I.D. Synthoil pilot plant at the conclusion of Run FB-53, showed substantial cementing of coal mineral matter to the surface of the catalyst. Unlike the sample taken from the upstream region of the 5/16 in. I.D. Synthoil reactor, the FB-53 catalyst had very little buildup of FeS_x on the external surface. The mineral matter cemented to the surface consisted primarily of clay, rutile and $CaCO_3$ reduction products.

Microreactor Engineering

The moment analysis of pulse microreactor data was extended to give a basis for investigation of fairly complex reaction networks. In particular the film model was extended to describe a two-phase catalyst. The transport in a spherical catalyst with reaction was compared critically to the film mode. A limited range of experiments with thiophene were conducted using a microprocessor to read out the

moments of the pulses. These data show the moment analysis is fairly powerful in systems of moderate complexity.

Table I is the actual milestone chart and time plan prepared for the work at the beginning of the grant period (in the Proposal). Hatching on the chart indicates that the activity (task) indicated is under active investigation; the number in the hatched region is an estimate of the percentage completion of this particular activity. Crosshatching on the chart indicates that an activity (task) has been completed. Table II gives the cumulative expenditures.

TABLE I TIME PLAN* AND MILESTONE CHART**

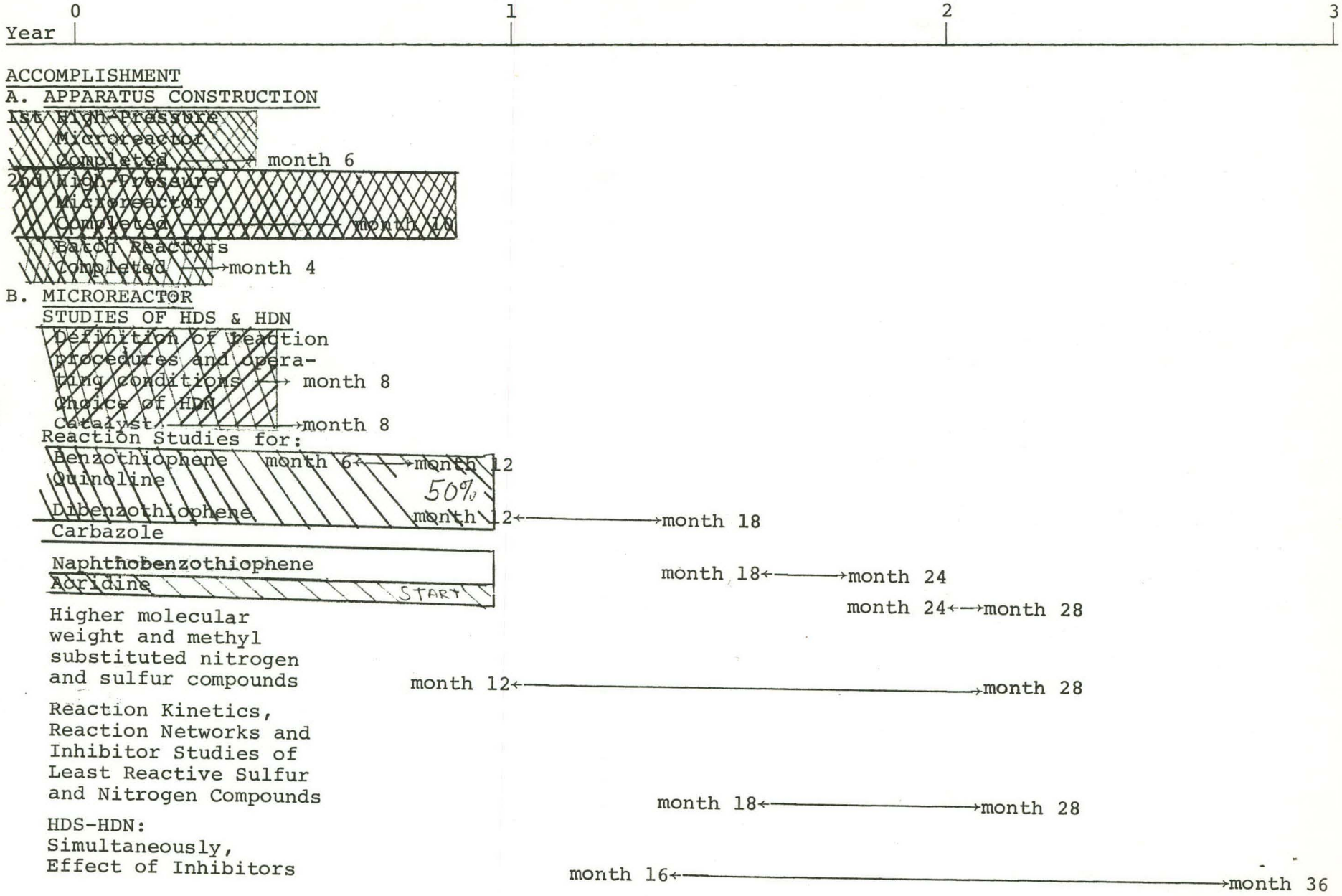

C. CATALYST DEACTIVATION

SYNTHOIL CATALYST:

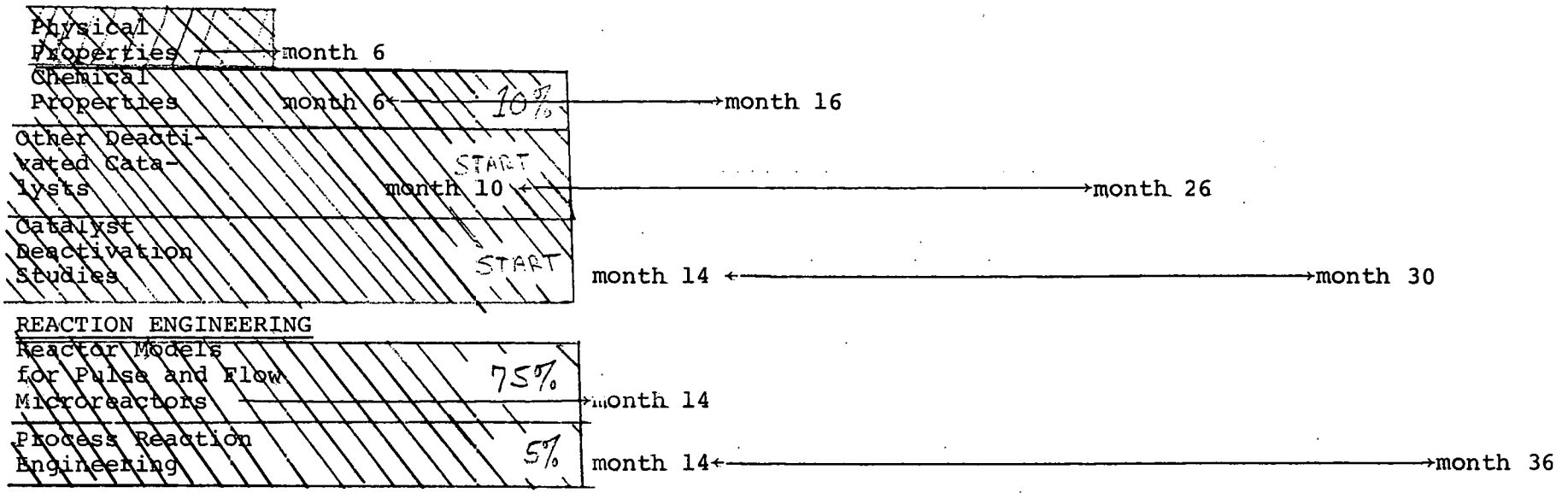

* Time Plan and Milestone Chart as Presented in Proposal

** Hatching indicates that activity indicated is under active investigation; number in hatched region indicates the percentage completed; crosshatching indicates that the task has been completed.

TABLE II

CUMULATIVE EXPENDITURES

ITEM \ QUARTER	First	Second	Third	Fourth
Personnel	$ 5,807	20,740	37,396	53,418
Travel	28	528	1,152	1,152
Supplies & Expenses	4,674	10,007	19,582	25,735
Occupancy & Maintenance	6,110	9,208	10,108	10,634
Equipment	610	17,978	30,704	34,930
Information Processing	--	--	--	97
Transfers (Overhead)	--	10,202	20,035	38,710

IV. DETAILED DESCRIPTION OF TECHNICAL PROGRESS

A. HYDROPROCESSING MICROREACTOR DEVELOPMENT

After the successful operation of the first high-pressure liquid-phase flow microreactor was demonstrated, a second unit was constructed incorporating a number of desirable changes into the design as reported in the last quarterly progress report. This unit has been operated successfully demonstrating the effectiveness of these design changes. Results of the initial hydrodenitrogenation studies with this second reactor are outlined in C. CATALYTIC HYDRODENITROGENATION. Based on the improved operability resulting from the design changes made in the second microreactor unit, some of these improvements are being incorporated into the first flow microreactor. Experience has now shown that about 55 hours is required to establish steady-state catalytic activity, and that although data can be readily obtained thereafter, the reactor cannot effectively be operated by several researchers. Therefore, based on the objectives of this work and the number of research personnel involved in it, a budget revision to allow the construction of a third high-pressure liquid-phase flow microreactor has been made. Of the two high-pressure liquid-phase flow microreactors now in use one has been constructed with funds from the Department of Chemical Engineering, and the second has been constructed with funds from this ERDA grant.

B. CATALYTIC HYDRODESULFURIZATION

1. Experimental

a. Liquid-phase high-pressure flow microreactor

Several modifications have been carried out on the high-pressure liquid-phase flow microreactor. These included installation of two three-way high-pressure valves, one before and one after the microreactor to enable *in situ* sulfiding of the catalyst (see Third Quarterly Progress Report). A four-way sampling valve has also been installed to replace the sample loop initially built into the system (see Second Quarterly Progress Report, page 12). The main advantage of the sampling valve is that it eliminates dead volume pockets present in the original sampling system.

b. Experimental operating conditions

All the experiments with the high-pressure liquid-phase flow microreactor, reported in this quarterly progress report were carried out under the same conditions described previously (see Third Quarterly Progress Report). They are summarized in the following:

* catalyst: HDS-16A, mass = 260 mg, volume of reactor bed = 0.30 cc, length of bed = 3.8 cm, catalyst particle size = 350 μ to 420 μ
* pretreatment: catalyst presulfided with 10% H_2S in H_2 for 2 hours at 400°C
* liquid flow rate: 1.2 cc/hr unless otherwise specified
* reactant mixture: 0.25 wt % n-dodecane, 0.25 wt % dibenzothiophene, n-hexadecane solvent
* reaction temperature: 350°C
* H_2 saturation pressure: 300 psig to 1050 psig.

c. Analytical

A flame-ionization gas chromatograph (Model Antek 440L) has been ordered, delivered and installed. The G.C. will be used for all analysis that can be done using flame-ionization detection including HDS and HDN product and cracking product analysis. A coated open-tubular column to achieve greater resolution of complex product mixtures is being installed in this unit. The testing and optimizing of the G.C. are underway. The addition of this unit to our analytical capabilities will reduce the backlog that is being experienced with the Perkin-Elmer gas chromatograph.

2. Hydrodesulfurization of Dibenzothiophene

a. Literature Review

Most studies of the kinetics and reaction network of catalytic hydrodesulfurization have been carried out either with a real hydrocarbon feed containing a mixture of sulfur compounds or with thiophene as a model compound. Little work has been reported on dibenzothiophene hydrodesulfurization. The published data is summarized below.

Reaction networks: Hoog (1950) reported that at 50 atm pressure and 375°C, dibenzothiophene hydrodesulfurization catalyzed by a cobalt-molybdenum type catalyst, gave a mixture of 35% 1,5-cyclohexadiene plus 6-cyclohexene and 65% phenylcyclohexane plus bicyclohexyl. Products corresponding to aromatic ring saturation of biphenyl were also reported by Landa and Mrnkova (1966). They found the following product distribution as a function of temperature for batch reactor operation at 100 atm hydrogen pressure (TABLE III).*

TABLE III

PRODUCT DISTRIBUTION FOR HYDRODESULFURIZATION OF DIBENZOTHIOPHENE OVER MoS_2 CATALYST*

T, °C	Biphenyl (BP), %	Phenyl-cyclohexane (PCH), %	Bicyclo-hexyl (BCH), %	Dibenzo-thiophene (DBT), %
300	20.9	7.6	8.6	62.9
320	18	32	24.2	25.8
340	11.1	22.4	46.7	19.8

*Landa and Mrnkova, 1966

The data of Table III show that increasing temperature favors aromatic ring saturation. Compounds of the phenyl cyclohexyl type have also been reported by Drushel and Sommers (1967).

Although the results tabulated above are consistent with a consecutive reaction network such as that shown in Figure 1, more experimental work using biphenyl, phenylcyclohexane, and hexahydrodibenzothiophene is needed to define the reaction network of dibenzothiophene hydrodesulfurization. Recently Urimato and Sakikawa (1972) studied the hydrodesulfurization of dibenzothiophene over molybdenum disulfide in a batch reactor. Their results are in partial disagreement with those of Landa and Mrnkova (1966), since products such as 1,2,3,4-tetrahydrodibenzothiophene, 1,2,3,4,10,11-hexahydrodibenzothiophene, and perhydrodibenzothiophene were identified. Moreover,

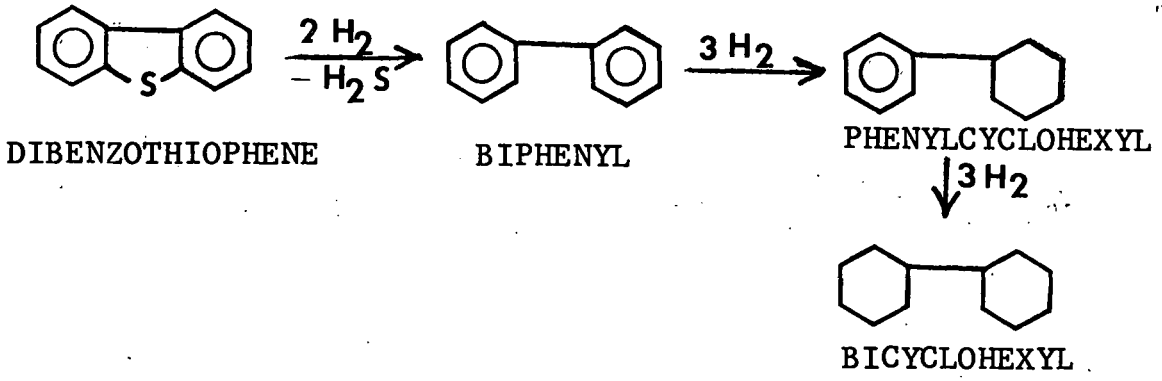

Figure 1. Proposed Reaction Network for Hydrodesulfurization of Dibenzothiophene involving Biphenyl Formation as a Primary Product.

---

substantial amounts of 3-methylcyclopentylcyclohexane and 3,3'-dimethyldicyclopentyl were obtained (Table IV). Urimoto and Sakikawa (1972) proposed a dibenzothiophene hydrodesulfurization reaction network in which direct hydrodesulfurization to biphenyl and a parallel reaction involving aromatic ring hydrogenation followed by desulfurization of the hydrogenated species occur simultaneously as shown in Figure 2.

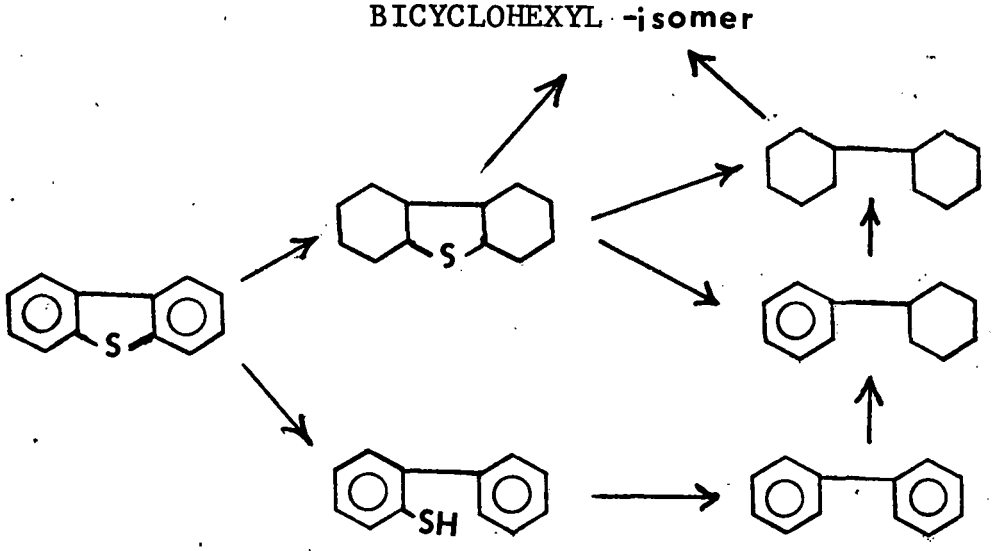

Figure 2. Reaction Network for Hydrodesulfurization of Dibenzothiophene involving Parallel Reaction Pathways (Urimoto and Sakikawa, 1972).

TABLE IV

PRODUCT DISTRIBUTION FOR DIBENZOTHIOPHENE HYDRODESULFURIZATION OVER MOLYBDENUM DISULFIDE CATALYST*

conditions			
	Reaction Temperature, ^{o}C	300	350
	Reaction Time, hr	4	4
	H_2 Pressure, kg/cm^2	50	50
wt % products	Dibenzothiophene	44.5	
	Perhydrodibenzothiophene	15.8	
	Hexahydrodibenzothiophene	3.6	
	Biphenyl	7.7	10.7
	Phenylcyclohexyl	8.6	17.6
	Bicyclohexyl	5.6	13.2
	3-methylcyclopentylcyclohexane	8.5	24.5
	3,3'-dimethyldicyclopentyl	3.2	16.5

Catalyst: Molybdenum sulfide
Catalyst surface area: 14 m^2/g
Catalyst wt: 1.9 g
Batch reactor
Dibenzothiophene added: 1.9 g
Unknown product: 17.5 wt %

*Urimoto and Sakikawa, 1972

A simplified reaction network has been proposed by Rollmann (1976), based on results obtained in high-pressure trickle-bed reactor studies. Rollmann demonstrated that the hydrodesulfurization of dibenzothiophene over Co-Mo/Al_2O_3 catalyst at 344°C, 700 psig, W.H.S.V.= 2, H_2/ feed = 8, (contained in a feed mixture containing various chemical types of sulfur-containing and nitrogen-containing compounds found in petroleum, shale oils and coal oils) lead to biphenyl as a primary product with over 90% selectivity. Rollmann proposed that the mechanism of sulfur removal is a simple cleavage of the C-S bond to give H_2S and the corresponding aromatic. Saturation of the aromatic rings attached to the sulfur ring is not required prior to the removal of the sulfur atom. Furthermore, the presence of trace amounts of mercaptan sulfur in the products indicated that the initial thiophene ring opening, and not thiol hydrogenation, was rate limiting.

The only work on hydrodesulfurization of dibenzothiophene at atmospheric pressure was reported by Bartsch and Tanielian (1974). Using a flow microreactor and Co-Mo/Al_2O_3 catalyst they observed that biphenyl was the only product formed. They also concluded that hydrogenation of an aromatic ring adjacent to the thiophene ring is not necessary to obtain easier ring opening and sulfur removal from the thiophene ring.

Kinetics: There are no systematic studies of the kinetics of dibenzothiophene hydrodesulfurization which include a clear definition of the absence of mass transfer effects and of the dependence on reactant and product concentrations. Frye and Mosby (1967) demonstrated that hydrodesulfurization of dibenzothiophene contained in light catalytic cycle oil (boiling range 450-600°K) over Co-Mo/Al_2O_3 catalyst was first order in the concentration of the sulfur compound and in the hydrogen pressure up to 400 psi. They observed inhibition by H_2S and aromatic hydrocarbons. In the atmospheric pressure studies of Bartsch and Tanielian (1974), first-order dependence on dibenzothiophene concentration and on hydrogen partial pressure was also observed. However, these authors reported that their kinetic measurements were not free from diffusional effects.

Thus although there is some information in the literature on the kinetics and reaction network for dibenzothiophene hydrodesulfurization, the information is not definitive with respect to either the reaction network or the kinetics. Resolution of

the questions which exist is desirable by itself but is necessary to provide a base on which to compare the behavior of dibenzothiophene with that of methyl substituted dibenzothiophenes and higher molecular weight analogues such as benzonaphthothiophene.

b. Experimental Results and Discussion

Thermal Reaction: The temperature required for thermal desulfurization of dibenzothiophene to be relatively rapid was determined by Druschel (1968) to be 800°C. Since the temperature range of our studies is 300-350°C, the hydrodesulfurization observed must be almost solely catalytic.

Kinetics: Order of reaction with respect to dibenzothiophene. In its simplest form the dibenzothiophene hydrodesulfurization reaction network can be illustrated by the following:

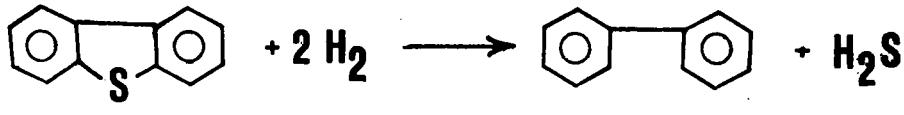

DIBENZOTHIOPHENE BIPHENYL

The reaction rate per unit volume of catalyst can be written as:

$$r = K\, C_s^{\alpha}\, C_{H_2}^{\beta} \qquad (1)$$

where K is the rate constant, C_s is the concentration of sulfur compound in the carrier oil, C_{H_2} is the concentration of hydrogen in the carrier oil and α and β are dimensionless constants. Written in this form K will depend on the concentration of products, solvent and temperature. Assuming a constant hydrogen concentration and omitting the influence of the products (Metcalfe, 1969), Equation (1) becomes

$$r = K'\, C_s^{\alpha} \qquad (2)$$

Equation (3) is the model equation for an ideal tubular flow reactor,

$$\frac{V_c}{V_f} = \frac{1}{L.H.S.V.} = \int_0^x \frac{dx}{(-r)} \qquad (3)$$

where V_c = volume of catalyst in the reactor, cm^3

V_f = volumetric flow rate of feed, cc/hr

x = degree of conversion of reactant

$(-r)$ = reaction rate per unit volume of catalyst, and

L.H.S.V. = liquid hourly space velocity, volume of feed/hr per volume catalyst, cm^3/cm^3-hr.

For small conversions where the rate of reaction across the reactor does not vary significantly (differential reactor operation) Equation (3) may be written in finite difference form

$$\frac{V_c}{V_f} = \frac{1}{L.H.S.V.} = \frac{\Delta X}{(-r)} \qquad (4)$$

and then

$$\Delta X = \frac{(-r)}{L.H.S.V.} \qquad (5)$$

where the rate of reaction (-r) can be determined directly from the slope of the linear portion of a plot of ΔX vs. $\frac{1}{L.H.S.V.}$ as $\frac{1}{L.H.S.V.}$ approaches zero. Rates obtained in this manner for a series of different conditions can then be correlated using Equation (1) or (2) to define the kinetics of the system. Figure 3 is a plot of this type for the hydrodesulfurization of dibenzothiophene. The run conditions included: Co-Mo/Al_2O_3 catalyst whose activity had been stabilized, run temperature = 350°C, 0.25 wt % dibenzothiophene in n-hexadecane, and H_2/dibenzothiophene molar ratio of 3.0.

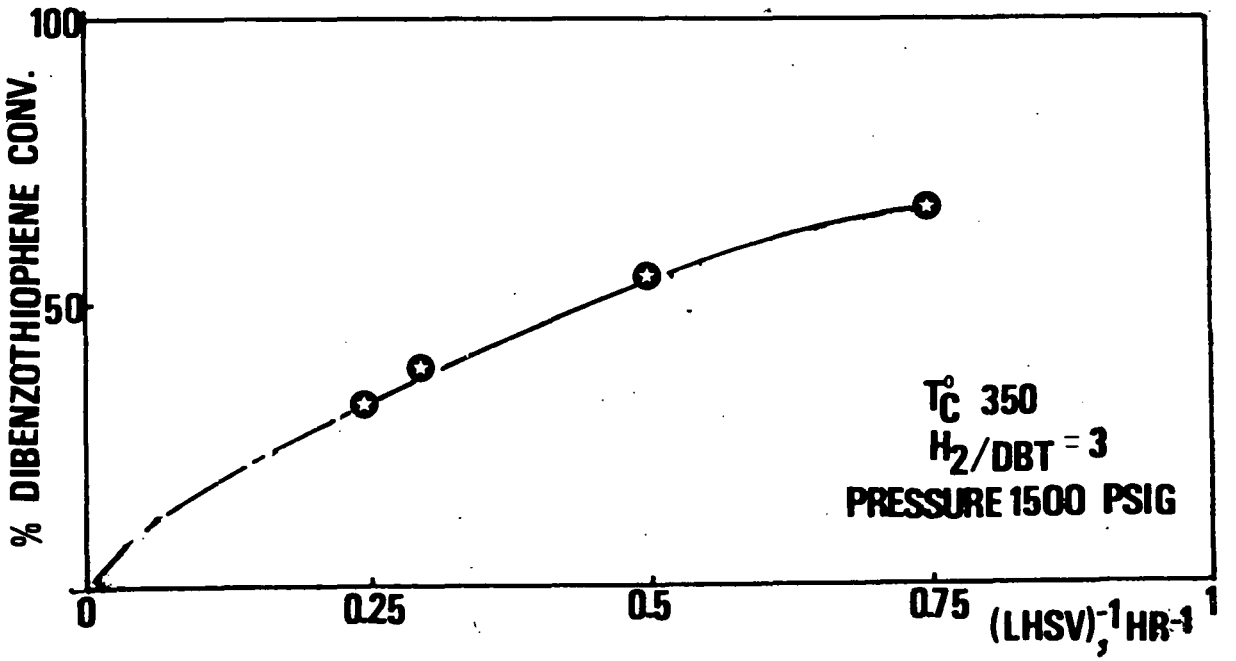

Figure 1. Demonstration of Differential Flow Reactor Operation in Dibenzothiophene Hydrodesulfurization for Conversions less than about 40% and Demonstration that the Data are not fitted by Zero-Order Kinetics: activity-stabilized presulfided Co-Mo/Al_2O_3 (Cyanamid HDS-16A), 350°C, saturation pressure 1500 psig, H_2/dibenzothiophene molar ratio = 3, 0.25 wt% dibenzothiophene in n-hexadecane.

If differential reactor operation is not achieved, Equation (2) can be substituted into Equation (3), and the integration can be performed with or without the assumption of a reaction order. For assumed first-order reaction:

$$\frac{1}{\text{L.H.S.V.}} = \int_o^x \frac{dx}{-K'C_s} \tag{6}$$

$$\frac{1}{\text{L.H.S.V.}} = -\frac{1}{K'C_{so}} \ln(1-X) \tag{7}$$

Reaction network

Three runs were carried out on Co-Mo/Al_2O_3 catalyst which had its activity stabilized. Reaction temperature, dibenzothiophene concentration, working pressure, and liquid hourly space velocity were kept the same; only hydrogen saturation pressure was varied between about 300 and 1,000 psia.

Analysis of sulfur products with the sulfur-specific detector showed that only unconverted dibenzothiophene was present; no thiol type compounds or partially hydrogenated dibenzothiophenes were detected. Gas chromatographic analysis of the hydrocarbon fraction showed that biphenyl was the main product with a selectivity of over 75%. Chromatographic analyses of products showed in addition to biphenyl, the presence of products which result from partial saturation of aromatic rings (phenyl cyclohexane and/or bicyclohexyl).

The presence of phenylcyclohexane and bicyclohexyl can be explained at least partially by hydrogenation of biphenyl formed upon sulfur removal from dibenzothiophene, since a solution of 0.2 wt % biphenyl in n-hexadecane underwent at our experimental conditions hydrogenation to compounds having one and two saturated rings.

Based on these results, a simple reaction network can be postulated and is shown by the solid lines in Figure 2. The reaction involves cleavage of C-S bond with the formation of a thiol which is probably only present as a surface intermediate; sulfur atom removal then occurs with biphenyl formation. Biphenyl can be further hydrogenated to phenyl cyclohexane and the latter to bicyclohexyl in a consecutive reaction network (Figure 2).

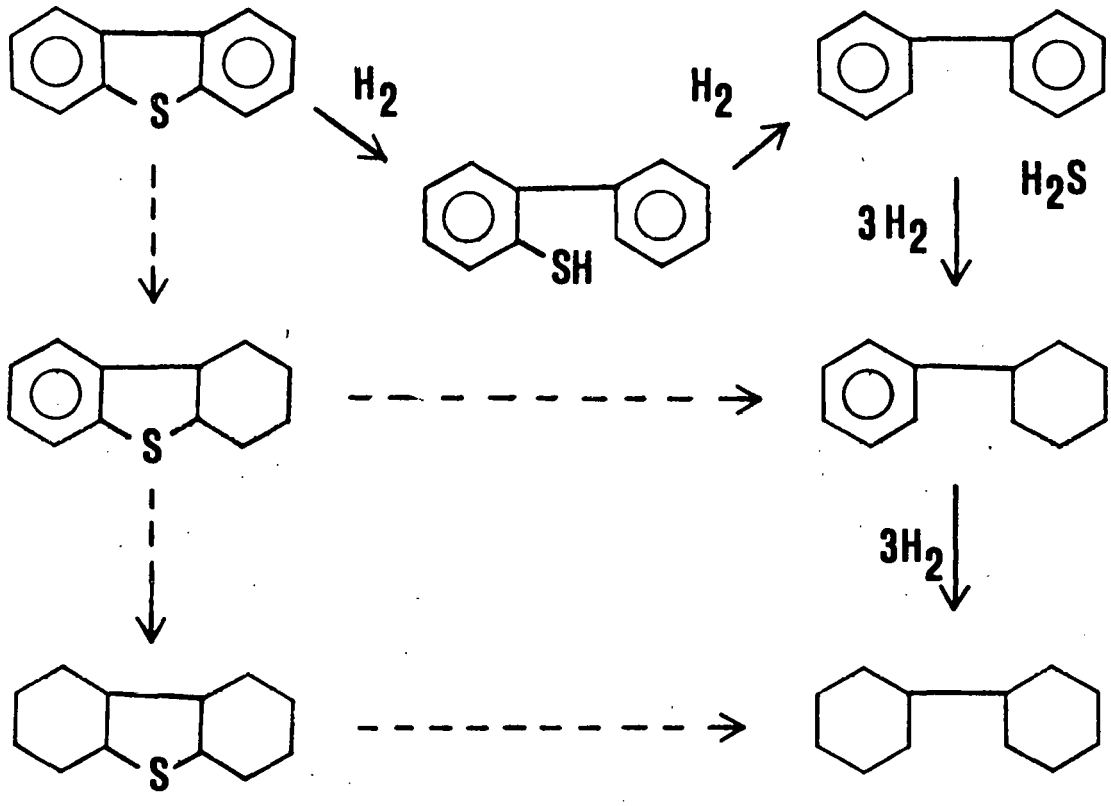

Figure 2 Proposed Reaction Network for Dibenzothiophene Hydrodesulfurization

Another pathway can be imagined in which phenylcyclohexane is formed by hydrogenation of dibenzothiophene to hexahydrodibenzothiophene, followed by sulfur removal. Similarly, hydrogenation of the other aromatic ring can occur before desulfurization. Although no hexahydrodibenzothiophene or other sulfur-containing products have been detected, the reaction network illustrated by dotted lines in Figure cannot be excluded.

c. Synthesis of sulfur-containing compounds

The program of synthesis of sulfur-containing compounds for use in the hydrodesulfurization studies has been initiated, and the work done to date is outlined below.

2,8-Dimethyldibenzothiophene has been synthesized from dibenzothiophene by the following reaction steps.

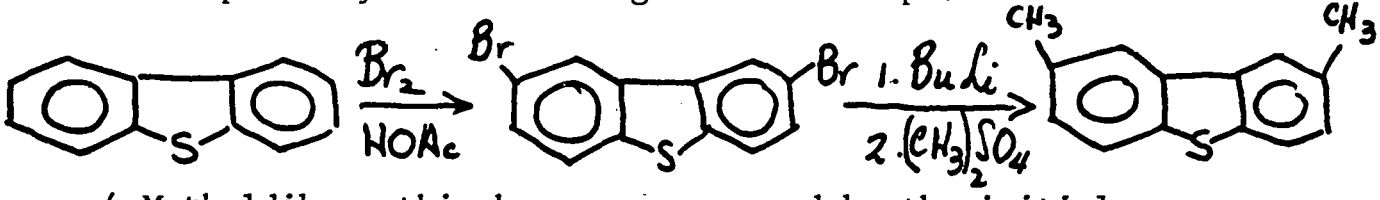

4-Methyldibenzothiophene was prepared by the initial reaction of dibenzothiophene with n-butyllithium in the ratio of 1:2 and subsequent methylation with $(CH_3)_2SO_4$.

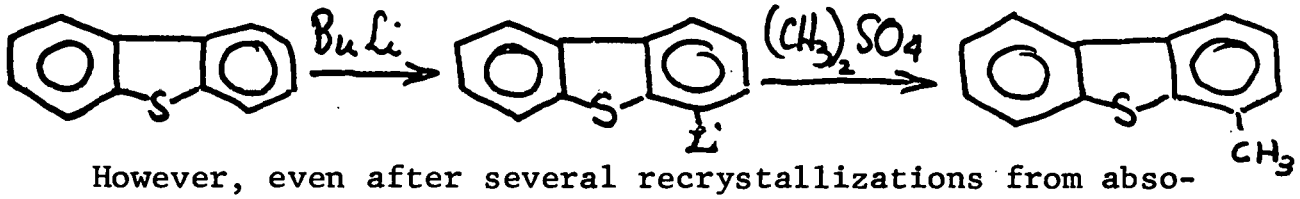

However, even after several recrystallizations from absolute alcohol, aqueous alcohol, methanol and methanol-benzene, the product is only about 85% pure and contains unreacted dibenzothiophene and 4,6-dimethyldibenzothiophene. An alternative procedure promising a purer product will be undertaken as described in a subsequent section of this report.

4,6-Dimethyldibenzothiophene has been prepared by similar procedure.

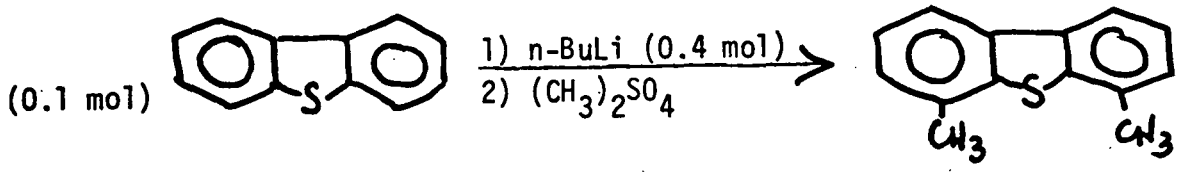

This product has about 2% 4-methyldibenzothiophene.

The preparation of 3,7-dimethyl-dibenzothiophene by the following reaction sequence has been started.

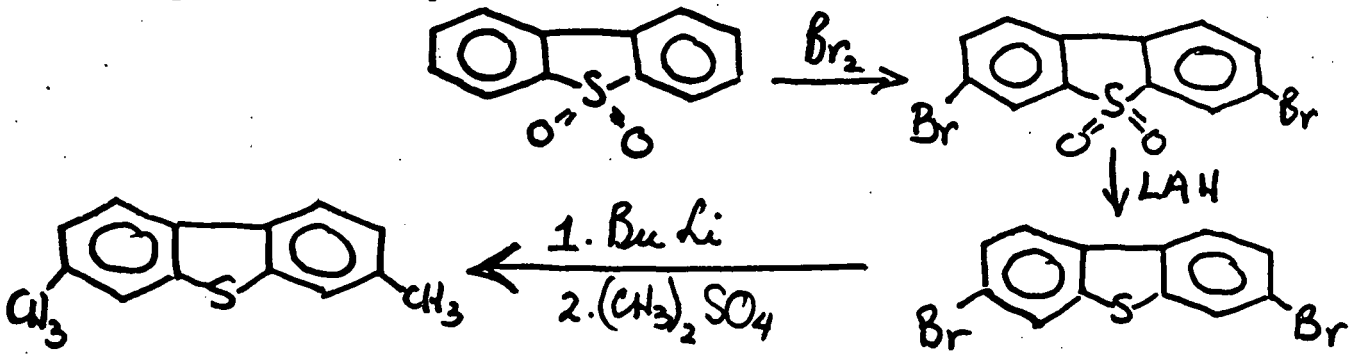

So far, 3,7-dibromodibenzothiophene has been obtained.

d. Research plans for the fifth quarter

1. Kinetics of Dibenzothiophene Hydrodesulfurization

Future studies of dibenzothiophene hydrodesulfurization will aim at establishing, in the form of a rate equation, the kinetics of hydrodesulfurization of dibenzothiophene. On the basis of our previous results the following measurements must be made, and the following papameters must be defined:

**The composition of the feed mixture, the amount of catalyst and feed flow rate which will lead to a reasonably small (differential) conversion must be determined.

**The experimental conditions where the observed rate of hydrodesulfurization is free from diffusional effects will also be determined to insure that intrinsic kinetics are being determined. The test for intraparticle mass transfer will involve measuring the rate of hydrodesulfurization for different particle sizes of the catalyst under the same operating conditions.

**White oil will be used instead of n-hexadecane after reproducible kinetic measurements and adequate product identification have been achieved. The rate of dibenzothiophene hydrodesulfurization with white oil as a solvent will be compared to our previous results obtained with n-hexadecane as a solvent.

**The inhibition effect of hydrogen sulfide on the hydrodesulfurization activity will also be examined. Inhibition by H_2S in hydrodesulfurization has already been reported by Metcalfe (1969), Philipson (1971), Cecil et al. (1968), Frye and Mosby (1967), Owens and Amberg (1962), and Satterfield and Roberts (1968).

**The effect of temperature, dibenzothiophene concentration and hydrogen concentration on the rate of hydrodesulfurization will also be determined. The influence of the products on the kinetics will be defined. A rate equation which will account for the cited effects will then be developed.

**The reaction network previously proposed will be refined in the light of the kinetic results.

2. Analysis

**The use of a coated open tubular column to achieve better separation of products formed will be evaluated.

**To avoid interference between cracking products from aromatic and straight chain hydrocarbons,the use of a high-pressure liquid chromatograph will be considered.

3. Synthesis of Sulfur-Containing Compounds

During the months of July and August, after completing the above-mentioned incomplete synthesis of 3,7-dimethyl-dibenzothiophene, the following compounds will be prepared by the methods indicated.

4-Methyldibenzothiophene:

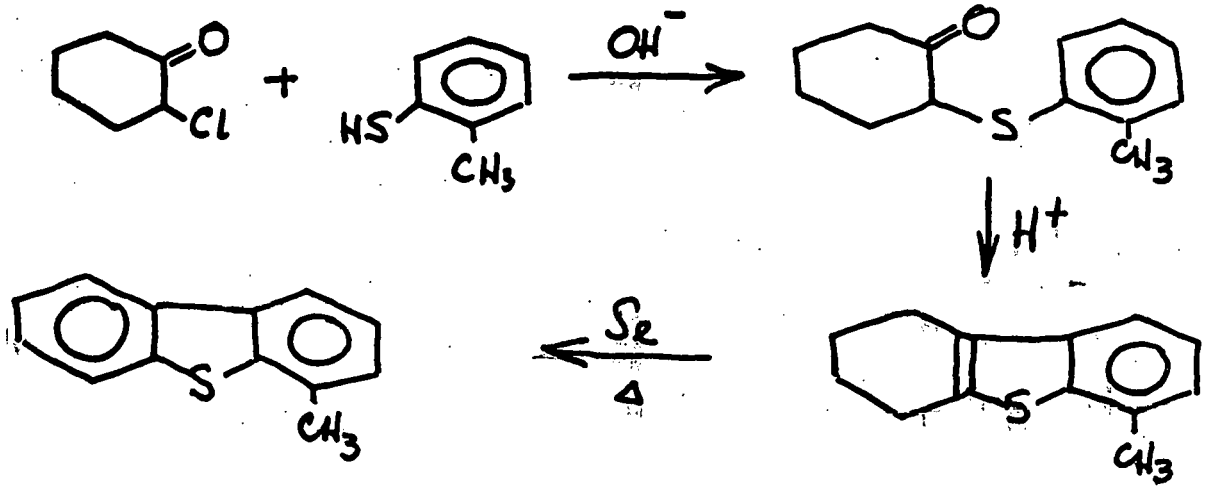

THIS PAGE

WAS INTENTIONALLY

LEFT BLANK

C. CATALYTIC HYDRODENITROGENATION

1. Summary

During this quarterly period, the construction of the second high-pressure liquid-phase flow microreactor was completed; both autoclave reactors and the flow microreactor were on stream producing data. A run with carbazole was carried out in an autoclave reactor to initiate the study of carbazole and acridine hydrodenitrogenation.

A kinetic model was proposed for the catalytic hydrodenitrogenation of quinoline. Based on the appropriate kinetic analysis, it is possible to calculate the rate constant of each reaction step in the reaction network of quinoline hydrodenitrogenation. By combining the results of kinetic analyses and the effects of hydrogen pressure, considerably detailed insight into the reaction mechanism of the catalytic hydrodenitrogenation of quinoline has been achieved. A few of the key experimental runs designed to probe the proposed reaction mechanism have been carried out. Additional supporting experiments of this nature are scheduled for the next quarterly period, including the effect of reaction temperature, the support activity, and the kinetics and reactivity of important reaction intermediates which occur in the hydrodenitrogenation of quinoline.

In the next quarterly period, the microreactor will continue to be used to study the steady-state catalyst activity in hydrodenitrogenation of quinoline. Studies of the hydrodenitrogenation of acridine and carbazole will be also undertaken.

2. Experimental Method

All hydrodenitrogenation studies were carried out over a pre-sulfided Ni-Mo/Al_2O_3 catalyst (Cyanamid HDS-9A). The catalyst was presulfided at 325°C in 10% H_2S/H_2 for two hours. For the autoclave reactor, the catalyst loading was 0.5 wt% in white oil. For the liquid-phase high-pressure flow reactor, the space velocity was 4 hr^{-1}. An amount of CS_2 equal to 0.05 wt% of CS_2 in the white oil was added to maintain a constant

sulfur level on the presulfided catalyst. Runs were carried out at 342°C unless otherwise stated. The liquid-phase samples were analyzed by gas chromatography with the aid of a nitrogen-specific detector. The detailed operational procedures for the autoclave can be found in the previous progress report.

3. Results and Discussion

a. Reaction Network for Quinoline Hydrodenitrogenation

A detailed reaction network showing all probable reaction pathways for quinoline hydrodenitrogenation is shown in Figure 3. Figure 4 shows the type of data which is obtained on the intermediates and which is used to define the most important parts of the network shown in Figure 3. As reported in the previous progress report, quinoline is rapidly hydrogenated on the nitrogen-containing ring before any nitrogen is removed. Several nitrogen-containing compounds are observed as reaction intermediates, including 5,6,7,8-tetrahydroquinoline (saturation of the benzene ring), decahydroquinoline, o-propylaniline and a trace amount of aniline (Figure 3). Kinetic analysis indicates that the data can be fitted to a first-order kinetic expression with respect to the nitrogen-containing compounds in the reaction network. Figure 5 shows that the kinetics for 1,2,3,4-tetrahydroquinoline plus quinoline and those for total nitrogen removal can be represented very well by a first-order rate expression over about a 95 and a 90 percent conversion range respectively. Based on this observation it was assumed that the reaction rate for each of the intermediate nitrogen-containing compounds could be expressed by a first-order kinetic expression. A nonlinear least squares regression computing program (Marquardt's Method) was used to estimate the reaction constants for each important step in the reaction network shown in Figure 3. The program and its application will be detailed in the next progress report. Typical results of this kinetic analysis together with the simplified reaction network are shown in Table V. The results shown in Table V are based on the data which are presented in Figure 4 and Figure 5.

Hydrogenation of quinoline on the nitrogen-containing ring to form 1,2,3,4-tetrahydroquinoline is a very fast reaction which attains thermodynamic equilibrium under the study conditions employed. However, hydrogenation to form 5,6,7,8-tetrahydroquinoline and complete hydrogenation to form decahydroquinoline are relatively slow. Although all these hydrogenation reactions have comparable equilibrium constants, only the formation of 1,2,3,4-tetrahydroquiniline is fast enough to reach thermodynamic equilibrium.

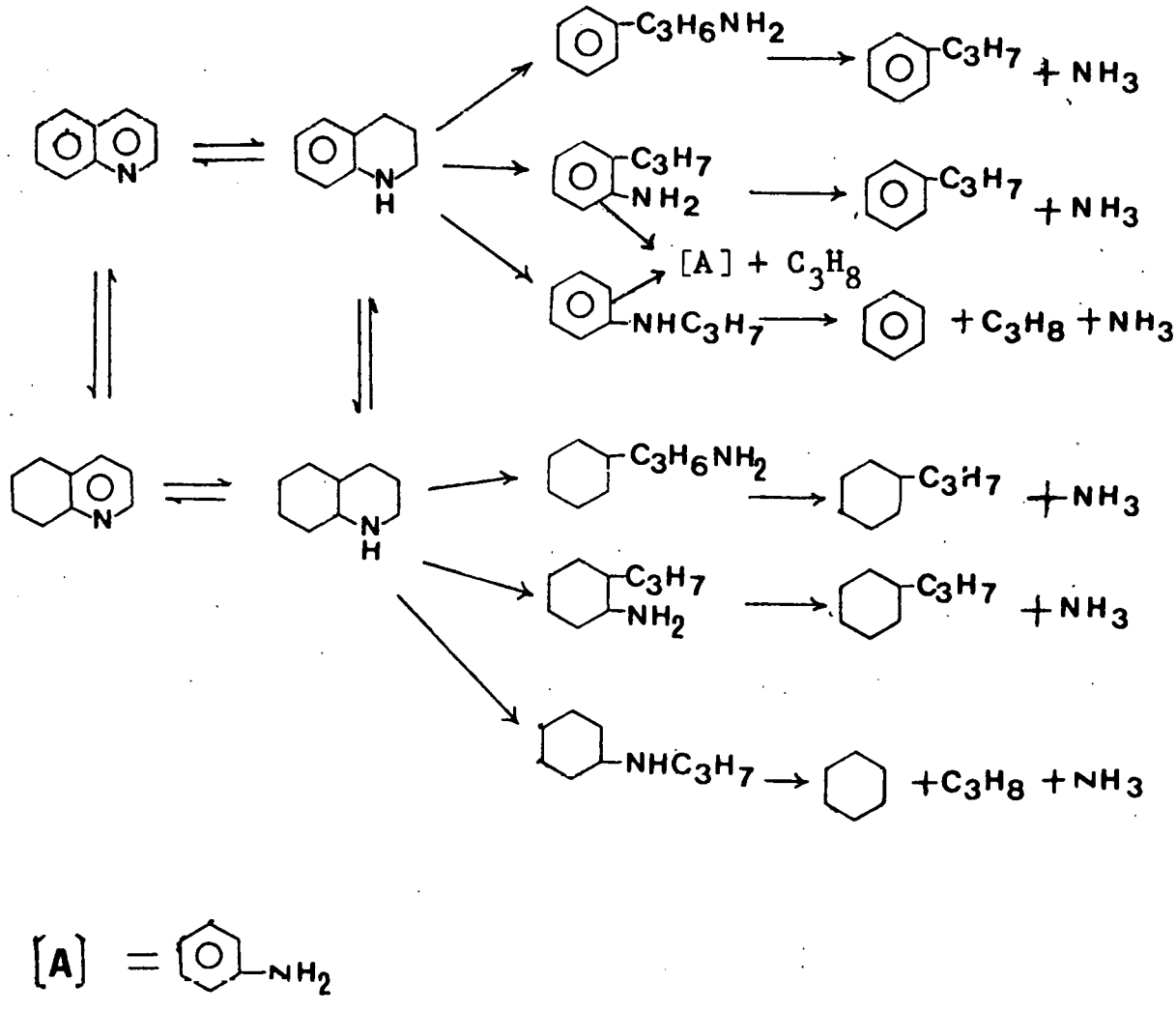

[A] = NH_2

Figure 3. Reaction Network showing all Probable Steps in the Hydrodenitrogenation of Quinoline.

THIS PAGE

WAS INTENTIONALLY

LEFT BLANK

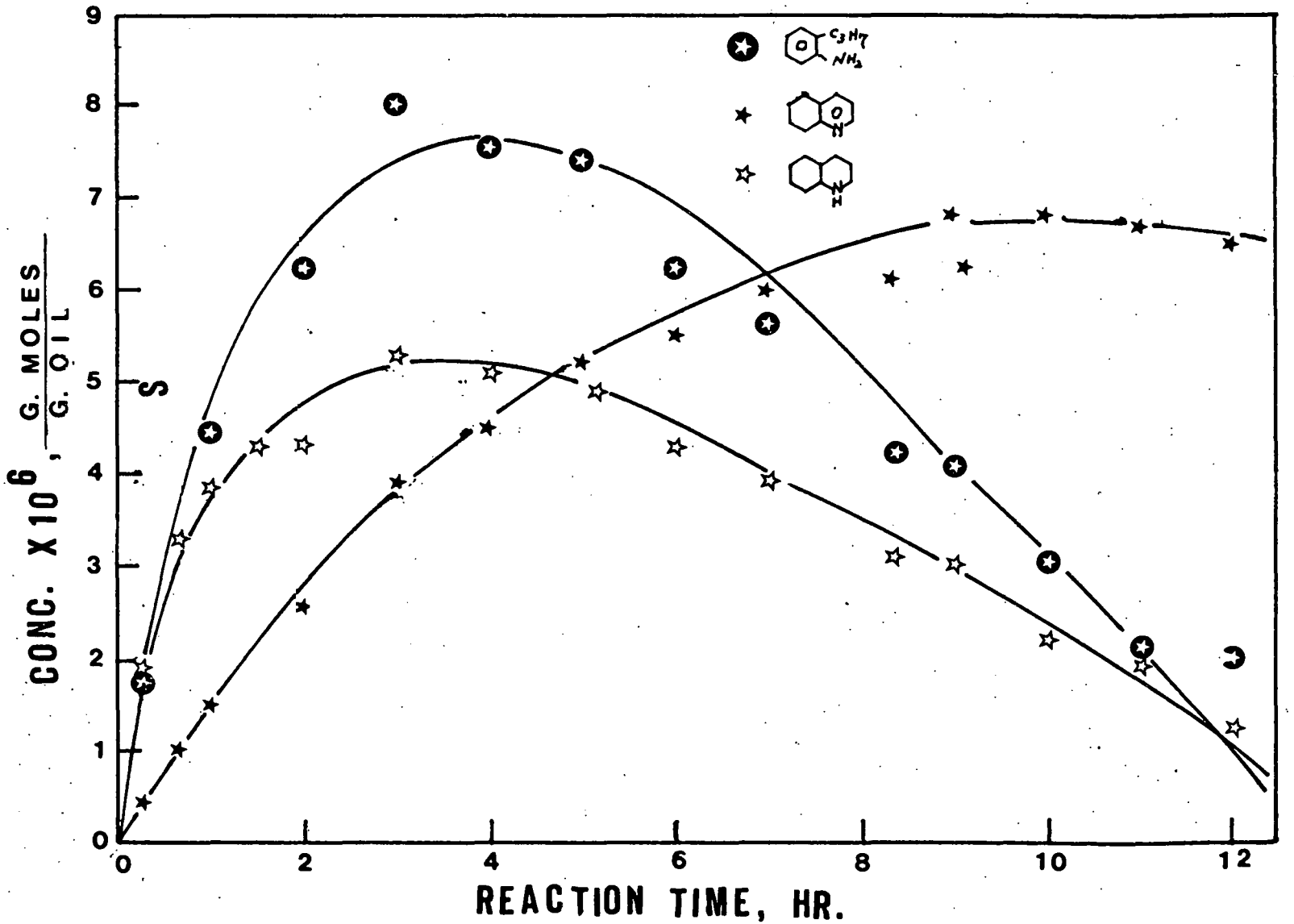

Figure 4. Hydrodenitrogenation of Quinoline in the Autoclave: presulfided Ni-Mo/Al_2O_3 catalyst, 342°C, 500 psig total pressure, 0.050 wt% of CS_2 in white oil, 0.50 wt% catalyst in white oil, and 1.0 wt% quinoline in white oil initially.

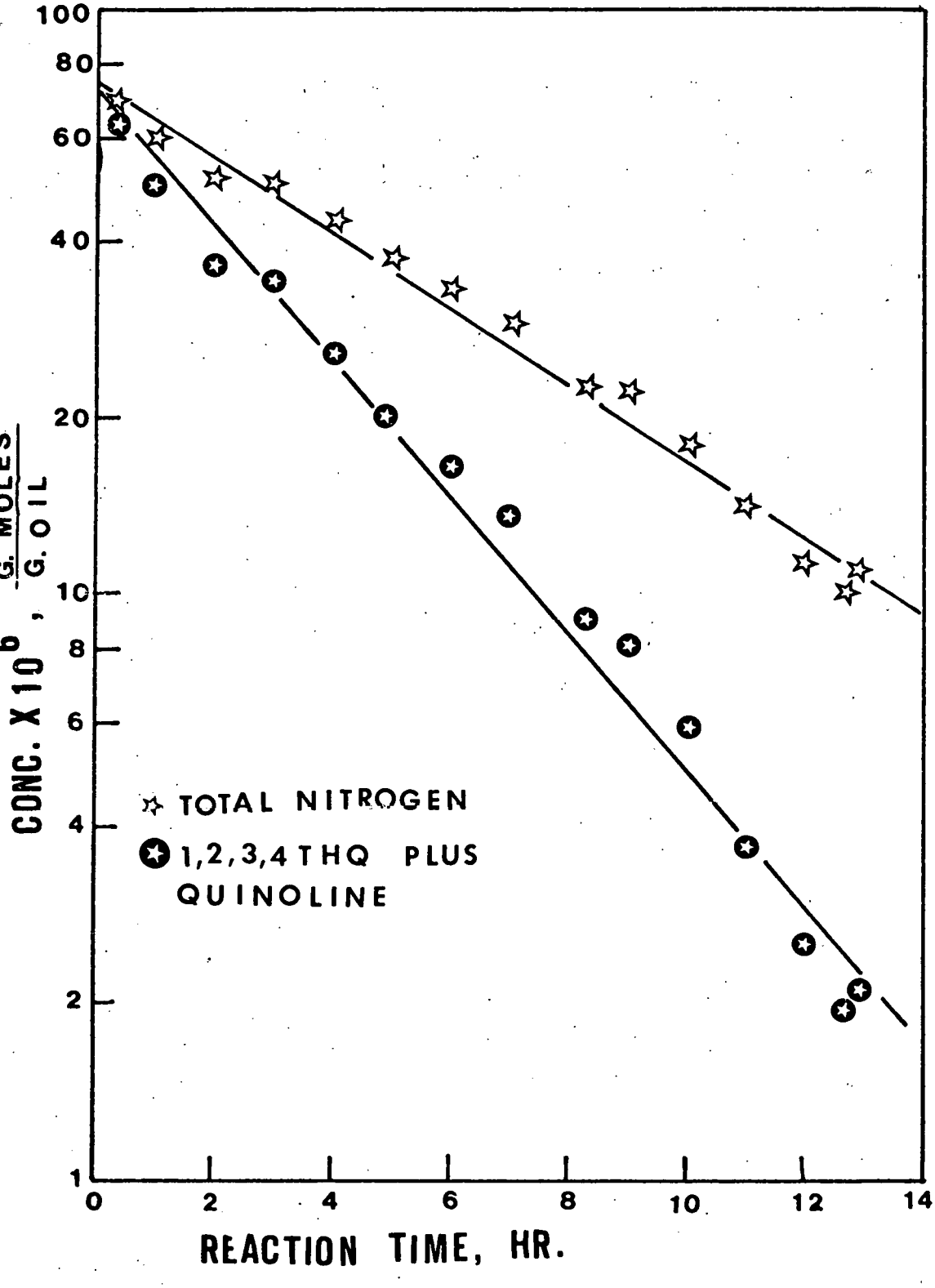

Figure 5. Hydrodenitrogenation of Quinoline in the Autoclave: presulfided Ni-Mo/Al_2O_3 catalyst, 342°C, 500 psig total pressure, 0.050 wt% of CS_2 in white oil, 0.50 wt% catalyst in white oil and 1.0 wt% quinoline in white oil initially.

TABLE V: KINETIC ANALYSIS OF THE CATALYTIC HYDRODENITROGENATION OF QUINOLINE

a. First-order rate constant for total nitrogen removal (from Figure 9).

$$\text{Total Nitrogen} \xrightarrow{K_{Total}} \text{Hydrocarbon} + NH_3$$

First-order rate constant:

$$K_{Total} = 0.56\ min^{-1}$$

b. First-order rate constant for the removal of quinoline plus 1,2,3,4-tetrahydroquinoline (from Figure 9).

$$\text{Quinoline} \underset{\text{very fast}}{\overset{\text{very fast}}{\rightleftharpoons}} \text{1,2,3,4-THQ}$$

$$\xrightarrow{K_{Q + THQ}} \text{Hydrogenated and Cracked Nitrogen-containing Hydrocarbons}$$

$$\frac{THQ}{Q} = 6.5$$

First-order rate constant:

$$K_{Q + THQ} = 0.88\ min^{-1}$$

TABLE V (continued)

c. First-order rate constants for the quinoline hydrodenitrogenation reaction network (from Figure 8 and Figure 9).

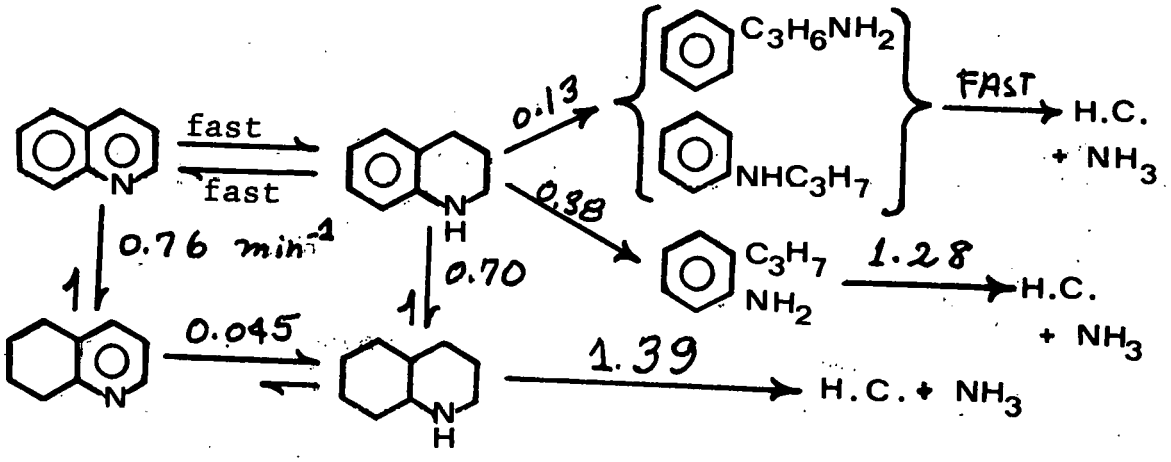

Reaction Conditions: Catalyst: HDS-9A (Ni-Mo/Al_2O_3), 2.0 grams
500 cc white oil
[CS_2]: 0.050 wt% in oil
Temperature: 342°C
Total Pressure: 500 psig
Total Reaction Time: 13 hrs
Initial Quinoline Conc.: 1.0 wt% in white oil

From Table VII, the relative reaction rates of the hydrogenation reactions, as shown by the first-order reaction constants, fall into the following sequence:

(quinoline ⟶ 1,2,3,4-tetrahydroquinoline) >>

(quinoline ⟶ 5,6,7,8-tetrahydroquinoline) >

(1,2,3,4-tetrahydroquinoline ⟶ decahydroquinoline) >

(5,6,7,8-tetrahydroquinoline ⟶ decahydroquinoline).

Since only the formation of 1,2,3,4-tetrahydroquinoline reaches equilibrium, the other hydrogenation reactions must be controlled by kinetic rather than thermodynamic factors.

It is not surprising that quinoline is very reactive toward partial hydrogenation of either the nitrogen-containing ring or the benzene ring due to activation by the adjacent aromatic ring. Similarly, naphthalene is more reactive for hydrogenation than benzene (Fieser and Fieser, 1957). It is worth noting that hydrogenation of the nitrogen-containing ring is much faster than the hydrogenation of the benzene ring. The higher electronegativity of the nitrogen atom and its unshared electrons clearly increase the electron density and consequent activation of the nitrogen-containing ring. Another possible explanation is that the basic nitrogen atom enhances adsorption of the nitrogen-containing ring on the catalyst surface enhancing hydrogenation of this ring vs. hydrogenation of the benzene ring.

The steric hindrance arising from the (non-planar) puckered conformation of the saturated ring may create difficulties for adsorption on the catalyst surface and thereby reduce the amount of material adsorbed or the rate of adsorption on the catalyst surface and thus retard reactivity. This is true for both of the possible tetrahydroquinoline hydrogenation intermediates [(I) and (II)] as can be seen in the representations of their structures:

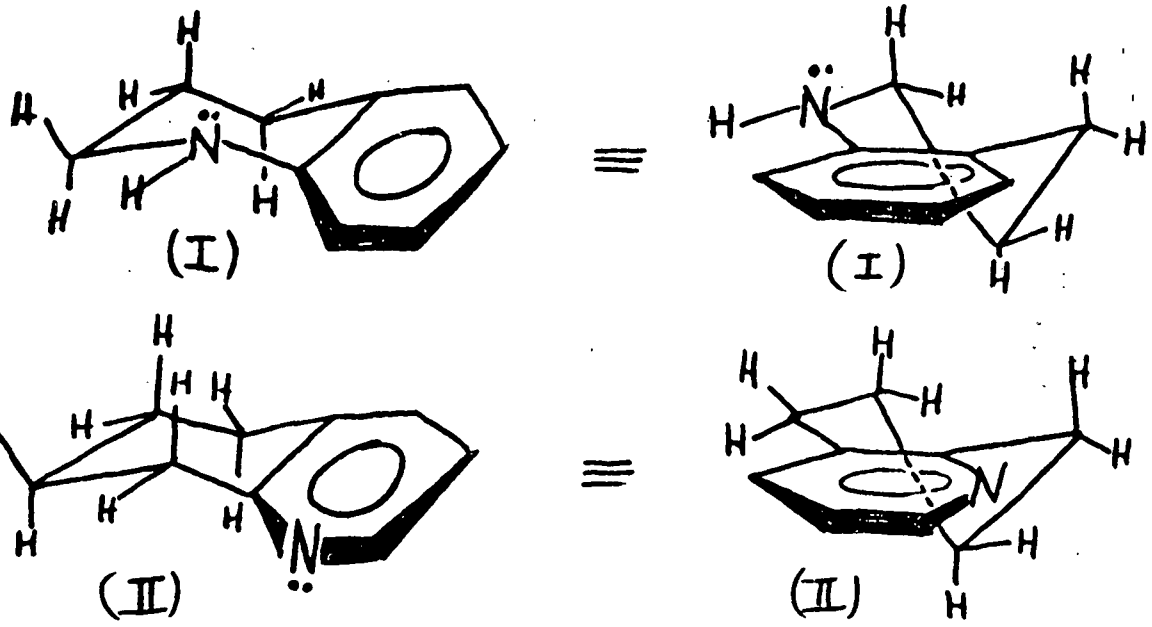

While adsorption of the residual aromatic ring in both (I) and (II) is somewhat retarded by steric influences, the pyridine moiety of (II) must be considerably less basic than the alkyl aniline-like centers of (I). This can be readily deduced from considerations of the basifying influences of the substituent structures in each case. Thus, any deviation from coplanarity of the (puckered cyclohexane) carbon substituents on the pyridine ring in (I) will only slightly diminish their (ordinarily) mildly basifying effect that can be perceived in the comparison of basicities of 2,3-dimethyl pyridine (pK_a = 6.57) and pyridine (pK_a = 5.25).

On the other hand, deviation in (I), from coplanarity of the nitrogen with the benzene ring to which it is attached is enforced by the puckering conformation of the fused, saturated ring. This greatly diminishes the resonance interaction which is ordinarily responsible for the depressed basicity of alkylanilines (N-ethylaniline pK_a = 5.12) compared to alkylamines (piperidine pK_a = 11.1). Thus, we can anticipate vastly increased basicity due to steric inhibition of aniline resonance in (I) and comparatively little alteration of the basicity of the pyridine ring in (II) (both) arising from the conformation of the fused, saturated ring. These differences in substituent effects of structure creating exalted basicity in (I) could account for its increased ease of adsorption on the electrophilic hydrogenation centers and greater reactivity.

The experimental results confirm that hydrogenation of 5,6,7,8-tetrahydroquinoline (II) is very slow as shown in Table V. It is speculated that the adsorption of 5,6,7,8-tetrahydroquinoline may be the rate determining step.

The cracking and hydrogenolysis of the saturated N-ring and the subsequent removal of nitrogen are more complex steps. They are the irreversible reactions displayed in Figure 3. More detailed discussion of reaction mechanism on cracking and nitrogen-atom removal will be presented in the next section.

b. Effect of hydrogen pressure and reaction mechanism.

As discussed in many examples in the literature, the reaction order with respect to hydrogen pressure is not consistent. The discrepancies may be caused by the differences in the range of hydrogen pressure, the type of feedstock and the characteristics of the catalyst; no study has provided a very complete evaluation of any one of these variables let alone of their effect in combination. The effect of hydrogen pressure on the hydrodenitrogenation of quinoline was studied during this quarterly period over a Ni-Mo/Al_2O_3 catalyst, between 300 and 1500 psig at 342°C. Figure 6 shows the effect of hydrogen pressure (i.e. total pressure) on the first-order rate constant for total nitrogen removal. In the low-pressure region the rate of total nitrogen removal increases with increasing hydrogen pressure; at high pressures the effect seems to level off or even decrease. A preliminary point at 1925 psig indicates that the rate may be decreasing at higher hydrogen pressures; confirmation is yet required. This type of behavior is indicative of a surface reaction mechanism involving adsorption of both the nitrogen-containing organic compound and the hydrogen on the same site on the surface with bimolecular surface reaction occurring between them. This suggests that the system might be well modeled by a Langmuir-Hinshelwood kinetic model for both total nitrogen removal and for quinoline plus 1,2,3,4-tetrahydroquinoline removal. Moreover a wealth of information can be obtained from the kinetic analysis of each reaction step in the reaction network as shown in Table V. The reaction network is partitioned among hydrogenation and hydrogenolysis steps. These will be discussed separately.

Hydrogenation Reactions. Figure 7 shows the effect of hydrogen pressure on the hydrogenation reactions. These results should be considered preliminary and will be firmed-up by experiments at higher pressures and by several repeat runs. As discussed previously, the hydrogenation of quinoline to 1,2,3,4-tetrahydroquinoline is so fast that the reaction rate cannot be measured under the conditions of the present study. Therefore, the reaction order with respect to hydrogen for this reaction is undetermined. For other hydrogenation reactions, the apparent reaction orders with respect to hydrogen are tabulated in Table VI.

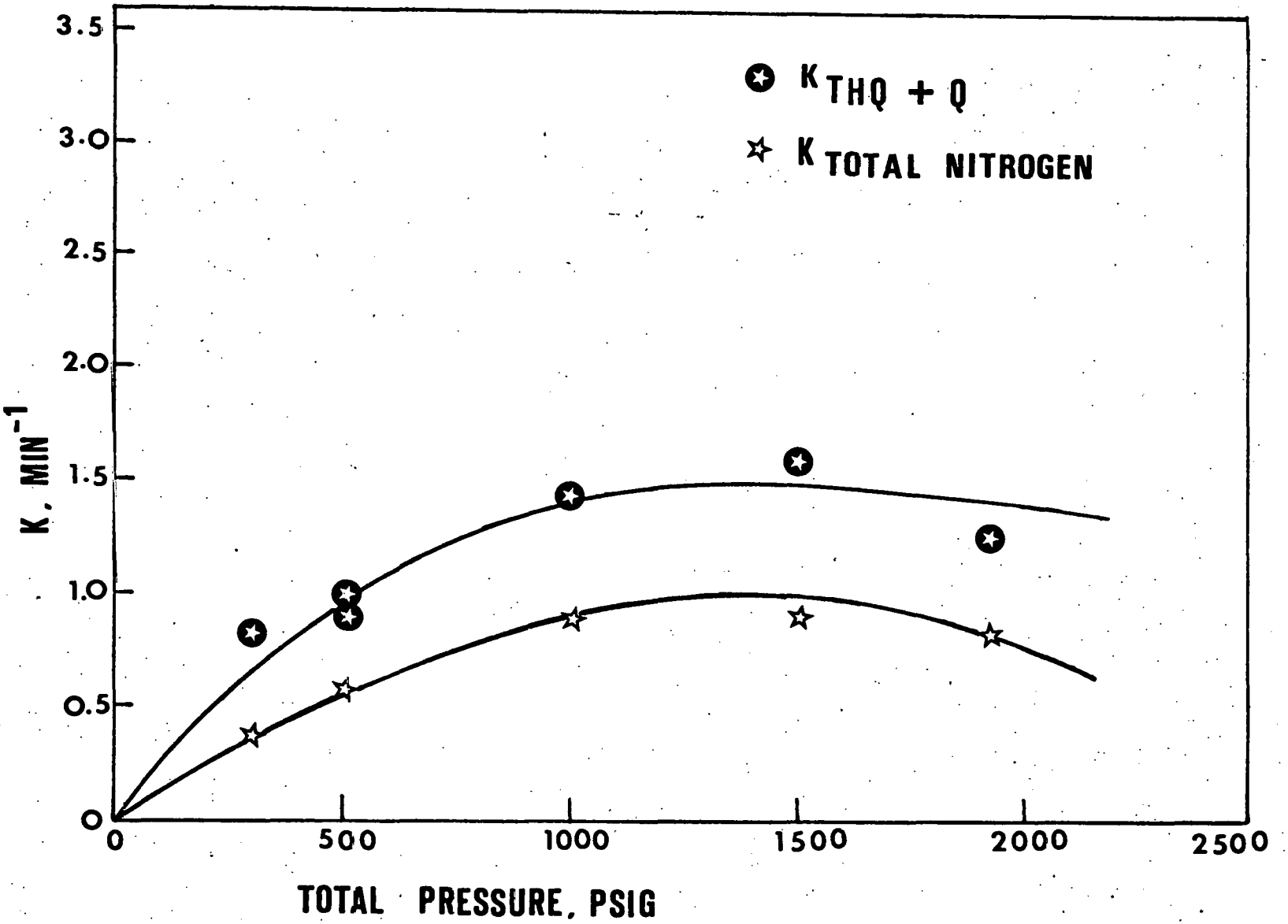

Figure 6. Effect of Total Pressure on Hydrodenitrogenation of Quinoline: Ni-Mo/Al_2O_3 catalyst, 342°C, 0.05 wt% of CS_2 in white oil, 0.50 wt% catalyst in white oil and 1.0 wt% quinoline in white oil initially.

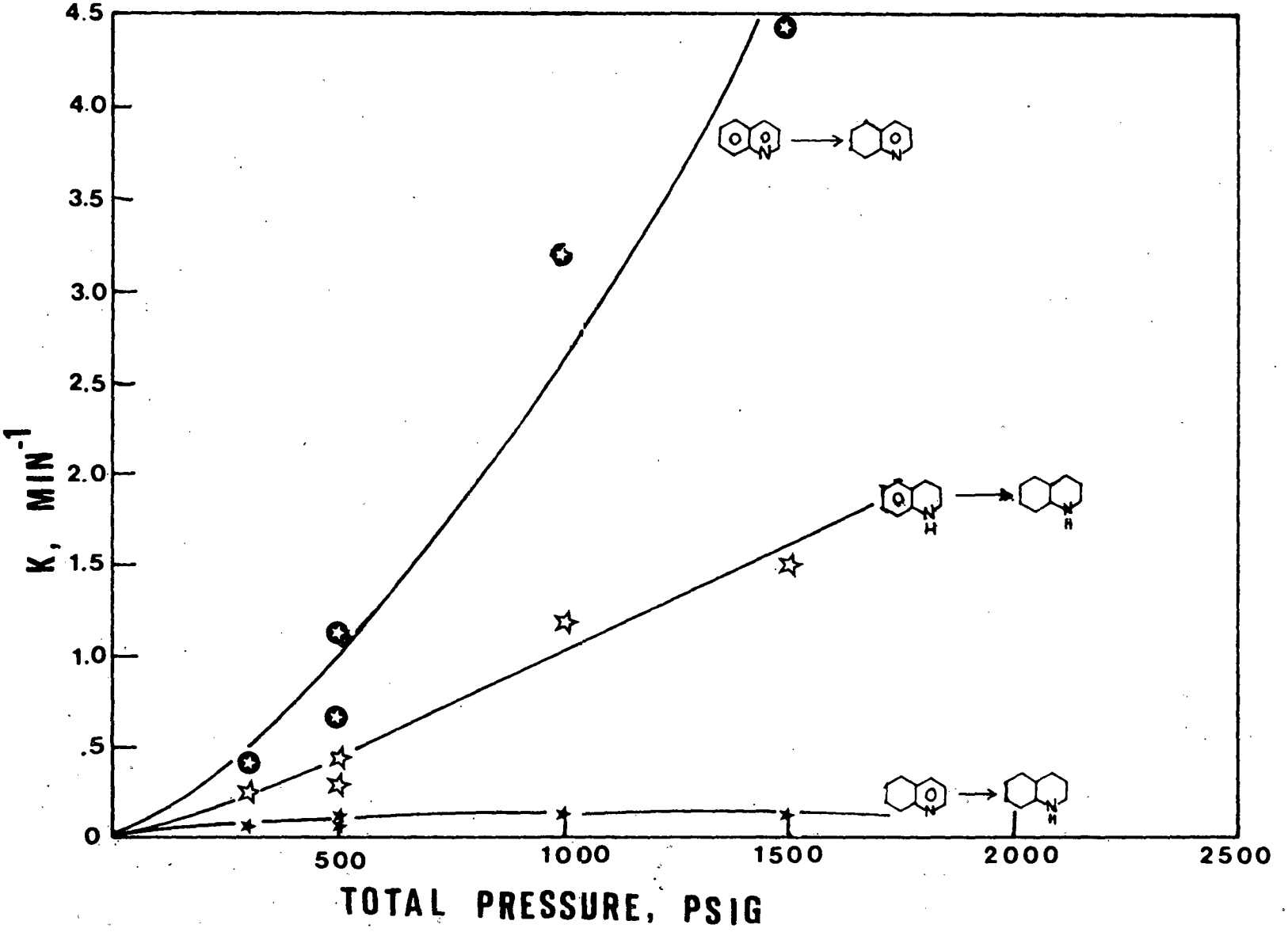

Figure 7. Effect of Total Pressure on Hydrodenitrogenation of Quinoline; Hydrogenation Reactions: Ni-Mo/Al_2O_3 catalyst, 342°C, 0.05 wt% CS_2 in white oil, 0.50 wt% catalyst in white oil and 1.0 wt% quinoline in white oil initially.

TABLE VI : REACTION ORDER WITH RESPECT TO HYDROGEN PRESSURE FOR HYDROGENATION REACTIONS

	Reaction order, n*
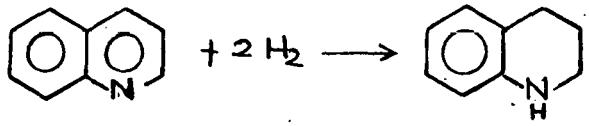	can't be measured
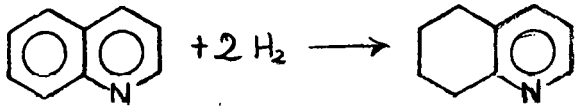	1.5
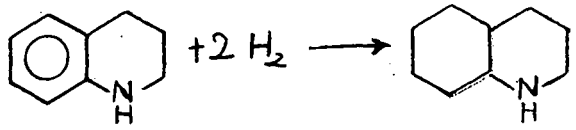	1.0
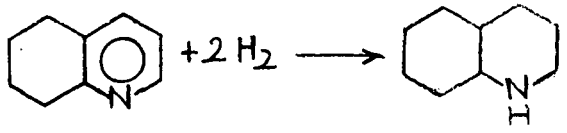	0

*$dC_i/dt = -K_i C_N P_{H_2}^n$

As shown in the Table VI the hydrogenation of quinoline to 5,6,7,8-tetrahydroquinoline appears to have a reaction order with respect to hydrogen which is greater than 1.0. For the hydrogenation of 1,2,3,4-tetrahydroquinoline to decahydroquinoline the reaction order in hydrogen is close to unity, and for the hydrogenation of 5,6,7,8-tetrahydroquinoline to decahydroquinoline the reaction order with respect to hydrogen is almost zero. Differences in reaction order with respect to hydrogen may reflect the differences in the rate determining steps of the pertinent hydrogenation reactions. Additional runs, particularly at higher pressures, will be carried out to establish the kinetic behavior with respect to hydrogenation.

For the hydrogenation of quinoline to 5,6,7,8-tetrahydroquinoline, the rate determining step is probably the surface reaction. The reaction supposedly takes place in two distinctive steps:

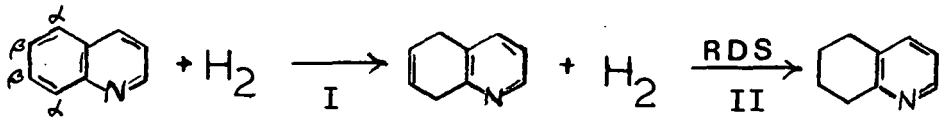

(8)

It is well known that α-positions (1,4,5,8) of naphthalene are more reactive than β-positions (2,3,6,7). If the second step is rate controlling, the overall reaction may well exhibit second-order behavior with respect to hydrogen pressure. Further studies will help define this.

If the nitrogen-containing ring has been hydrogenated, in the course of subsequent hydrogenation (of the benzene ring) the rate determining step may shift to step 1 leading to a first-order reaction in hydrogen, since the difference in reactivity between the α and β positions still prevails. In Table VI it can be seen that the hydrogenation of 1,2,3,4-tetrahydroquinoline to decahydroquinoline has a reaction order in hydrogen of approximately one. The role of steric effects is probably also important, but it is not yet clear how it is involved in these reactions.

For the hydrogenation of 5,6,7,8-tetrahydroquinoline to decahydroquinoline, the hydrogenation reaction may be sterically hindered and the adsorption of the 5,6,7,8-tetrahydroquinoline may be reduced by the cyclohexane ring as discussed previously. These steric effects may well explain the very low reactivity of 5,6,7,8-tetrahydroquinoline toward hydrogenation, as would reduced adsorption. If the slow rate were due to steric effects or particularly if the rate limiting step were adsorption because of steric hindrance,the rate could well show a very weak dependence on hydrogen partial pressure as observed.

Hydrogenolysis and Nitrogen removal. The effect of hydrogen pressure on the hydrogenolysis of the nitrogen-carbon bonds is shown in Figure 8. Removal of nitrogen as NH_3 must take place first via cracking the saturated nitrogen-containing

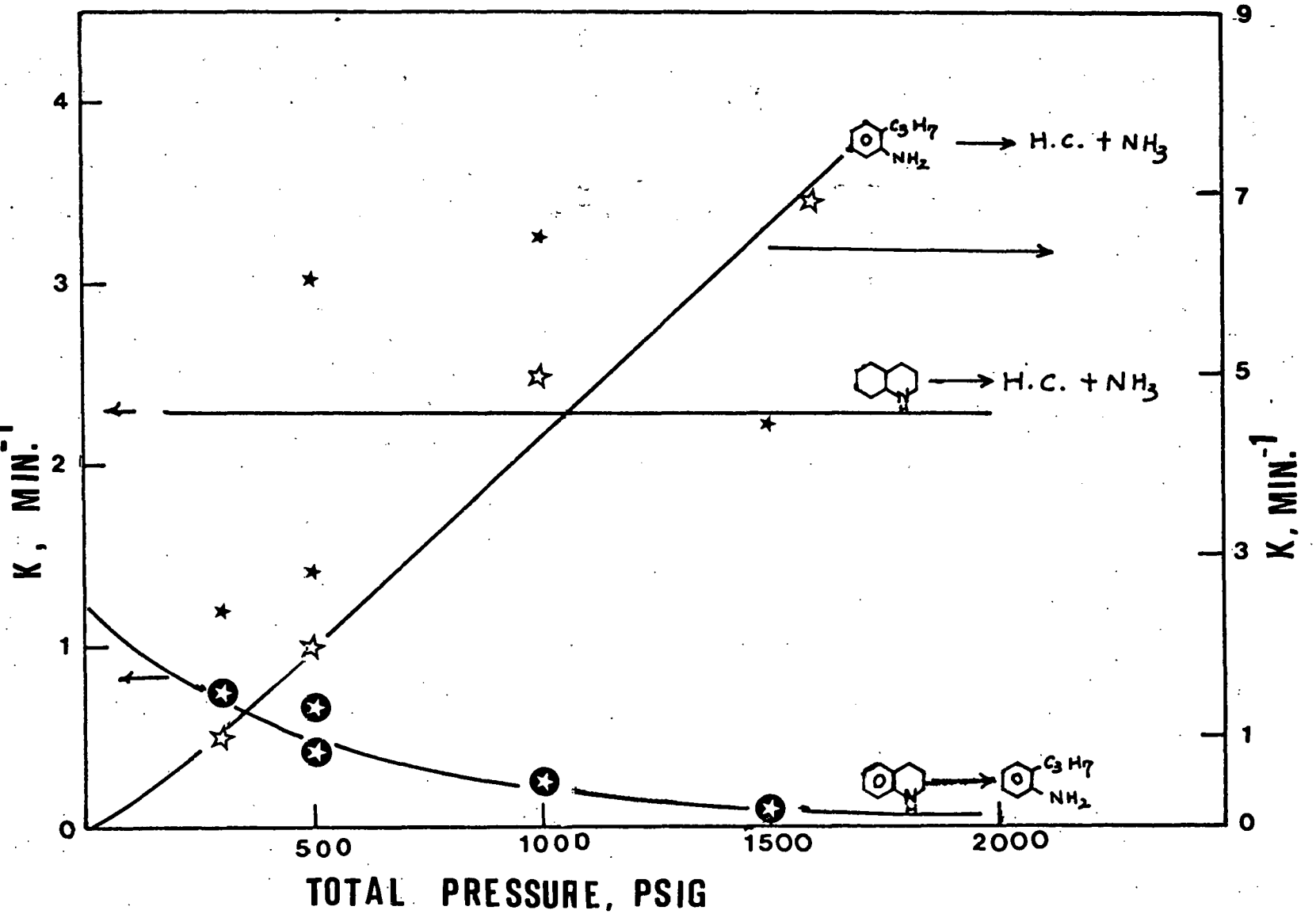

Figure 8. Effect of Total Pressure on Hydrodenitrogenation of Quinoline, Hydrogenolysis Reactions: Ni-Mo/Al_2O_3 catalyst, 342°C, 0.050 wt% of CS_2 in white oil, 0.50 wt% catalyst in white oil, and 1.0 wt% quinoline in white oil.

ring and then deamination of the amine or aniline formed. There are two intermediates with a saturated nitrogen-containing ring: 1,2,3,4-tetrahydroquinoline and decahydroquinoline. For 1,2,3,4-tetrahydroquinoline, three positions can be cracked as shown below:

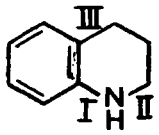

The C-N bond strength at (a) is expected higher than the C-N bond strength at the (b) position since the (a) position can be stabilized through the resonance with the adjacent benzene ring:

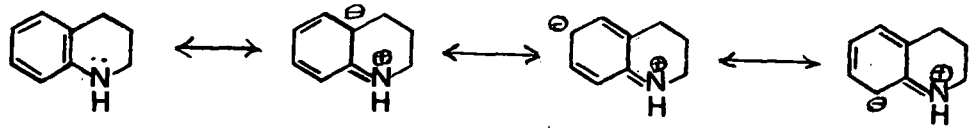

(9)

The average energies of the relevant bonds are shown in Table VII.

TABLE VII. BOND ENERGIES IN POLYATOMIC MOLECULES

Bond	Energy*	Bond	Energy*
C-H	99	N-H	93
C-C	83	C-N	73
C=C	146	C=N	147
C≡C	200	C≡N	213

*Bond energy given in kcal/mole.

Source: Roberts, J. D., Stewart, R., and Caserio, M. C., Organic Chemistry p. 25, W. A. Benjamin, Inc., Menlo Park, California, 1971.

Judging from the bond energies listed in Table VII, the bond strength of (a), (b), and (c) fall into the following order:

$$(a) \geq (c) > (b)$$

Cracking at position (a) leads to the formation of γ-phenyl-n-propyl amine, which is an aliphatic primary amine. Aliphatic amines are much more reactive in hydrogenolysis than aromatic nitrogen-containing compounds (Flinn et al., 1963). γ-phenyl-n-propyl amine was not observed as an intermediate in the current study, which, in all likelihood, is a reflection of this high reactivity toward hydrogenolysis.

Cracking reactions at (c) and (b) positions lead to the formation of o-propylaniline and n-propylaniline respectively. Both compounds are expected to be unreactive because of the nitrogen resonance with the adjacent benzene ring. n-propylaniline was not observed as a reaction intermediate. However, trace amounts of aniline which were detected in the current study could originate from n-propylaniline via β elimination of the propyl group either thermally or catalytically. The o-propylaniline is a refractory intermediate; it is only slowly denitrogenated and could also be the precursor of aniline.

An attractive and well precedented (though here purely hypothetical) mechanism for homogeneous reactions in solution is β-elimination. This mechanism provides two roles for the catalyst surface and suggests the need for two sites; one site is an electrophilic site which enhances the bond breaking activity for the leaving group, the nitrogen, and the second site is an electron donor site coordinating the hydrogen transferred concomitantly with the bond breaking. This reaction is illustrated in the following scheme:

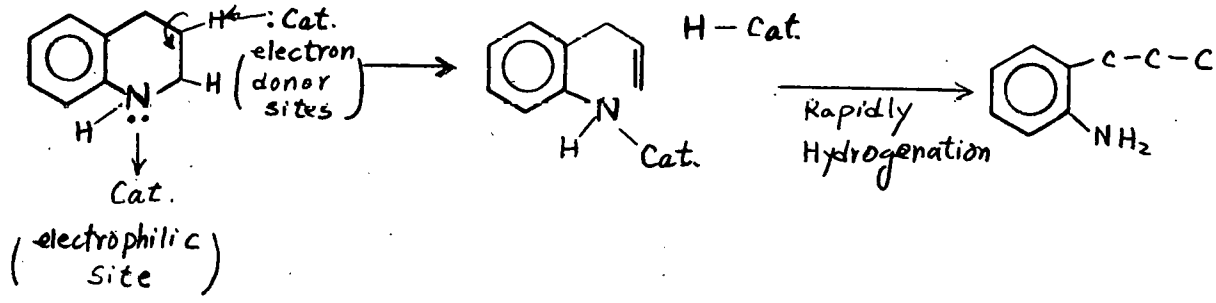

This type of process is commonly designated as an E-2 Hofmann Elimination reaction. The negative order with respect to hydrogen pressure in the conversion of 1,2,3,4-tetrahydroquinoline to o-propylaniline, shown in Figure 12, is consistent with the bifunctional activity of the catalyst in this β-elimination mechanism in that increasing hydrogen pressure results in a decrease of the sites available to carry out a bifunctional elimination. Such acid-base site pairs appear on the surface of alumina upon dehydration under the conditions used here (Peri, 1965, 1965a). Suppression of their frequency would be expected upon increasing hydrogen pressure.

On the other hand, if dehydrogenation of 1,2,3,4-tetrahydroquinoline occurs readily on the catalyst, the catalyst assisted cleavage of the C-N bond may involve a carbonium ion and possibly a resonance stabilized carbonium ion intermediate as illustrated in the following scheme:

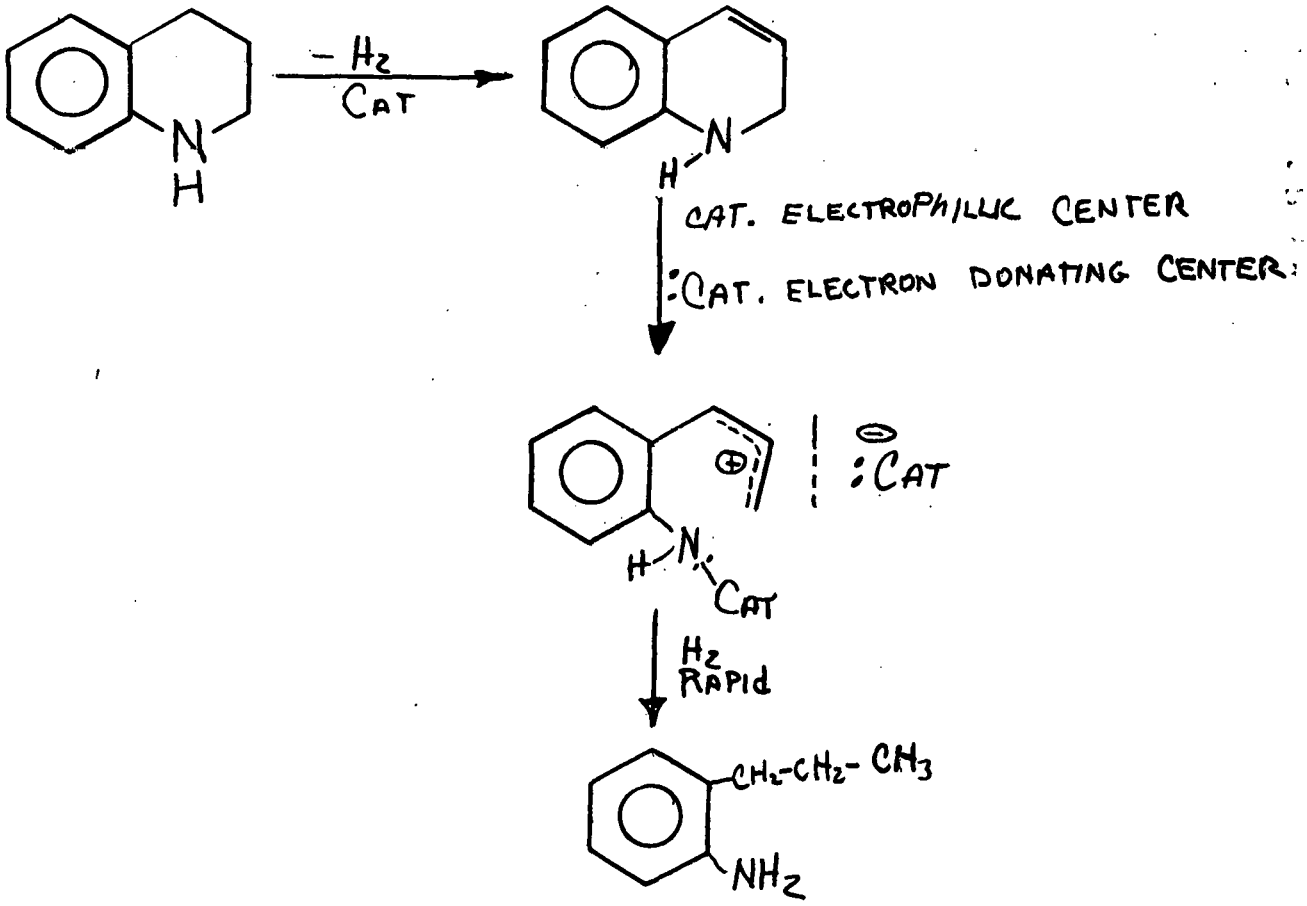

This type of reaction mechanism is commonly designated as an E-1 Hofmann process. This scheme is also in consonance with the negative order of reaction with respect to hydrogen pressure exhibited in Figure 8 since hydrogen will quench carbonium ions. There are at least two alternative ways of explaining the data in Figure 8, and further experimentation is required to distinguish between the alternatives.

As discussed previously, the aromatic C-N bond in o-propylaniline is relatively strong due to the resonance with the benzene ring. For hydrodenitrogenation of o-propylaniline, the benzene ring probably must be hydrogenated to weaken the C-N bond sufficiently for hydrogenolysis to occur:

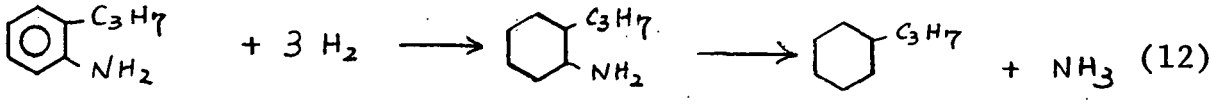

(12)

Hydrogenation of the benzene ring is probably the rate determining step. As shown in Figure 8 , the hydrodenitrogenation rate of o-propylaniline increases with increasing hydrogen pressure. Cracking of decahydroquinoline will lead to the formation of aliphatic amines. Since the hydrodenitrogenation of aliphatic amines should be very fast, they would not be expected to appear as high concentration intermediates; no amines were observed in measurable quantities. The reaction order with respect to hydrogen for the cracking of decahydroquinoline is somewhat uncertain since the data shown in Figure 8 are quite scattered. However, the cracking rate for decahydroquinoline is evidently faster than the rate for 1,2,3,4-tetrahydroquinoline. This is in keeping with the fact that in decahydroquinoline there are many more opportunities for β-elimination (E-2 or E-1) as compared to 1,2,3,4-tetrahydroquinoline, and in one of these additional modes, as is illustrated below, a tertiary hydrogen (normally more reactive) can be eliminated

c. Effect of H_2S on Quinoline Hydrodenitrogenation

The overall, qualitative discussion of the effect of H_2S on the hydrodenitrogenation of quinoline has been presented in the previous progress report.[2] Since the current kinetic model, as discussed in the previous sections, provides detailed information about the kinetic parameters in the reaction network, it is desirable to review the effect of H_2S on catalytic hydrodenitrogenation, especially to emphasize the effect on each step in the reaction network and to elucidate the change of catalyst parameters.

Generally, H_2S promotes the hydrodenitrogenation reaction. Table VIII shows the effect of H_2S pressure on the total nitrogen removal rate. Little insight can be obtained by examining only the effect on total nitrogen removal. More detailed information concerning the changes induced in the kinetic parameters by H_2S is given in the Figure [9]. The effect on hydrogenation and cracking reactions will be discussed separately.

Hydrogenation: Only the rate of hydrogenation of quinoline to 5,6,7,8-tetrahydroquinoline is increased by increasing H_2S partial pressure. The rate of hydrogenation of 1,2,3,4-tetrahydroquinoline to decahydroquinoline and that of hydrogenation of 5,6,7,8-tetrahydroquinoline to decahydroquinoline are independent of H_2S partial pressure. However, as discussed previously, the steric hindrance of cyclohexane-ring in 5,6,7,8-tetrahydroquinoline and in 1,2,3,4-tetrahydroquinoline may create difficulties for further hydrogenation of the other ring, possibly even leading to the rate limiting step becoming adsorption and thus altering the effect of system parameters on the hydrogenation rate. Thus changes in the catalytic hydrogenation activity might not affect the reaction rate. On the other hand the rate of hydrogenation of quinoline to 5,6,7,8-tetrahydroquinoline appears to be limited by surface reaction between adsorbed quinoline and hydrogen. Thus increasing the H_2S concentration increases the catalytic hydrogenation activity in the conversion of quinoline to 5,6,7,8-tetrahydroquinoline which enhances the overall reaction rate although not by a first-order dependence because this is only one of several important steps along two parallel paths leading to nitrogen removal.

TABLE VIII EFFECT OF H_2S CONCENTRATION ON THE CATALYTIC HYDRODENITROGENATION OF QUINOLINE

CS_2, wt% in oil	P_{H_2S}, vol% in gas-phase	K_{total}, min^{-1}	$K_{1,2,3,4\text{-THQ+Q}}$, min^{-1}	1,2,3,4-THQ / Q
0.00	0.017%	0.410	0.83	8.0
0.05	1.46 %	0.57	1.04	6.5
0.50	13.92 %	0.80	1.46	5.5

Reaction Conditions:

Loading: Catalyst HDS-9A ($Ni\text{-}Mo/Al_2O_3$) 2.0 grams
White Oil: 500 cc
Quinoline: 4.0 grams = 0.90 wt%

Temperature: 342°C
Total Pressure: 500 psig
Kinetic expressions:

$$-r_{\text{Total N}} = K_{\text{Total}}\, C_N.$$

$$-r_{1,2,3,4\text{-THQ+Q}} = K_{1,2,3,4\text{-THQ+Q}}\; C_{1,2,3,4\text{-THQ+Q}}$$

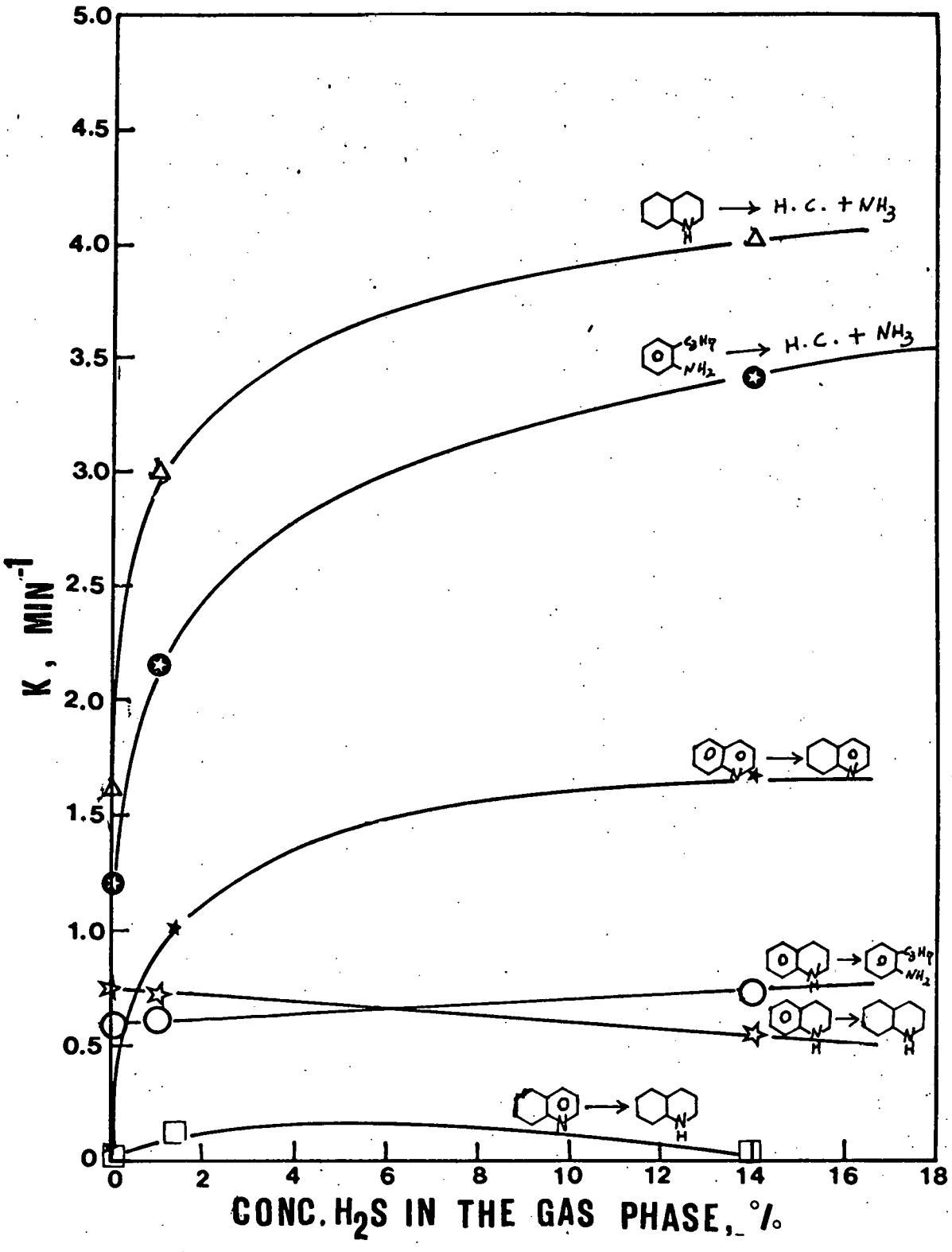

Figure 9. Effect of H_2S on Hydrodenitrogenation of Quinoline: presulfided Ni-Mo/Al_2O_3 catalyst, 342°C, 500 psig total pressure, CS_2 added to the white oil, 0.50 wt% catalyst in white oil, and 0.90 wt% quinoline in white oil initially.

A similar argument can be made for the denitrogenation of o-propylaniline. The hydrodenitrogenation of o-propylaniline probably proceeds via hydrogenation of the benzene ring of o-propylaniline followed by nitrogen removal from the amine. As shown in Figure 9 , increasing the H_2S partial pressure causes an increase in the rate of hydrodenitrogenation of o-propylaniline. Based on the above observations, H_2S seems to promote the hydrogenation of the benzene ring in molecules where steric hindrance problems are not present.

Hydrogenolysis: For the cracking reactions, the effect of H_2S depends on the reaction as shown in Figure 9 . H_2S promotes the cracking of decahydroquinoline, but there is evidently no promoting effect on the cracking of 1,2,3,4-tetrahydroquinoline. The reason for these differences is not entirely clear; further work may help clarify it. Increasing H_2S concentration should result in increased protonic acidity on the support. If the hydrogenolysis (cracking) reactions require protonic acidity, H_2S should have a beneficial effect. H_2S should also quench carbonium ions and reduce Lewis acidity of the catalyst. Thus it might also cause a reduction in the rate of reaction through the above effects. Possible mechanisms for the hydrogenolysis reactions were discussed above and will not be repeated here.

d. Relative catalyst activity

Similarly, the kinetic analysis of the reaction network for quinoline hydrodenitrogenation for the series of hydrotreating catalysts examined is summarized in Table IX and Table X. The overall catalytic activity in terms of total nitrogen removal is tabulated in Table IX, and the detailed kinetic analysis of the reaction network is shown in Table X.

Although the rate constant data are somewhat scattered (Table X), several interesting trends are observed. Since different catalysts were supplied by different producers (Table IX), pore volume, surface area and preparation procedure are significantly different from one catalyst to another. An interesting point is the fact that the rate of several reactions is constant for one specific parameter. For example, hydrogenation of 1,2,3,4-tetrahydroquinoline to decahydroquinoline has a constant reaction rate for all Ni-W catalysts, implying that this reaction is monofunctional and will therefore not be influenced significantly by the catalyst support. The

TABLE IX. FIRST-ORDER RATE CONSTANTS FOR QUINOLINE HYDRODENITROGENATION OVER A SERIES OF HYDROTREATING CATALYSTS

RANK	CATALYST	1st ORDER RATE CONSTANT, $\frac{g[THQ+Q]}{g\ cat\text{-}min}$	1st ORDER CORRELATING COEFFICIENT (-r)	1st ORDER RATE CONSTANT, $\frac{g[THQ+Q]}{g\ cat\text{-}min}$	1st ORDER RATE CONSTANT, $\frac{g[Total\ N]}{g\ cat\text{-}min}$	SURFACE AREA, m^2/g	PORE VOLUME, cc/g
		Autoclave No. 1	Autoclave No. 1	Autoclave No. 2	Autoclave No. 2		
1	CYANAMID AERO HDS-9A ($Ni\text{-}Mo/Al_2O_3$)	1.08	0.993	1.00	0.410		
2	NALCO NT-550 ($Ni\text{-}W/Al_2O_3$)	0.95	0.997	0.85	0.278	225	0.60
3	HARSHAW Ni-4303* ($Ni\text{-}W/Al_2O_3$)	0.69	0.976	0.97	0.237	152	0.54
4	HARSHAW Ni-4301 ($Ni\text{-}W/SiO_2\text{-}Al_2O_3$)	0.58	0.989	0.54	0.191	228	0.37
5	CYANAMID AERO HDS-16A ($Co\text{-}Mo/Al_2O_3$)	0.45	0.984	0.42	0.180		

*Sulfided at 325°C for one hour only.

Detailed operation conditions are described in Table XII.

Kinetic Analysis: Rate equations are based upon the disappearance of (Q) Quinoline plus (THQ) 1,2,3,4-tetrahydroquinoline or total nitrogen concentration in solution.

TABLE X: KINETIC ANALYSIS OF QUINOLINE HYDRODENITROGENATION REACTION OVER A SERIES OF HYDROTREATING CATALYSTS

	K_Q → 	K 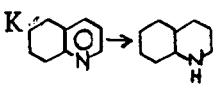	K 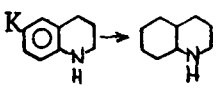	K 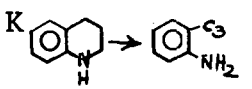	K 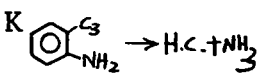	K 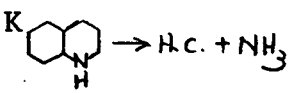
CYANAMID HDS-9A ($Ni\text{-}Mo/Al_2O_3$)	~ 0	~ 0	0.76	0.58	1.21	1.63
NALCO NT-550 ($Ni\text{-}W/Al_2O_3$)	0.24	~ 0	0.48	0.41	0.88	1.06
HARSHAW Ni-4303* ($Ni\text{-}W/Al_2O_3$)	~ 0	~ 0	0.49	0.26	0.87	0.22
HARSHAW Ni-4301 ($Ni\text{-}W/Al_2O_3\text{-}SiO_2$)	~ 0	~ 0	0.49	0.40	0.40	0.22
CYANAMID HDS-16A ($Co\text{-}Mo/Al_2O_3$)	~ 0	~ 0	0.32	0.29	1.42	1.53

Reaction Conditions: 342°C
500 psig
Stirring speed 1250 RPM
Catalyst particle size 100-140 mesh
Initial quinoline concentration ~ 66 X 10^{-6} g mole/ g oil
No CS_2 added to white oil

Presulfiding: All catalysts were presulfided for two hours @ 325°C with 10.3% H_2S in H_2 gas mix.

*Sulfided for one hour only.

cracking of decahydroquinoline and subsequent denitrogenation of its cracking products are significantly controlled by the support properties. As shown in Table X, HDS-9A and HDS-16A are made of similar supports and reveal similar reaction rates for this reaction.

e. Effect of Initial Quinoline Concentration

As reported previously the total nitrogen removal (percentage removal) increases with decreasing initial quinoline concentration. Table XI gives the first-order rate constant for total nitrogen removal as a function of the initial quinoline concentration. The data fit the following empirical equation:

$$K_{\text{Total N}} = \frac{K'}{1 + AC_{Q_o}} \qquad (12)$$

Based on data in Table XI , K' and A can be calculated from Equation 12 giving the results shown in Equation 13.

$$K_{\text{Total N}} = \frac{1.075}{1 + 1.257\, C_{Q_o} \times 10^4} \qquad (13)$$

The kinetic analysis for the quinoline hydrodenitrogenation reaction network is shown in Figure 10 and Figure 11. Figure 10 and Figure 11 show that the effect of the initial quinoline concentration on the individual rate constants for each reaction step is similar.

f. Results from the High-Pressure Liquid-Phase Flow Microreactor

Basically data taken from the autoclaves gives the initial catalytic activity. The high-pressure liquid-phase flow microreactor will provide data on the steady-state activity. Data obtained by the two methods will be compared carefully.

The first run for hydrodenitrogenation of quinoline on the flow microreactor has been successfully completed. The results of the experiment are presented below.

The conditions for the sulfiding of the catalyst and for the hydrodenitrogenation reaction are summarized in Table XII. Figure 12 shows a typical analysis of a sample taken during

TABLE XI: EFFECT OF INITIAL QUINOLINE CONCENTRATION ON THE HYDRODENITROGENATION OF QUINOLINE

$[C_{Q_o}]$, $\frac{\text{g-mole}}{\text{g-oil}}$	K_{Total}, min^{-1}
73×10^{-6}	0.57
21×10^{-6}	0.80
8×10^{-6}	1.05

Reaction Conditions:

Loading: Catalyst - Cyanamid HDS-9A ($Ni\text{-}Mo/Al_2O_3$) 2.0 grams
White oil - 500 cc
CS_2 0.050 wt% oil

Temperature: 342°C
Total Pressure: 500 psig
Kinetic Expressions:

$$-r_{Total\ N} = K_{Total\ N}\, C_{Total\ N}$$

$$K_{Total\ N} = \frac{1.075}{1 + 1.257\, C_{Q_o}}$$

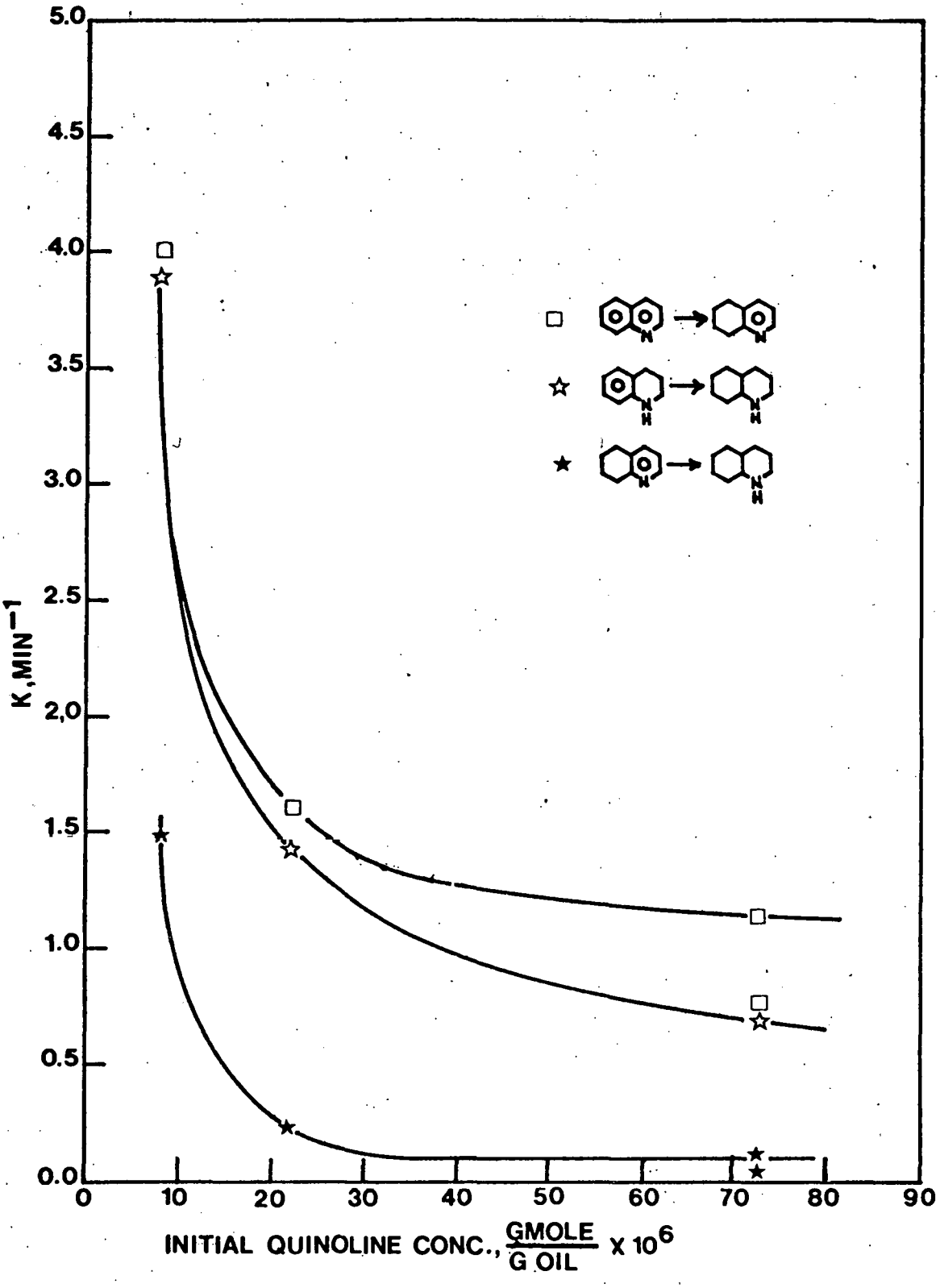

Figure 10. Effect of Initial Quinoline Concentration on Hydrodenitrogenation of Quinoline, Hydrogenation Reactions: presulfided Ni-Mo/Al_2O_3 catalyst, 342°C, 500 psig total pressure, 0.050 wt% of CS_2 in white oil, and 0.50 wt% catalyst in white oil.

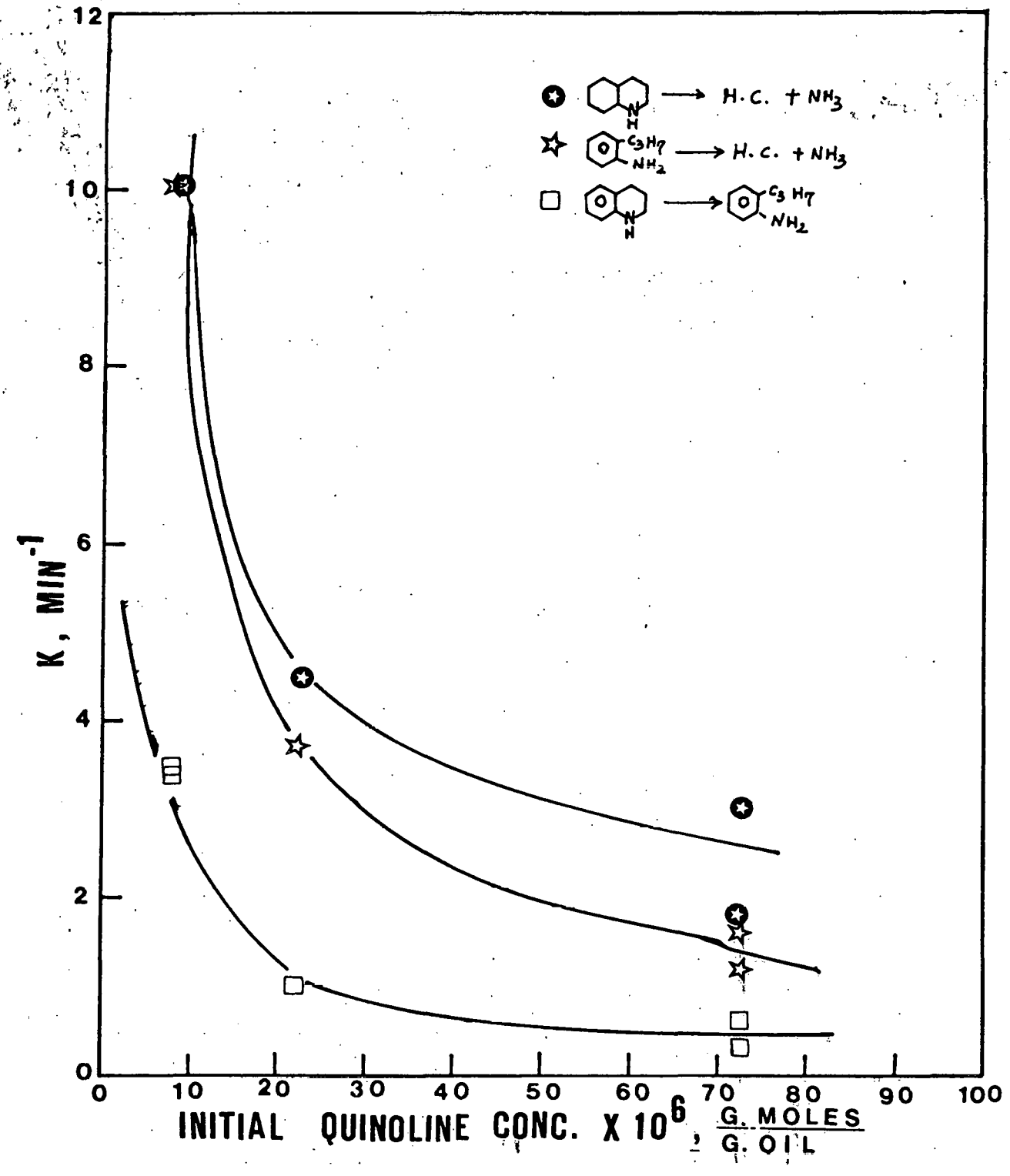

Figure 11. Effect of Initial Quinoline Concentration on Hydrodenitrogenation of Quinoline, Hydrogenolysis Reactions: presulfided Ni-Mo/Al_2O_3 catalyst, 342°C, 500 psig total pressure, 0.050 wt% of CS_2 in white oil, and 0.50 wt% catalyst in white oil.

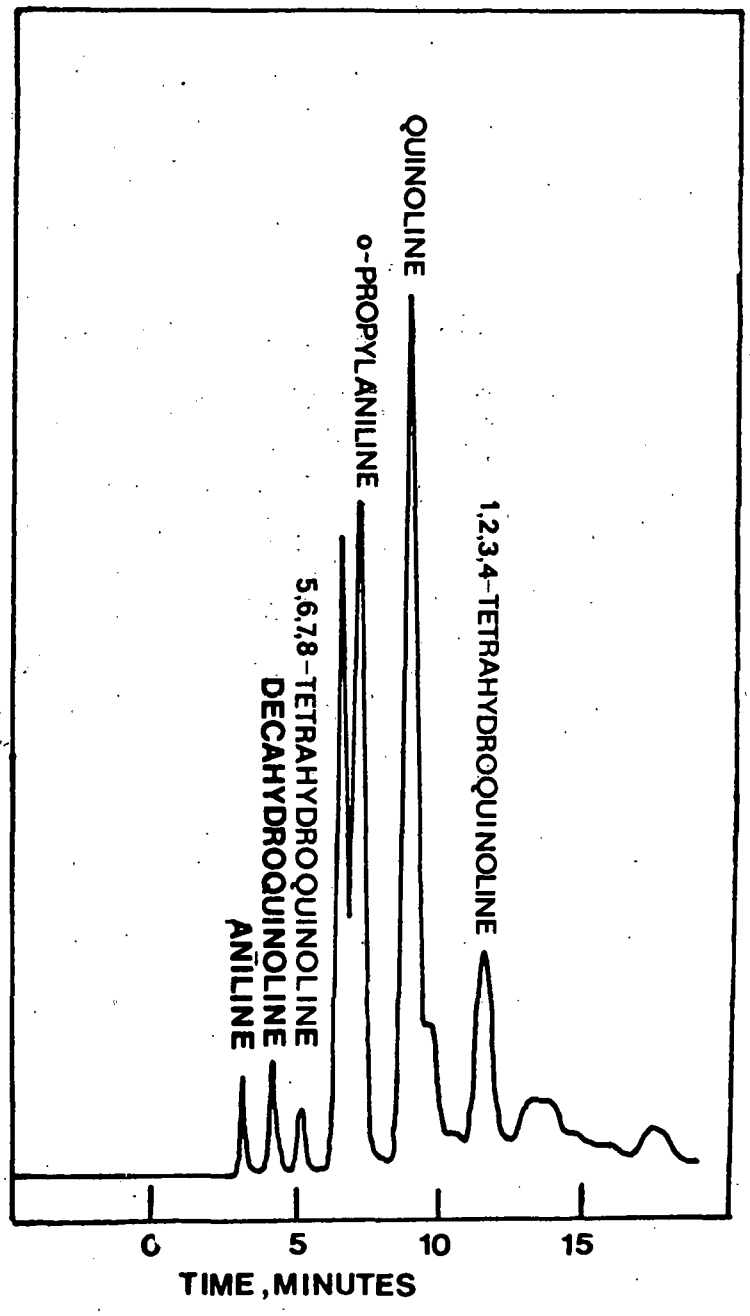

Figure 12. Gas Chromatogram Using Nitrogen-specific Detector of Early-time Product Sample from Quinoline Hydrodenitrogenation in High-Pressure Liquid-Phase Flow Microreactor: in situ sulfided Ni-Mo/Al_2O_3, white oil saturation pressure 690 psig H_2, operating pressure 1500 psig, 350°C and LHSV of 4.0.

TABLE XII

OPERATING CONDITIONS FOR HYDRODENITROGENATION OF QUINOLINE IN THE HIGH-PRESSURE LIQUID-PHASE FLOW MICROREACTOR

1) Compound(s) and Initial Concentration: quinoline in white oil - 8.07×10^{-5} g atom N/cc of white oil.

2) Catalyst: Cyanamid HDS-9A, Ni-Mo/Al_2O_3

   Weight of catalyst: 0.515 g
   Sulfided at: 350°C for 3 hours
   Catalyst size: 60-100 mesh

3) White oil saturation pressure: 690 psig of H_2

   Total pressure of operation of the flow microreactor: 1500 psig

4) Reaction temperature: 350°C

5) Flow rate: 1.83 cc liquid oil feed per hour
   LHSV = 4.0 hr^{-1}

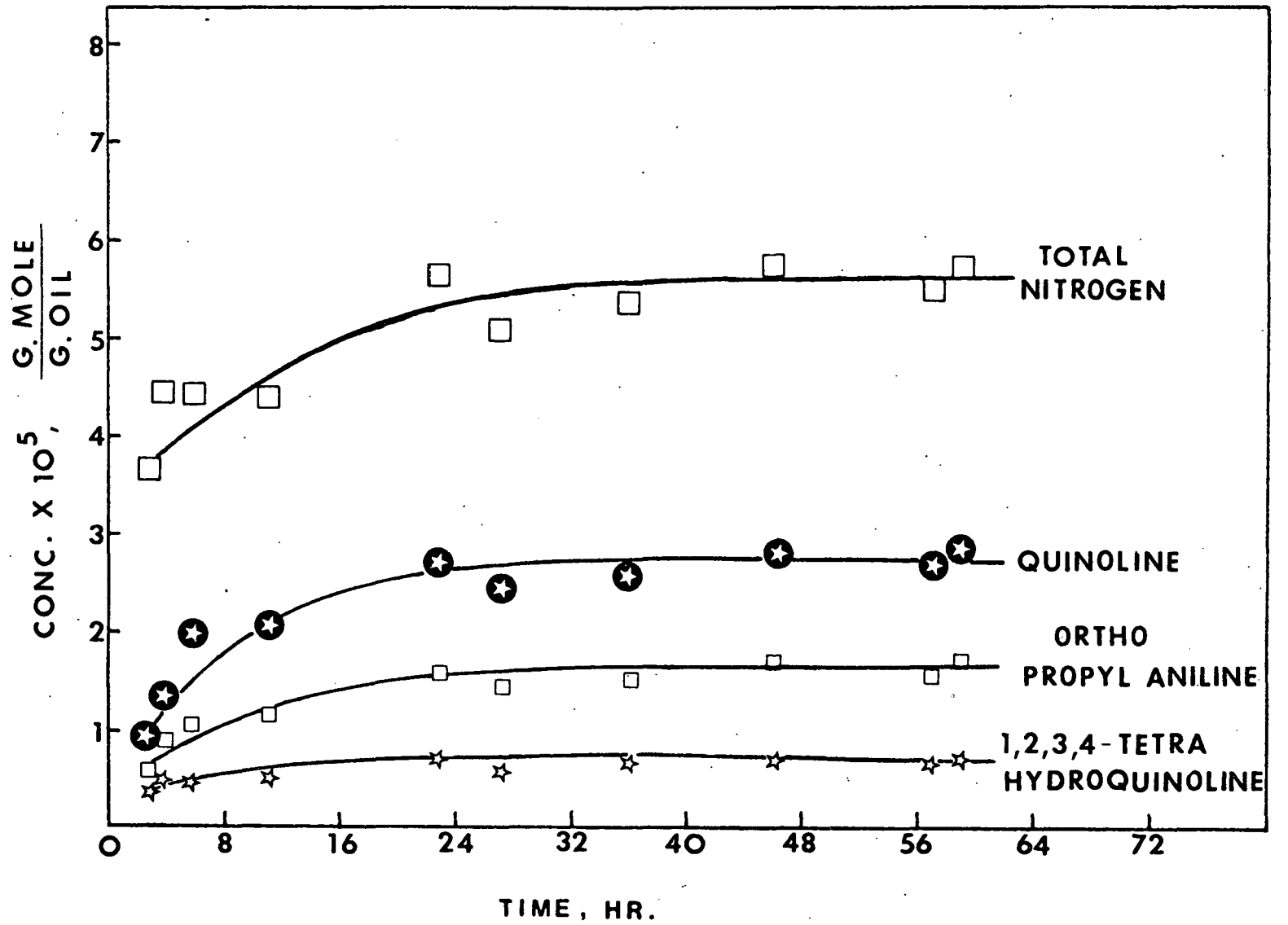

Figure 13. Hydrodenitrogenation of Quinoline in the High-Pressure Liquid-Phase Flow Microreactor: presulfided Ni-Mo/Al_2O_3 catalyst, 350°C, 690 psig hydrogen saturation pressure, 1500 psig operating pressure, 4 hr^{-1} LHSV.

TABLE XIII TABULATED PRODUCT CONCENTRATIONS FOR THE HYDRODENITROGENATION OF QUINOLINE IN THE HIGH-PRESSURE LIQUID-PHASE FLOW MICROREACTOR

Sampling Time (Hrs.)	Comp. #1 RT=0.5 min. g. atom N / cc. oil X 10^6	Comp. #2 RT=1.7 min. g. atom N / cc. oil X 10^6	Comp. #3 RT=2.1 min. g. atom N / cc. oil X 10^6	Comp. #4 RT=3.1 min. g. atom N / cc. oil X 10^6	Comp. #5 RT=4.1 min. g. atom N / cc. oil X 10^6
	unknown	unknown	unknown	aniline	decahydro-quinoline
1:14	-	0.0102	0.0269	1.51	3.43
1:50	-	-	0.0111	1.05	1.10
2:45	-	-	-	0.72	1.10
3:45	0.0213	-	0.0158	0.58	0.96
5:45	-	-	-	0.57	0.87
11:00	-	-	-	0.46	0.72
22:45	-	-	0.0139	0.40	0.72
27:00	-	-	-	0.37	0.74
36:00	0.0195	-	0.0148	0.37	0.71
46:00	-	-	-	0.33	0.80
57:00	-	-	0.0083	0.34	0.76
59:00	-	-	0.0158	0.36	0.74

TABLE XIII. TABULATED PRODUCT CONCENTRATIONS FOR THE HYDRODENITROGENATION OF QUINOLINE IN THE HIGH-PRESSURE LIQUID-PHASE FLOW MICROREACTOR

(continued)

Sampling Time (Hrs.)	Comp. #6 RT=5.2 min. g. atom N / cc. oil X 10^6	Comp. #7 RT=5.9 min. g. atom N / cc. oil X 10^6	Comp. #8 RT=6.5 min. g. atom N / cc. oil X 10^6	Comp. #9 RT=7.1 min. g. atom N / cc. oil X 10^6	Comp. #10 RT=8.9 min. g. atom N / cc. oil X 10^6
	unknown	unknown	5,6,7,8 tetrahydro-quinoline	o-propyl-aniline	quinoline
1:14	1.28	0.166	8.55	9.99	39.3
1:50	1.00	0.065	7.26	4.46	10.0
2:45	1.05	-	8.06	4.53	7.5
3:45	0.58	-	5.88	7.49	11.4
5:45	0.43	-	5.14	8.82	16.6
11:00	0.27	-	3.36	9.87	17.0
22:45	0.23	-	2.82	13.16	22.6
27:00	0.22	-	2.49	11.86	20.5
36:00	0.21	-	2.47	12.79	21.6
46:00	0.22	-	2.27	13.82	23.5
57:00	0.22	-	2.24	13.03	22.6
59:00	0.27	-	2.31	13.80	23.8

TABLE XIII. TABULATED PRODUCT CONCENTRATIONS FOR THE HYDRODENITROGENATION OF QUINOLINE IN THE HIGH-PRESSURE LIQUID-PHASE FLOW MICROREACTOR

(continued)

Sampling Time (Hrs.)	Comp. #11 RT=9.7 min. g. atom N / cc. oil X 10^6	Comp. #12 RT=11.6 min. g. atom N / cc. oil X 10^6	Comp. #13 RT=13.7 min. g. atom N / cc. oil X 10^6	Comp. #14 RT=16.3 min. g. atom N / cc. oil X 10^6	Comp. #15 RT=17.8 min. g. atom N / cc. oil X 10^6
	unknown	1,2,3,4 tetrahydro-quinoline	unknown	unknown	unknown
1:14	5.39	5.90	5.64	0.825	4.25
1:50	2.43	2.51	1.98	-	1.76
2:45	1.64	2.95	1.46	-	1.69
3:45	1.77	3.95	1.22	-	1.37
5:45	-	3.68	0.97	-	-
11:00	-	4.03	1.13	-	-
22:45	-	5.61	1.60	-	-
27:00	-	4.96	1.26	-	-
36:00	-	5.41	1.37	-	-
46:00	-	5.63	1.43	-	-
57:00	-	5.37	1.23	-	-
59:00	-	5.64	1.23	-	-

TABLE XIII. TABULATED PRODUCT CONCENTRATIONS FOR THE HYDRODENITROGENATION OF QUINOLINE IN THE HIGH-PRESSURE LIQUID-PHASE FLOW MICROREACTOR

(continued)

Sampling Time (Hrs.)	Total Nitrogen $\frac{\text{g. atom N}}{\text{cc. oil}} \times 10^6$	$\frac{1,2;3,4\text{-THQ}}{\text{quinoline}}$
1:14	86.2	0.15
1:50	33.6	0.25
2:45	30.7	0.39
3:45	37.1	0.35
5:45	37.1	0.22
11:00	36.8	0.24
22:45	47.1	0.25
27:00	42.4	0.24
36:00	45.0	0.25
46:00	48.0	0.24
57:00	45.8	0.24
59:00	38.1	0.24

TABLE XIV.

SUMMARY OF KINETIC ANALYSIS FOR QUINOLINE HYDRODENITROGENATION IN THE HIGH-PRESSURE LIQUID-PHASE FLOW MICROREACTOR

The first-order rate constants for hydrodenitrogenation of quinoline on Ni-Mo/Al_2O_3 catalyst corrected to 500 psig H_2 saturation:

@ 2-45 hrs K = 0.18 g oil/g cat-min (Initial Activity)

@ 46 hrs K = 0.10 g oil/g cat-min (Stabilized Activity)

cf. K = 0.41 g oil/g cat-min for hydrodenitrogenation of quinoline in autoclave.

initial high activity conditions of the catalyst. Concentrations of various nitrogen compounds with respect to time are plotted in Figure 13. The results in terms of all nitrogen-containing compounds observed (Table XIII) and the rate constant K based on total nitrogen removal (Table XIV) are summarized and compared to those obtained in the batch reactors in Table XIV. The steady-state activity corrected to 500 psig is one fourth of the activity obtained with the autoclave reactors.

The run was carried out in the absence of any sulfur in the feed and the activity of the catalyst appears to be stabilized after about 24 hours. However, from batch reactor studies completed to date in this laboratory, it is quite clear that the presence of sulfur in the feed results in a higher hydrodenitrogenation activity of the catalysts. Also part of the deactivation observed may have been due to stripping sulfur from the catalyst by the sulfur-free hydrogen-hydrocarbon feed. Hence, future runs with this reactor will be carried out in the presence of sulfur by saturating the reaction mixture with an H_2-H_2S mixture of appropriate concentration.

g. Hydrodenitrogenation of Carbazole

One experimental run was made using carbazole as the nitrogen-containing reactant. Figure 14 shows the results of this work. An aromatic-enriched solvent (85 wt% white oil; 15 wt% 1-methylnaphthalene) was used due to the low solubility of carbazole (<100 ppm) in pure white oil. However, even with aromatic-enriched solvent 0.5% carbazole was not soluble at ambient conditions. It was presumed that 0.5 wt% carbazole was soluble at reaction conditions because a precipitate formed in the liquid samples taken from the heated reactor after the samples cooled. Figure 14 indicates that less than 20% of the carbazole reacted in the autoclave batch reactor after 170 minutes at 342°C and 500 psig. For comparison at these experimental conditions, approximately 40% of an initial quinoline reactant in pure white oil would be expected to have reacted. Four nitrogen-containing compounds were observed as reaction intermediates. The major species among these is presented in Figure 14. The three other compounds were present in very low concentrations and are not shown in Figure 14. Further work will emphasize identification of these compounds and development of a better analytic procedure for the analysis of the compounds formed in this system.

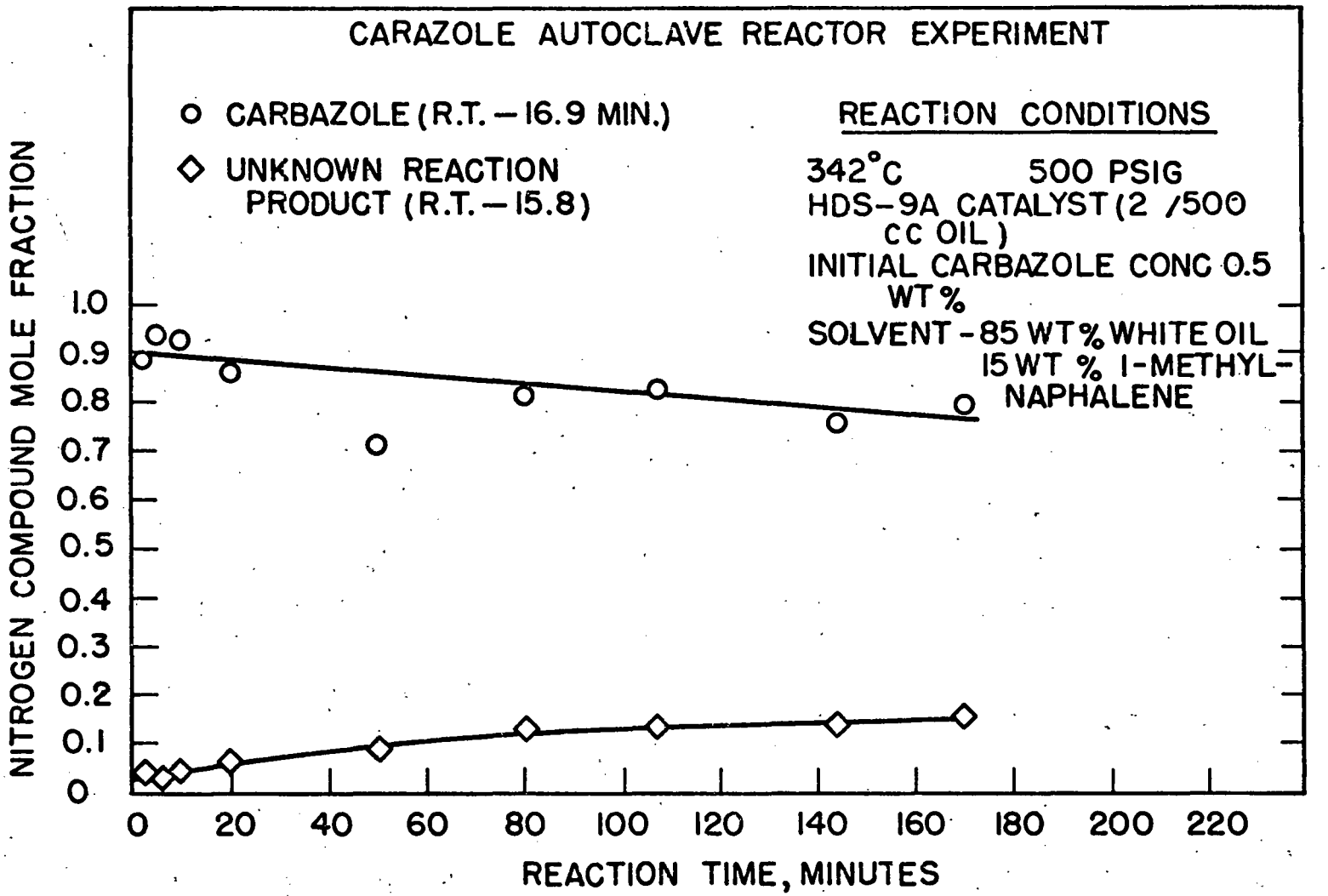

Figure 14. Hydrodenitrogenation of Carbazole in the Autoclave: presulfided Ni-Mo/Al_2O_3, 342°C, 500 psig total pressure, 0.050 wt% CS_2 in 85 wt% white oil - 15 wt% 1-methylnaphthalene mixture, 0.50 wt% catalyst in white oil, and 0.50 wt% carbazole in carrier oil.

h. Synthesis of Methyl-Substituted Nitrogen-Containing Compounds

Several methyl or dimethyl substituted nitrogen containing compounds have been prepared during this quarterly period. The compounds and synthesis methods are summarized below.

Hexahydrocarbazole was obtained by the reduction of tetrahydrocarbazole with tin and concentrated HCl.

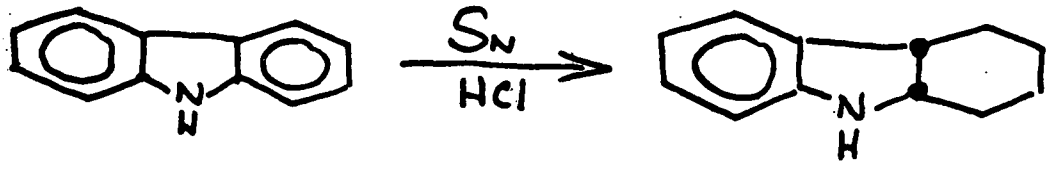

1,8-Dimethylcarbazole was obtained by the following reaction steps.

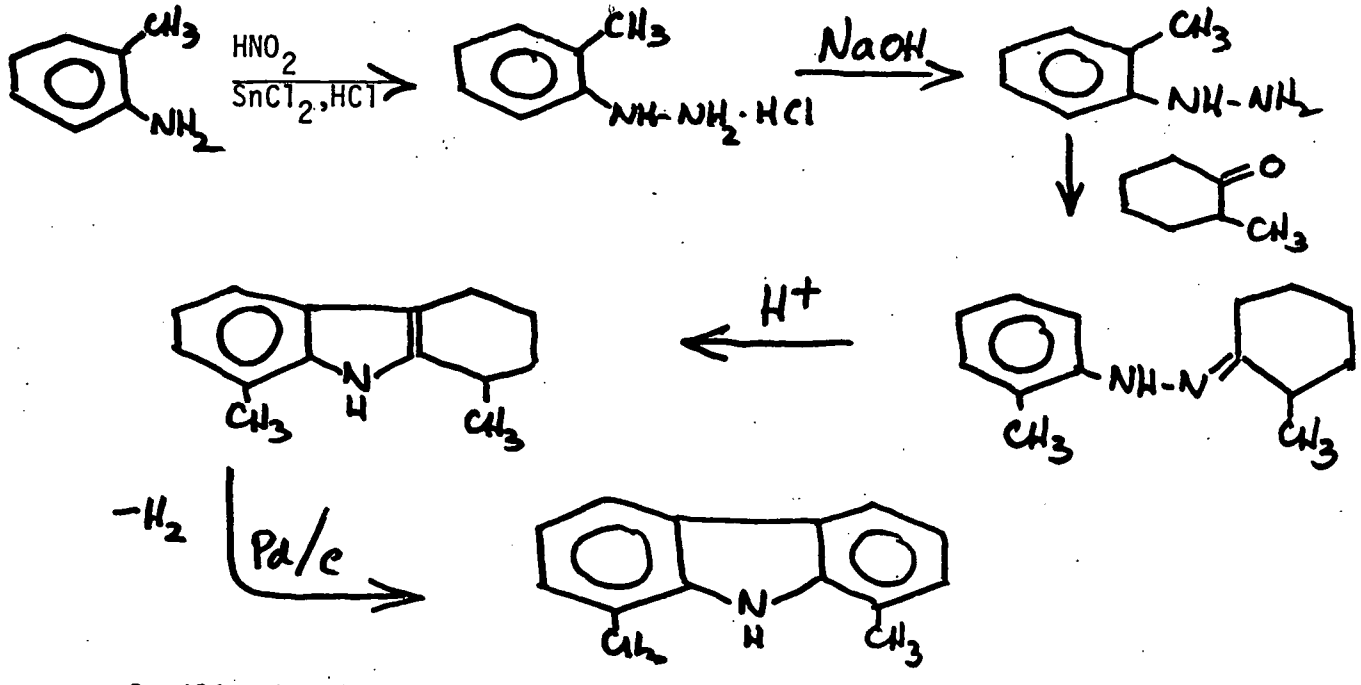

o-propylaniline has been prepared by nitration of n-propylbenzene and subsequent reduction of o-nitropropylbenzene

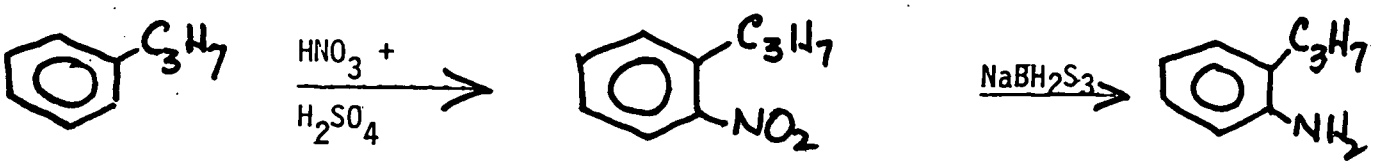

The preparation of 4,5-dimethylacridine has been undertaken by the following procedure (presently in progress).

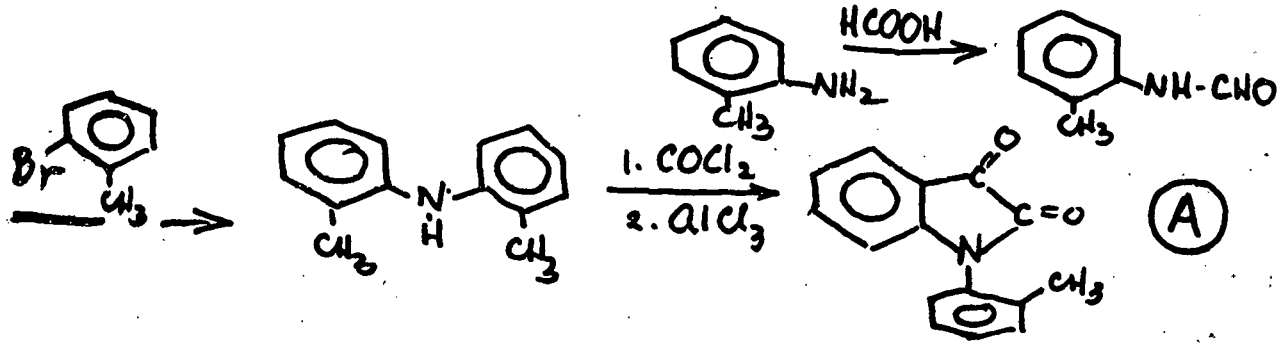

At this writing, the synthesis has progressed to the preparation of 1-o-tolyl-7-methylisatin.

The preparation of 2,8-Dimethylquinoline has been undertaken by the condensation of crotonaldehyde with o-toluidine

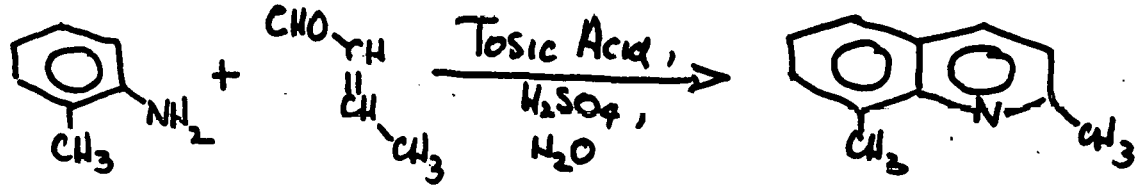

The crude product has already been isolated and purification is underway.

The synthesis of Decahydroquinoline and 5,6,7,8-Tetrahydroquinoline has been undertaken by the following method.

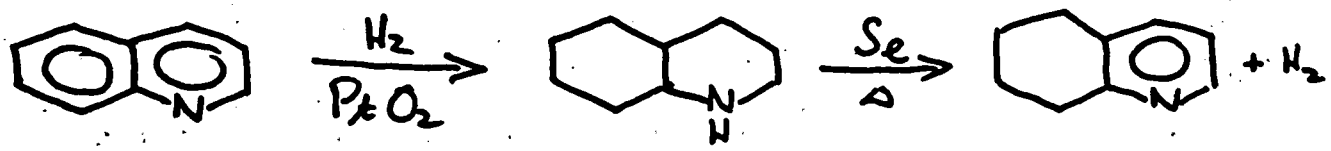

The crude decahydroquinoline has been isolated at this stage.

The preparation of 4-methylacridine was attempted by the following reaction sequences.

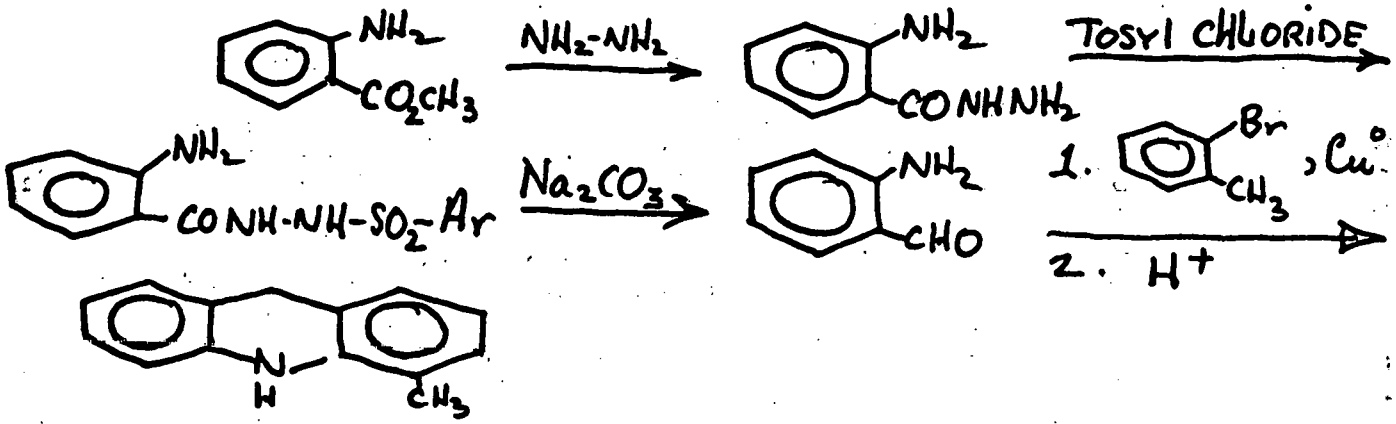

However, the yield of o-aminobenzaldehyde from the three step reactions was only about 10% and so an alternative procedure involving the reduction of o-nitrobenzaldehyde is scheduled for trial in the interests of obtaining an improved yield.

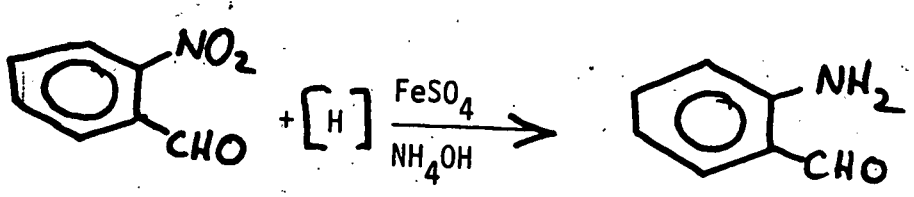

4. Research Plans for the Fifth Quarter

The future work for the next quarterly period for catalytic hydrodenitrogenation will emphasize hydrodenitrogenation of acridine, carbazole, quinoline and methyl substituted compounds. For acridine and carbazole the work will concentrate on identification of reaction products with mass spectroscopy and determination of the reaction network for hydrodenitrogenation. Work will also concentrate on determining the relative reactivity of carbazole, acridine and methyl-substituted species; reaction kinetics will then be studied on the less reactive species. All of these compounds and their methyl-substituted compounds will be studied in the autoclave reactor.

uinoline will be studied both in the autoclave reactor and the flow microreactor, and the steady-state kinetics and reaction network of quinoline hydrodenitrogenation will be obtained from the flow microreactor. In the autoclave reactor, quinoline will be studied in the wide range of temperature and kinetics of methyl substituted compounds will be examined. Besides kinetic study, the total material balance including hydrocarbons will be tested in the next quarterly period. The activity of support, and the kinetics of important intermediates for hydrodenitrogenation of quinoline also will be studied to further clarify the reaction mechanism of each step in the quinoline reaction network.

During the months of July and August, after completing the above mentioned incomplete synthesis, the following compounds will be prepared by the methods indicated.

1-Methylcarbazole:

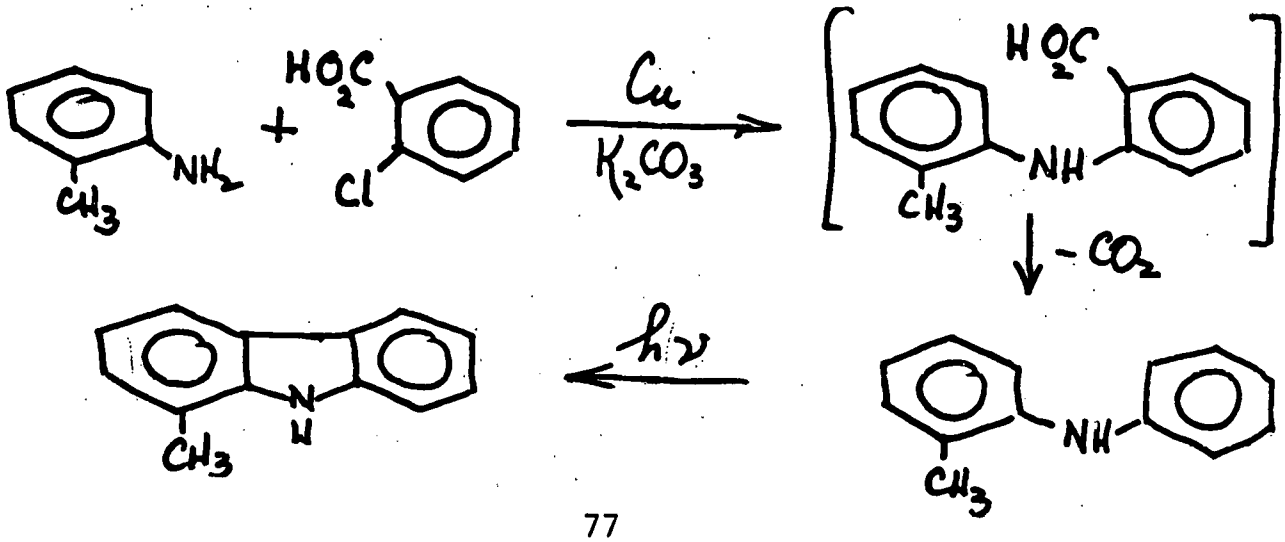

Similarly 2-methylquinoline, 3-methylquinoline, 8, methylquinoline and 2,8-dimethylquinoline will be synthesized. As the need appears for the synthesis of other nitrogen-containing reaction intermediates for the carbazole and acridine studies, these will be undertaken.

D. CATALYST DEACTIVATION

During this quarter the SEM-electron microprobe analysis of spent Synthoil catalyst has been continued. The sample was provided by Dr. Sayeed Akhtar of ERDA Bruceton and was taken from the front two inches of the entrance of the 1.1 in. ID pilot plant reactor at the conclusion of Run FB-53. The reactor ran for 24 days on Homestead Mine mixed Kentucky coal. The analysis of this coal is given in part in previous reports(Akhtar et al., 1975).

The operation of the 1.1 in. ID pilot plant is not equivalent to the 5/16 in. ID unit; in Run FB-53 there was a separate preheater ahead of the reactor. Consequently, the sample from Run FB-53 corresponds to the downstream sample previously described if the inert support in the preheater acts as a base for the deposition of coke and coal mineral matter.

The results of the investigation are shown on Figures 15-18. These figures show scanning electron micrographs (SEM) of fractured pellets which have been plasma etched, SEM plates of polished and plasma etched pellets, scanning electron microprobe plates for various elements present in coal mineral matter and electron microprobe concentration profiles of the mineral matter deposited near the external surface of the catalyst. The plates will be discussed in that order.

Figure 15 shows two views of a fractured pellet. The broken surface of 15a is in the lower left hand side of the plate, and the mineral matter deposits can be seen on the curved exterior surface of the catalyst. Obvious mineral matter deposits cover one-third of the surface. Figure 15b shows a zone of heavy deposition of mineral matter. The picture was taken at low angle to the surface to provide high contrast between the surface and the deposit.

Figure 16 shows additional views of the mineral matter crust formed externally to the catalyst. Energy dispersive X-ray analysis (EDAX) of these crusts is only qualitative

because the surfaces are rough. Nevertheless the titanium signal is unusually large and aluminum, silicon, sulfur, calcium and iron also appear. The composition of the crust is very heterogeneous and every element found in the traditional ash analysis is found in the crust.

Figure 17 shows two SEM (17 a and b) views of the crust along with the EDAX analysis. The crust found at the edge (b and d) of the fracture clearly is polycrystalline in which 5μ crystals are visible. On the other hand the somewhat different textured region 1 of Figure 17a contains FeS. The deposition of small amounts of FeS was found in the upstream sample described in the first progress report.

Figure 18 (which appears on two pages) is a series of SEM micrographs of polished cross sections of the catalyst exterior. Figures a and b show an agglomeration of coal mineral matter cemented to the surface of the Synthoil catalyst. The various regions have nearly the same EDAX analysis (region "1" was expected to be quite unlike single crystal regions 2, 3 and 4); the EDAX output is nearly identical to that for Figure 19 c. The crust shown on Figure 19 appears to have been formed from the clay mineral matter in the coal.

Figure 18c and d are two magnifications of the same cross section of an external deposit. The cross section suggests the deposition of the clay by cementing; the region appears to be produced by a backflow eddy. Since the catalyst particles were relatively clean, the deposit probably is not an artifact of the method for cooling down the reactor. Although the turbulence in the Synthoil reactor is high, mineral matter still can cement to the surface.

Figure 19 shows a few regions in which distinctly different mineral forms were found. Region 2 and 2' of Figure 19 a appear to be an agglomeration of cemented clay represented by EDAX 19c. Region 1 of Figure 19a is a mixture of CaS and some TiO_2. The calcium sulfide probably was formed from the reaction $CaCO_3$ with H_2S in the reducing environment. This reaction yields much larger crystals than are found in the coal. Regions 1 and 2 of Figure 19 d appear to be TiO_2 polycrystalline deposits while region 3 of Figure 19 d contains more clay. Taken as a whole Figures 18 and 19 show

that nonreactive coal mineral matter is cemented on the surface and that some reduction of mineral matter yields patches of external crystalline growth. These deposits obviously reduce the efficiency of the catalyst.

Figure 20 is a series of electron microprobe scans of a polished cross section. In these scans, unlike those in the previous report, regions of high concentration of an element appear white. Plates 20 a and b show the region of this investigation at low magnification with optical and electron image recording. Although the resolution of the electron microprobe is not quite as good as the SEM pictures, the polycrystalline nature of the deposits is quite clear. The distribution of the various elements is shown in the scans 20 d-m, and the electron image, 20c, shows that the deposit has formed in a small interstitial zone between two catalyst pellets. The separate element micrographs suggest the following:

20d Aluminum appears in highest concentration in the catalyst support which has a number of large cracks. The external coating contains a lower concentration of aluminum which is uniformly distributed in the solid portions of the coating. The exception is the circular ("fisheye") region at the upper right of the plate. The fisheye is primarily SiO_2.

20e Silicon appears in the catalyst support as a stabilizer. In addition there are zones of higher concentration of silicon in the catalyst where clay mineral matter appears to have penetrated into the catalyst along cracks. The external coating has the highest concentration of silicon in the aforementioned fisheye. Silicon also appears in the external coating at a level between the fisheye and the catalyst support. There are several distinct grains which are approximately rectangular with a linear dimension of 2-6 μm. These grains probably are SiO_2.

20f Titanium is found in high concentration in Kentucky coal, and the SEM-EDAX studies yielded large titanium signals. This plate shows that the titanium is deposited fairly uniformly in the external crust where the Al and Si signals are large. In addition titanium decorates the cracks of the catalyst near the surface. Titanium is found as rutile in Kentucky coal and also is found in the CH organic fraction. Titanium appears to be deposited on the catalyst from both of these sources.

20g Oxygen does not yield a large signal in X-ray fluorescence detection, and the oxygen level in the catalyst is uniform. The dark zones are potting compound.

20h Carbon is a major constituent of the potting polymer. Nevertheless there is a significant carbon concentration on the catalyst.

20i and j Sulfur and iron are found together as small crystals (3-5 μm) distributed throughout the external crust of the catalyst. The sulfided catalyst also has a moderate concentration of sulfur in the catalyst. The uneven zones of high concentration of sulfur in the catalyst correlate with zones of high molybdenum concentration.

20 k Molybdenum is the major catalytically active material and is found distributed throughout the catalyst. In addition there is a small amount of molybdenum distributed throughout the external deposit.

20l Calcium is present in coal as $CaCO_3$. The carbonate is quite reactive under reaction conditions. The general penetration of calcium throughout the external layer and into the cracks of the catalyst stems from this reactivity.

20m The cobalt distribution correlates quite closely with the molybdenum signal. Cobalt apparently migrates to the surface of the cracks inside the catalyst. The migration of Co and Mo has been seen in all of the samples and therefore appears to be general.

The electron microprobe was also used to obtain concentration contours of a series of elements near the external surface of the catalyst. The microprobe beam was focused to 0.5 μm diameter and this beam was swept over a 100 μm line parallel to the tangent of the sphere. The line was mechanically driven over a 800 μm span near the surface of the catalyst. The signal is approximately proportional to the concentration of the element in this zone. The magnitude of the signal was adjusted to maximum sensitivity or to a gain which scaled the maximum signal to the maximum response of the recorder.

The aluminum signal identifies the edge of the original catalyst and shows further the attachment of a substantial quantity of aluminum from the clays in coal mineral matter.

The cobalt and molybdenum signals show large noise in the interior of the catalyst. This noise probably is caused by the low signal level (shot noise) for Co-Mo in the catalyst. The diffusion of Co and Mo into the external layer is minimal. The titanium peak is nearly entirely outside of the catalyst; this profile shows that the crust contains rutile and relatively little organo titanium. The silicon signal shows the deposition of clays on the surface in addition to the migration of some silicon down cracks in the catalyst.

The calcium signal shows substantial penetration into the interior of the catalyst. The most prevalent form of calcium in coal is $CaCO_3$ which can be reduced to CaS. The reduced CaS apparently can penetrate into the catalyst skin.

The iron and sulfur peaks show a near perfect correlation in the external layer; previous work indicates the formation of $FeS_{1.1}$. There is a small penetration of iron into the catalyst interior. The sulfided catalyst yields a signal in the interior which is greater than that from the FeS_x in the crust. Comparison of this response with previous work shows that the laydown of FeS_x is much reduced in the FB-53 run.

Taken as a whole these studies of the Synthoil catalyst show that the turbulence of the system does not provide enough shear to prevent coal mineral matter from cementing to the surface of the catalyst. The laydown of FeS is reduced substantially from the heavy crust observed on the upstream catalyst of the 5/16 inch ID reactor. Therefore, the FeS laydown is sensitive to temperature (the current reactor is expected to have a higher inlet temperature than the previous unit) and/or the FeS laydown occurs in the preheater. The data suggest severe and immediate pore mouth blockage of the catalyst.

Plans for Future Work

This task is limited currently by the availability of catalyst samples. Verbal promises of additional catalyst have been given by three outside laboratories. The next major task is to burn off the carbon on the catalyst and test for recovered activity. The outline for this work is as follows:

1. Extract tar and solvent from the catalyst with benzene
2. Determine the pore size distribution
    a. crushed
    b. uncrushed
3. Microactivity test of unregenerated catalyst
4. Controlled burn off of carbon
5. Pore size distribution measurement
6. Microreactivity test of regenerated catalyst
7. Comparison of these activities to fresh catalyst.

The catalysts will be sulfided before microreactivity tests.

Figure 15
Fractured Pellets
Overview

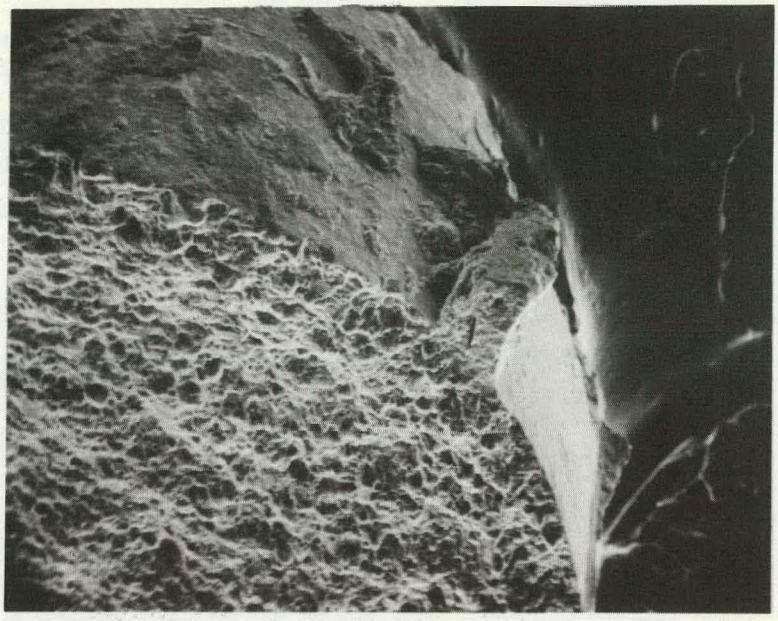

50X

a.

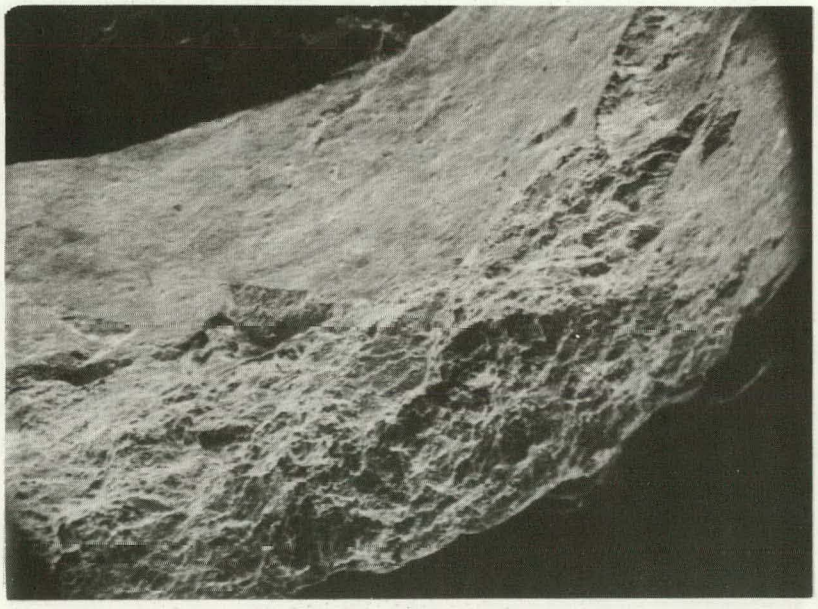

100X

b.

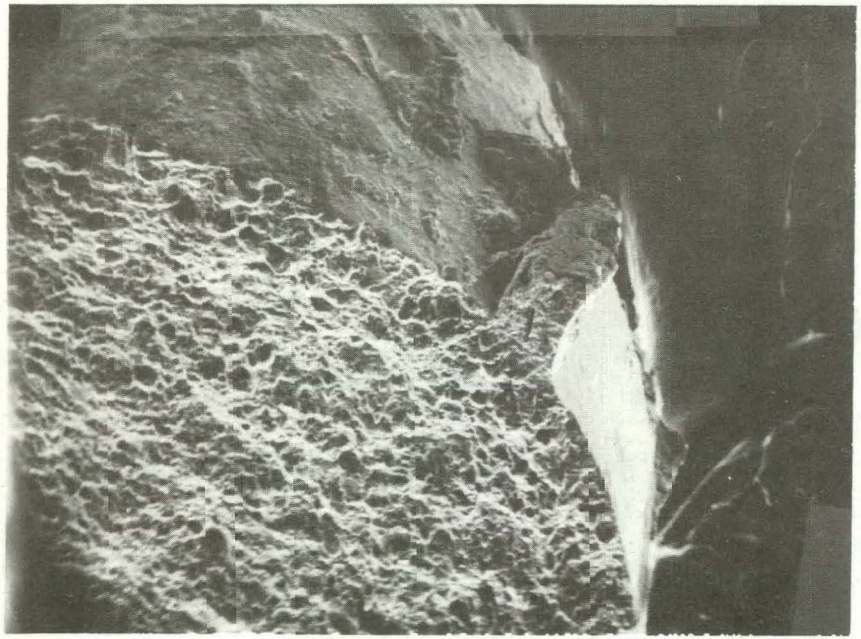

a. SEM at 50X

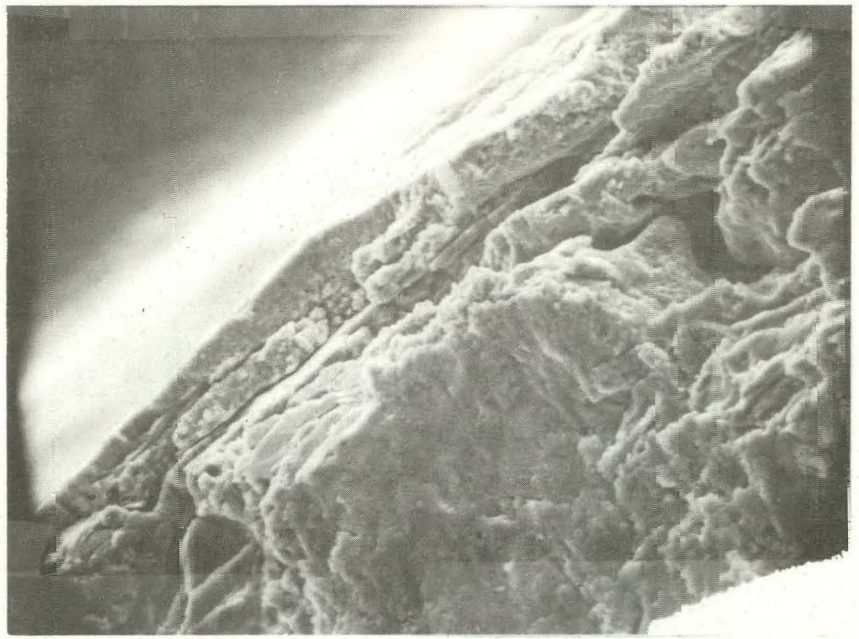

b. SEM at 500X

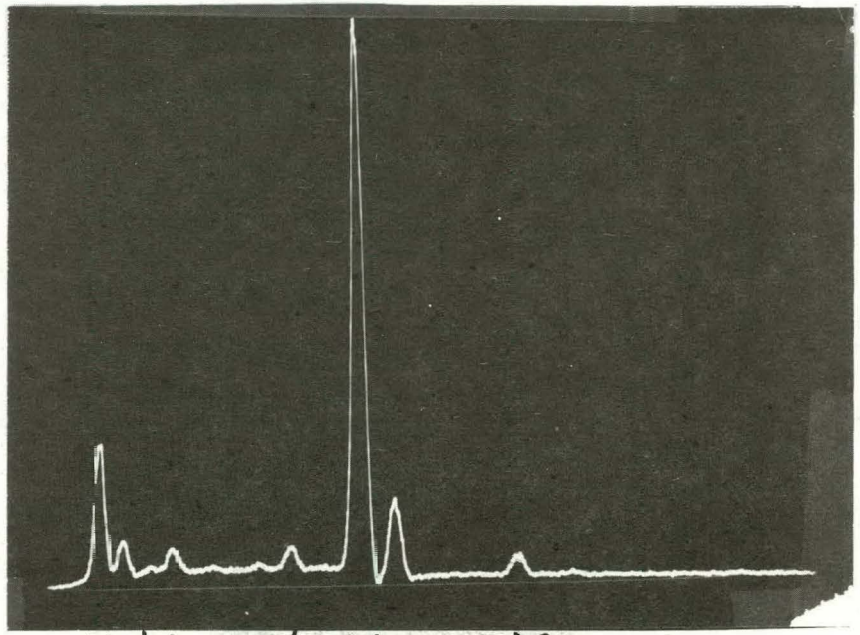

EDAX at 1,2 and 3

Figure 16 New Fractured Pellets

a. SEM at 100X

b. SEM at 3 2000X

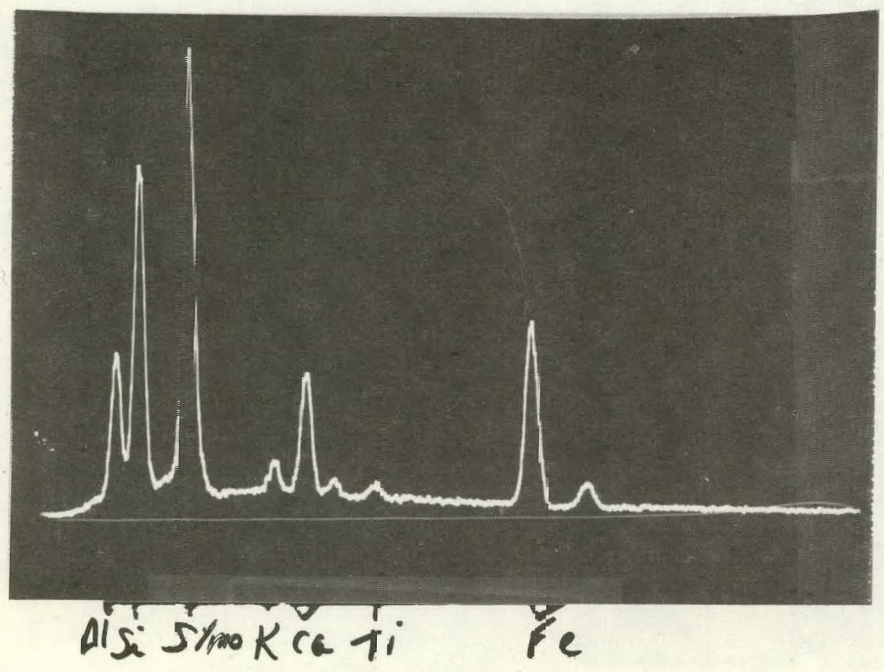

c. EDAX at 1

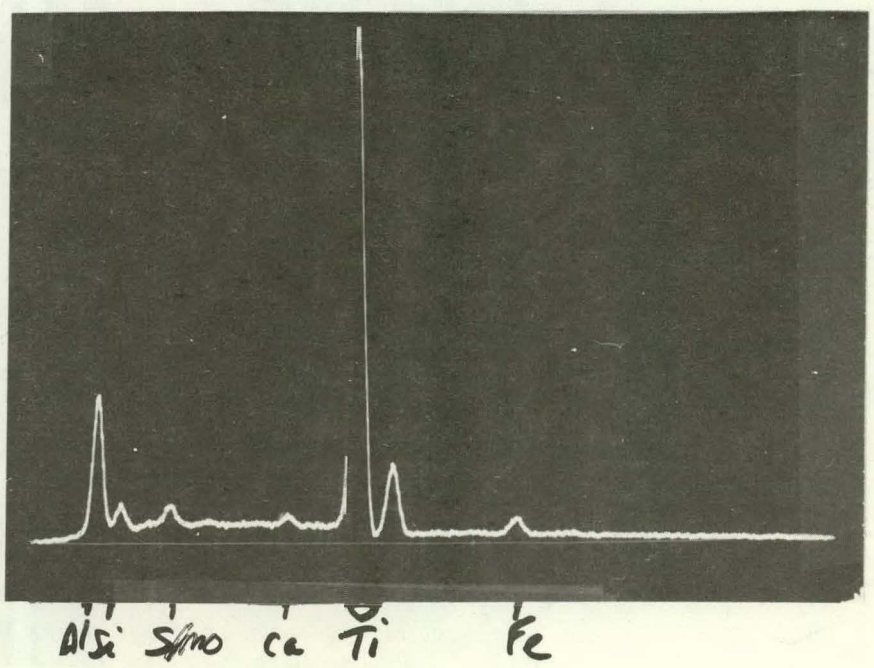

d. EDAX at 2

Figure 17 Fractured Pellets Mounted

Figure 18

Polished Cross Sections

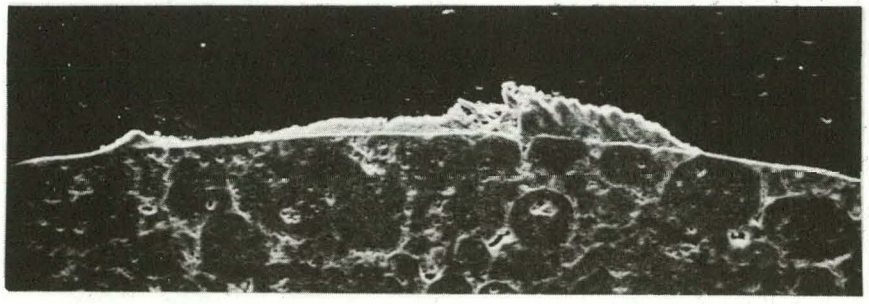

a.

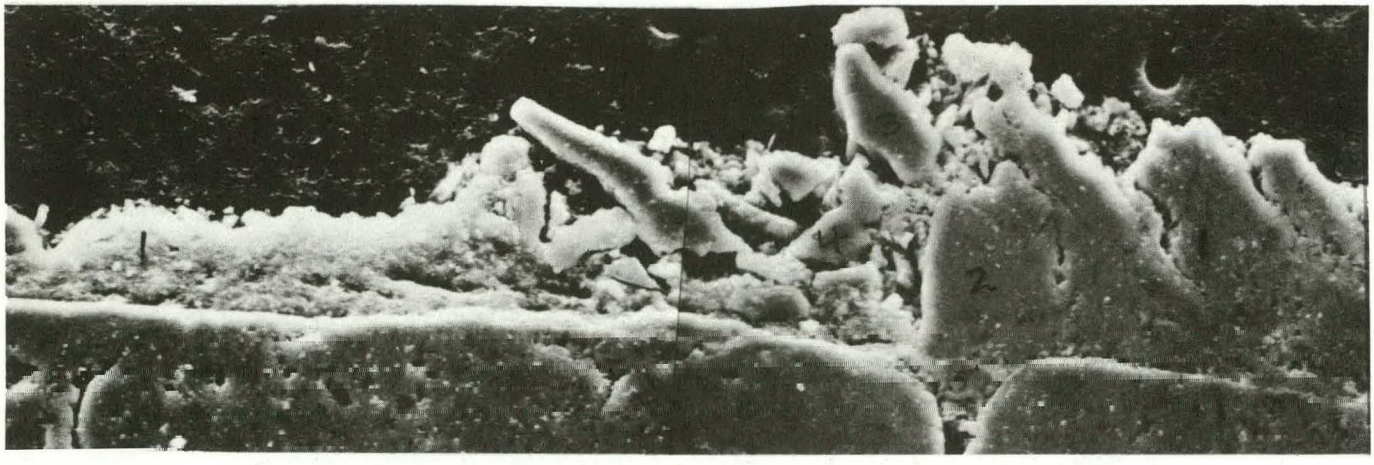

b.

10μ

Figure 18 cont'd

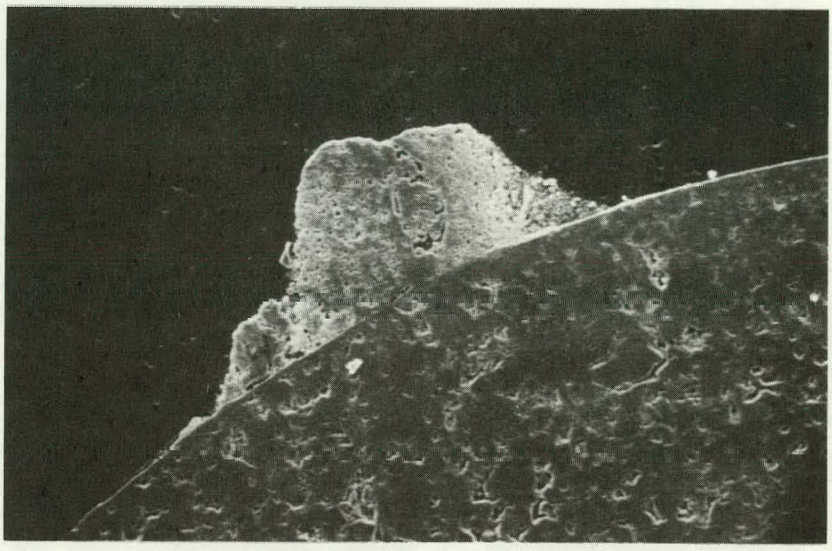

c.

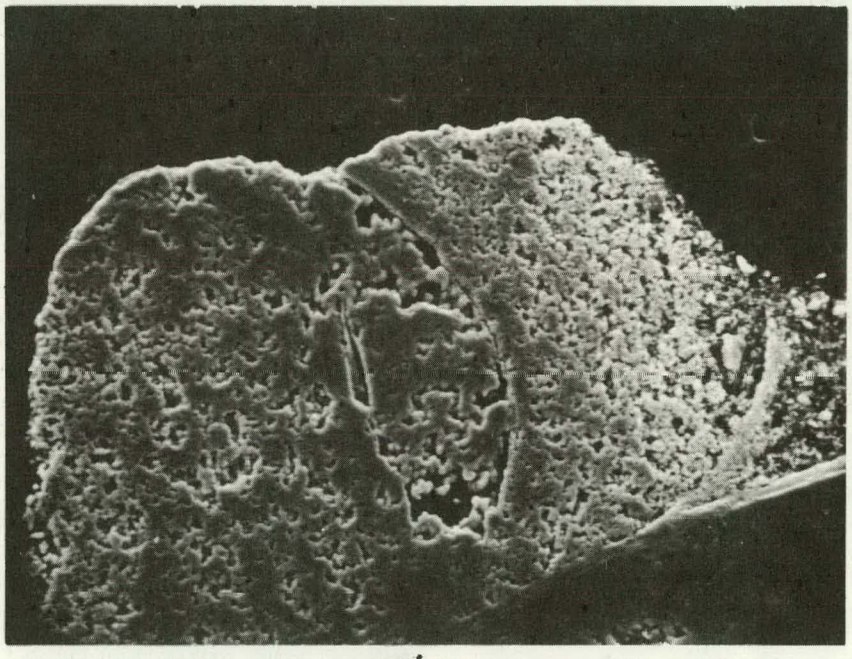

d.

50 μ

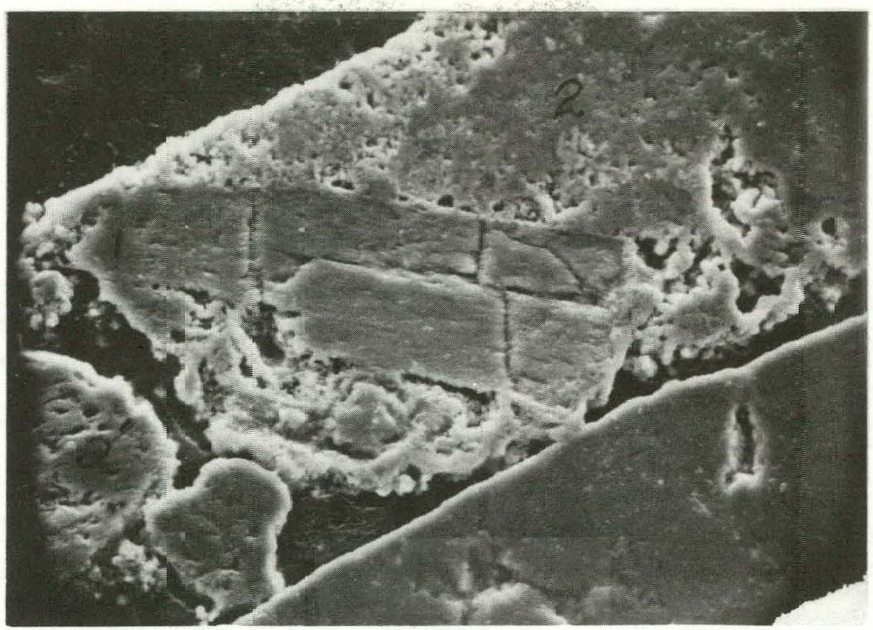

a. SEM at 1000X

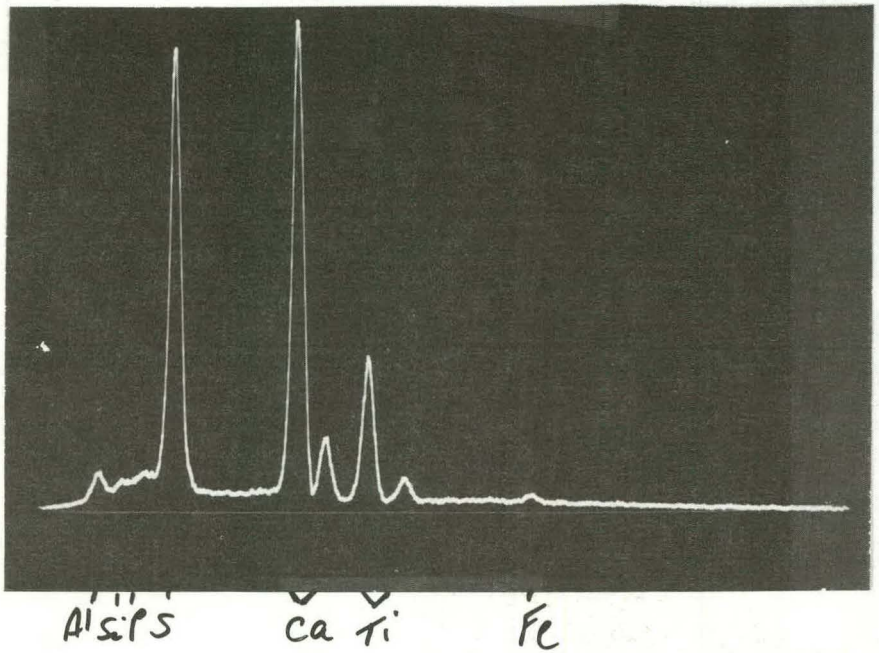

b. EDAX at 1

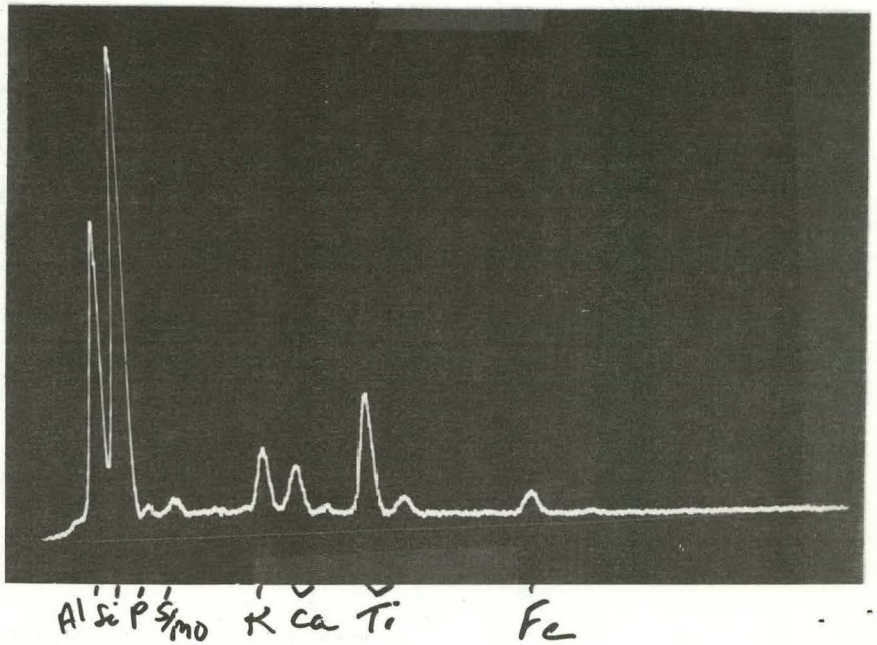

c. EDAX at 2

Figure 19 Polished Cross Sections

d. SEM at 2000X

e. EDAX at 1 and 2

f. EDAX at 3

Figure 19 cont'd Polished Cross Sections

Figure 20 Electron Microprobe Scans

Sample: FB-53 (Inlet)

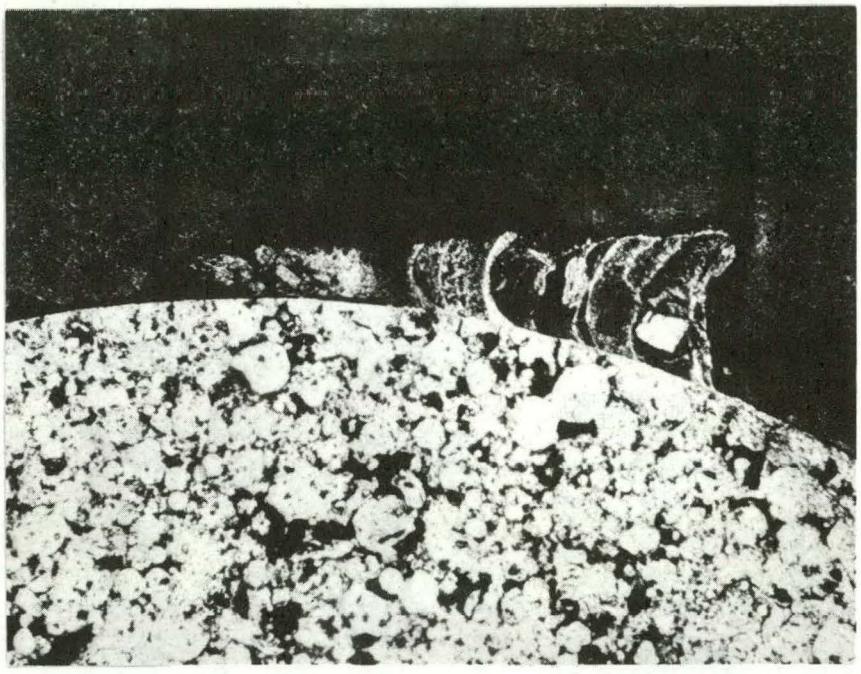

a. Optical Micrograph 100X

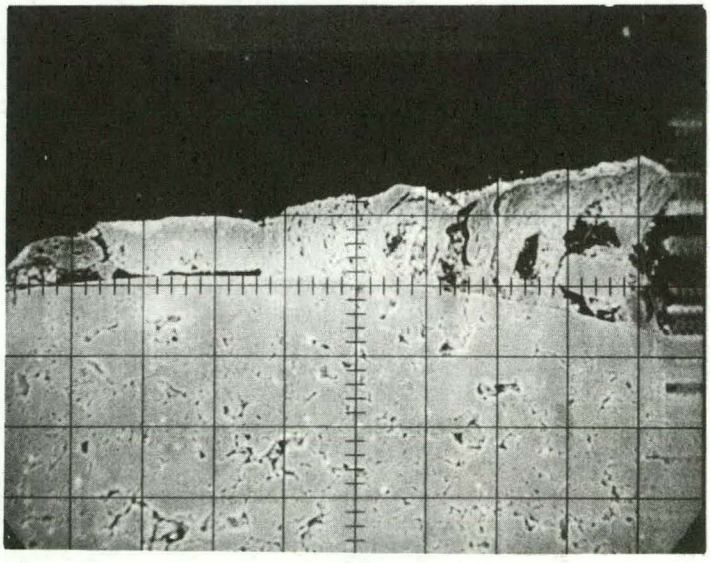

b. Electron Image ~110X

Figure 20 continued

Sample: FB-5[3] (Inlet)

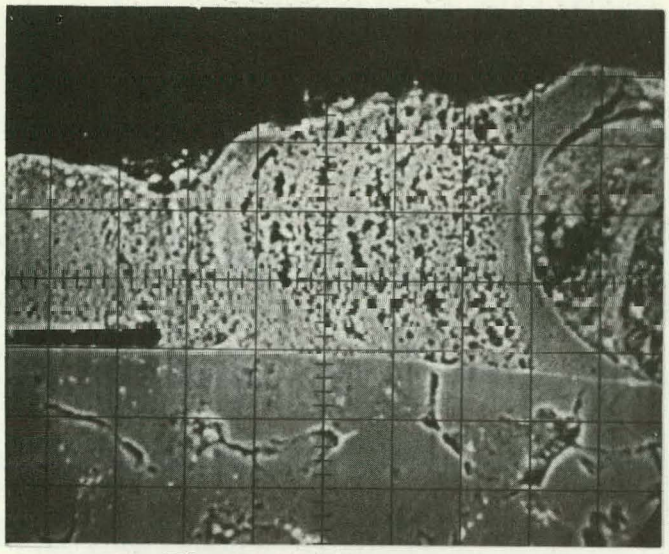

c. Electron Image

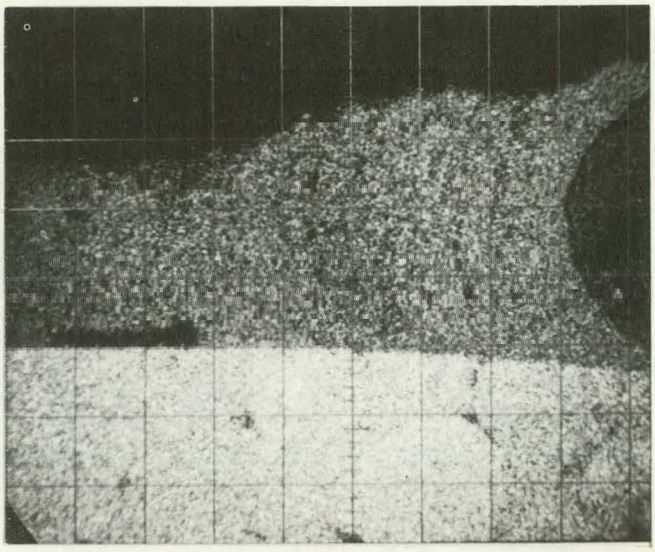

d. Al X-ray Image

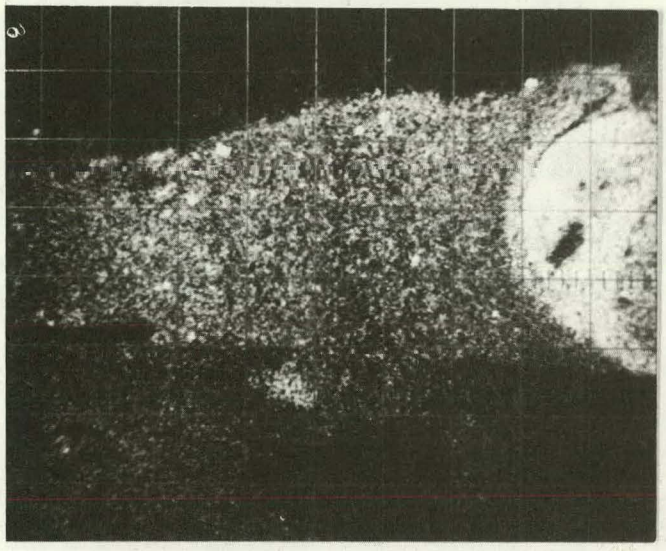

e. Si X-ray Image

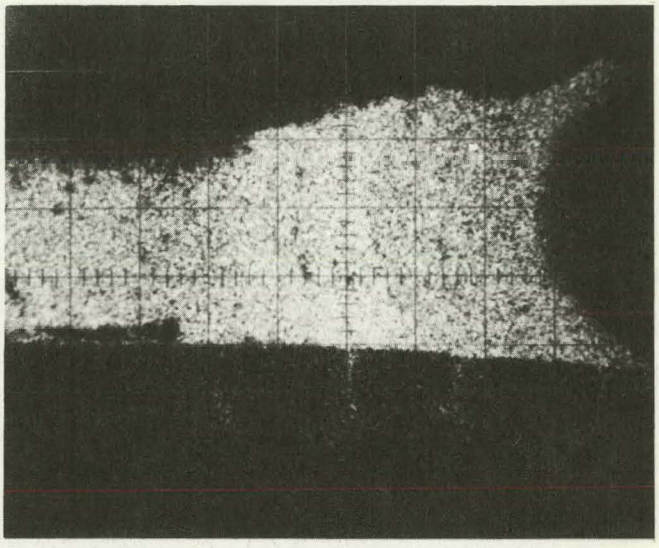

f. Ti X-ray Image

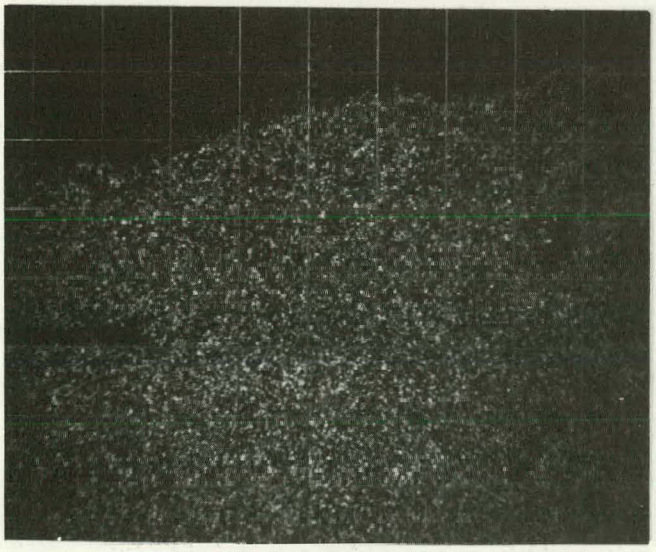

g. O X-ray Image

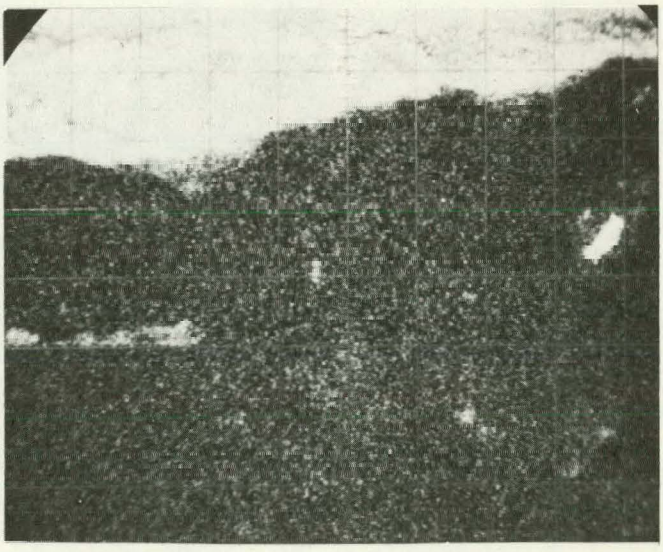

h. C X-ray Image

Magnification 333X

Figure 20 continued

Sample: FB-5[3] (Inlet)

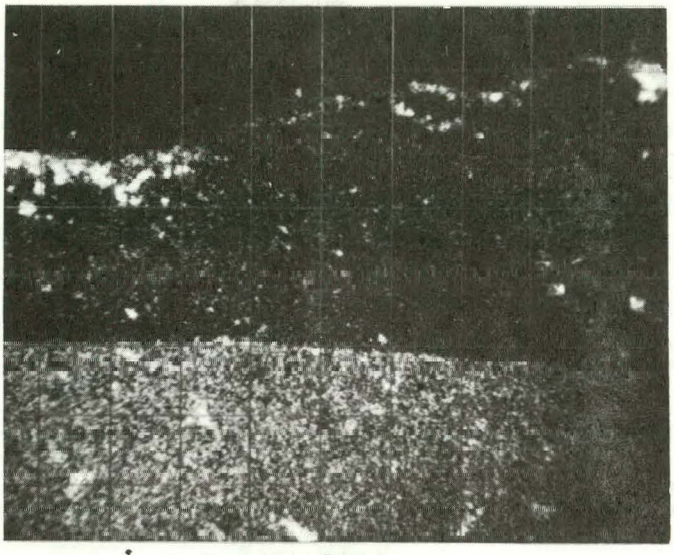

i. S X-ray Image

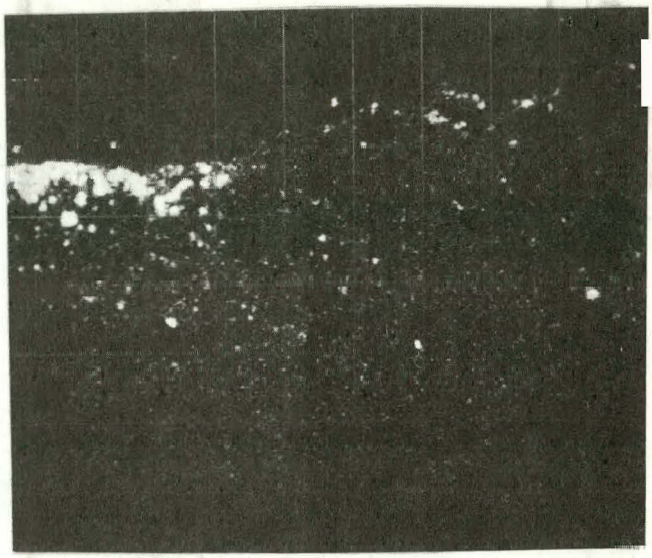

j. Fe X-ray Image

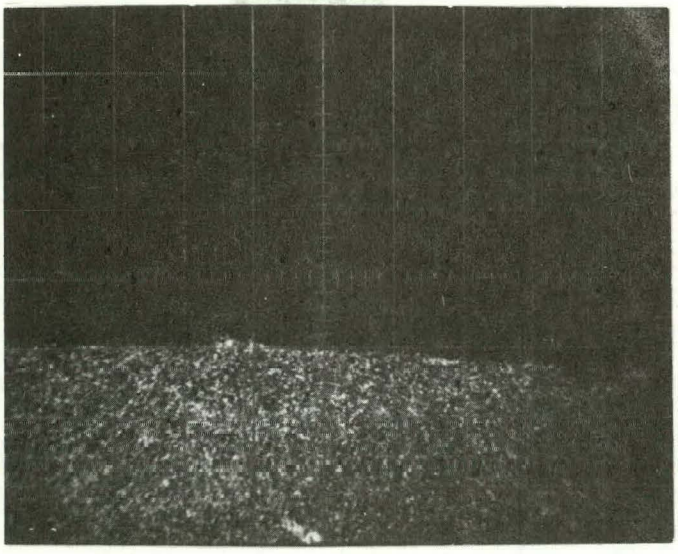

k. Mo X-ray Image

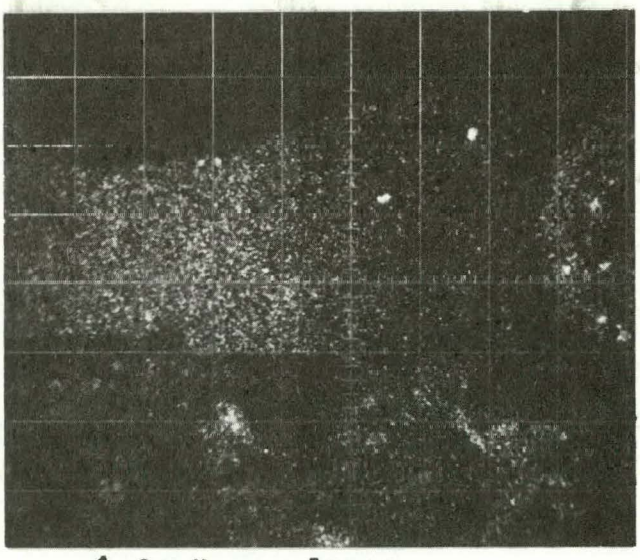

l. Ca X-ray Image

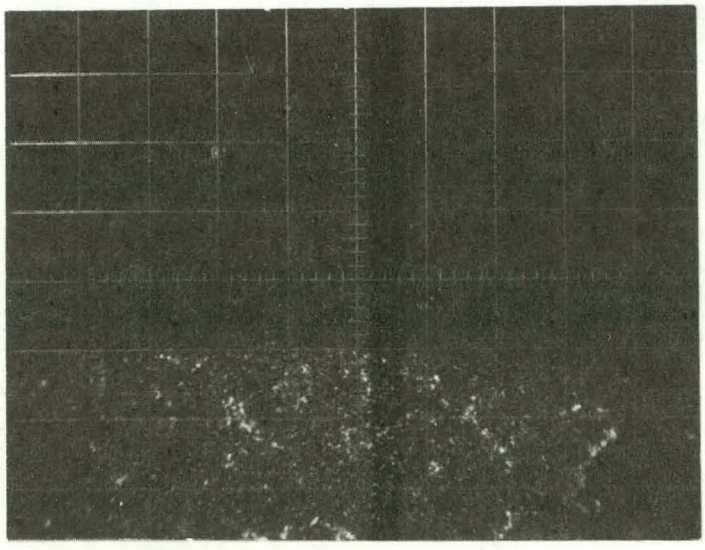

m. Co X-ray Image

Magnification 333X

Figure 21

Microprobe Profiles

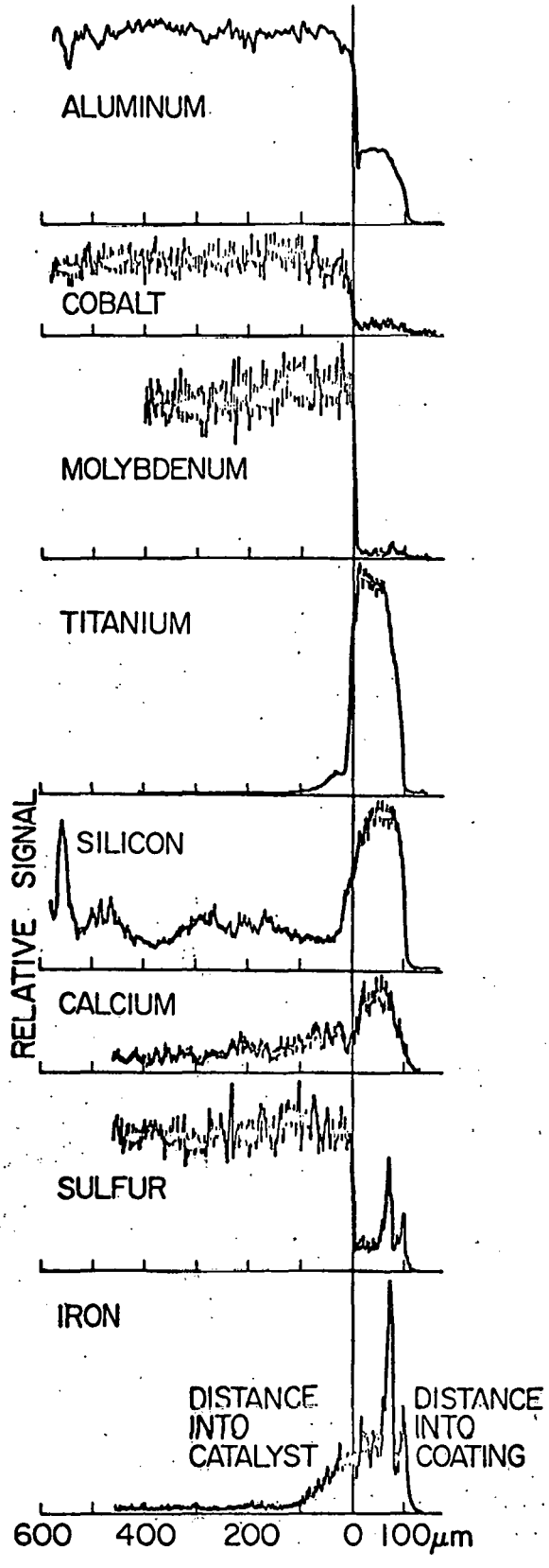

E. HYDROPROCESSING REACTION ENGINEERING

1. Pulse Microreactor Engineering

a. Film model

This report reviews and extends the model for a pulse passing through a microreactor. The purpose of this analysis is to discover the parameters which delay and change the shape of the pulse. Figure 22 shows a block diagram of a microreactor equipped with detectors before and after the microreactor. These detectors are used to signal the beginning and the end of the reaction and to provide for injection of the reaction products into the gas chromatograph. The pulses also contain information on the behavior of the pulse in the reactor. The function of this report is to demonstrate how the properties of the input and output pulses are related to a fairly simple model.

The approach used in the development is to consider a prototype reaction system in which a single reactant is converted into a single product by first-order reaction kinetics. The amount of reactant and product which remain can be measured with a gas chromatograph. The microreactor is operated with a small quantity of catalyst, and consequently there is no chromatographic separation of the reactant and the product. (More precisely, the separation of the reactant and product cannot be observed directly.) Therefore the two detectors shown on Figure 22 measure the pulse behavior of a mixture of reactant and product.

The analysis proceeds by developing a component material balance and a rate equation for the two components in the mixture seen by the detector. These equations are converted into moment equations by the Laplace transform. The differences in the moments of the pulses seen by detectors 1 and 2 of Figure 22 then are related to the basic parameters of the system.

A material balance on the fluid phase of a microreactor yields the partial differential equation

$$\mathcal{D}_{ax}\,\epsilon_g\,\frac{\partial^2 c}{\partial z^2} = v_i\,\epsilon_g\,\frac{\partial c}{\partial z} + \epsilon_g\,\frac{\partial c}{\partial t} + k_g\,a_s\,\epsilon_s\,(c - c_i) \qquad (5.1)$$

Figure 22

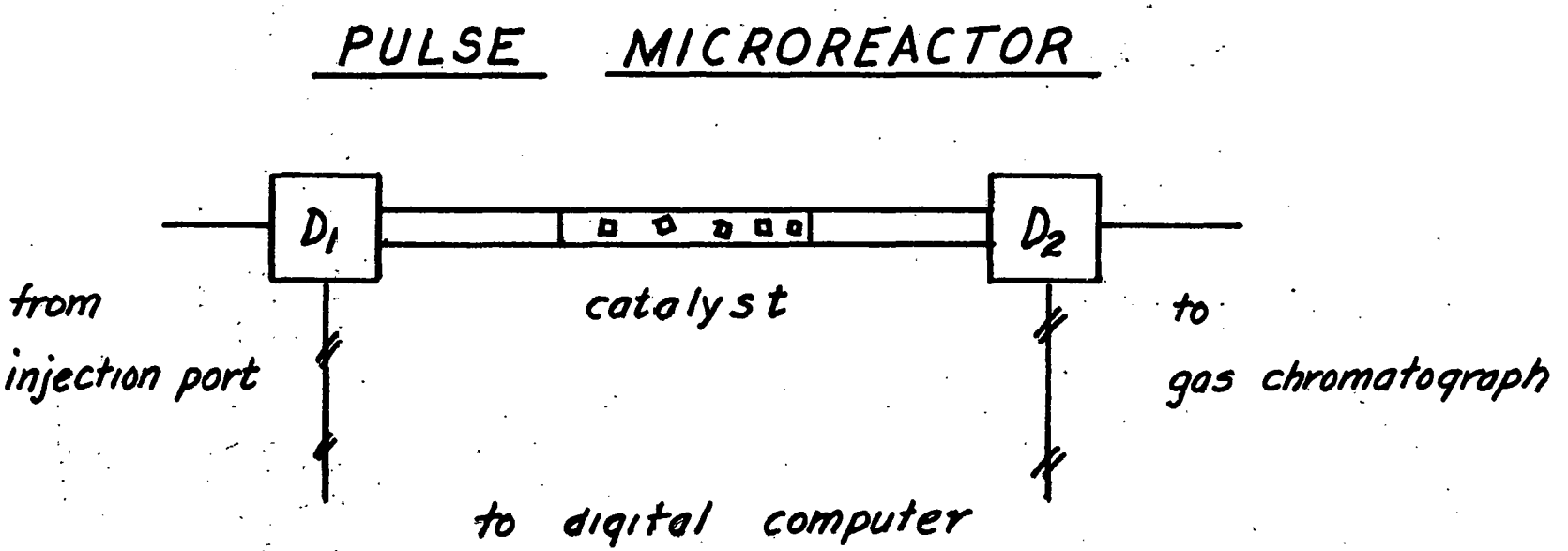
PULSE MICROREACTOR
D1
D2
from
injection port
catalyst
to
gas chromatograph
to digital computer
Reactants and products
do not separate

The first term in Eq. 5.1 denotes component transport by axial dispersion (deviations from piston flow); experimentally this term is found to be small. The second term represents convection, the third accumulation in the gas phase and the fourth represents mass transfer from the fluid phase to the catalyst surface. Using the notation given at the end of this section, eqn. 5.1 transforms to

$$B\frac{\partial^2 \mathbb{C}}{\partial Z^2} = \frac{\partial \mathbb{C}}{\partial Z} + \frac{\partial \mathbb{C}}{\partial T} + F\Lambda(\mathbb{C} - \mathbb{C}_i) \qquad (5.2)$$

The chemical reaction occurs in the catalyst phase. In this development the transient adsorption coupled with reaction is written in terms of the average concentration in the solid phase by use of a solid phase film coefficient. This approach is useful when the reaction rate is slow to moderate; an alternative view will be developed later. The solid phase material balance equation then is

$$\frac{\partial q}{\partial t} = k_s a_s (q_i - q) - k_r q \qquad (5.3)$$

which in dimensionless terms yields

$$\frac{\partial Q}{\partial T} = S(Q_i - Q) - KQ \qquad (5.4)$$

The continuity of flux across the gas film surrounding the catalyst particle yields the relation

$$F(\mathbb{C} - \mathbb{C}_i) = SE(Q_i - Q) = R(\mathbb{C} - Q) \qquad (5.5)$$

where R, the total number of transfer units is given as

$$R^{-1} = F^{-1} + (SE)^{-1} \qquad (5.6)$$

The overall component material balance for the reactant in the microreactor is found by combining eqns. 5.3, 5.4 and 5.5 to yield

$$B\frac{\partial^2 \mathbb{C}}{\partial Z^2} = \frac{\partial \mathbb{C}}{\partial Z} + \frac{\partial \mathbb{C}}{\partial T} + \Lambda E\frac{\partial Q}{\partial T} + \Lambda E K Q \qquad (5.7)$$

Experimentally the magnitude of the inverse Bodenstein number is small enough that this term can be neglected in the preliminary model development. Consequently the boundary conditions on the equation set are

$$C(0,T) = \delta(T) \qquad \text{Dirac forcing function} \qquad (5.8a)$$

$$C(Z,0) = 0 \qquad (5.8b)$$

$$Q(Z,0) = 0 \qquad (5.8c)$$

The solution of this equation set is found by taking the Laplace transform. The Laplace transformed equation is

$$\frac{d\bar{C}}{dZ} + (s + g_1(s))\,\bar{C} = 0 \qquad (5.8)$$

where

$$g_1 = ER\Lambda\,\frac{s+K}{Es+R+KE}$$

s = Laplace transform variable

the solution of this equation is

$$\bar{C} = e^{-(s+g_1)Z} \qquad (5.9)$$

The moments of concern are the zeroth and first moments about the origin and the second (central) moment about the mean. These moments are found as

$$m_0 = \lim_{s\to 0} \bar{C}(1) \qquad (5.10a)$$

$$m_1 = 1 + \lim_{s\to 0} \frac{d}{ds} g_1(s) \qquad (5.10b)$$

$$m_2 = \lim_{s\to 0} -\frac{d^2}{ds^2} g_1(s) \qquad (5.10c)$$

The moments then are found by tedious application of the chain rule. The zeroth moment is equivalent to the fraction of the reactant remaining. This fraction is

$$m_0 = e^{-r}$$

$$r = EK\Lambda\eta_g$$

$$\eta_g = \left(1 + \frac{EK}{F} + \frac{K}{5}\right)^{-1} \tag{5.11}$$

The zeroth moment is measured from the chromatographic analysis of the reaction pulse.

The first moment for the reactant alone is

$$m_1 = 1 + E\Lambda\eta_g^2$$

This moment can be observed when the extent of reaction is very small. In addition this moment is identical to the form of Susuki and Smith (1971) when the film model is transformed into the model form used by these authors.

The mean takes on a simple interpretation. The mean is the ratio of the holding time of an unadsorbed pulse in the reactor to a pulse with substantial adsorption. The parameter Λ is the volume ratio of active adsorbant to inert fluid space, and the parameter E is the ratio of the equilibrium adsorption in the catalyst to the gas phase concentration.

Similarly, the second central moment about the mean is found to be

$$m_2 = \frac{2E^2\Lambda\eta_g^3}{R} \tag{5.12}$$

This moment describes the spreading of the pulse caused by finite rate of mass transport in the catalyst. The second moment also is increased by axial dispersion, but the contribution of axial dispersion is not significant in the experiments considered thus far.

The product formed by the reaction is represented by two partial differential equations

$$\frac{\partial C^P}{\partial Z} + \frac{\partial C^P}{\partial T} + R_p\Lambda\left(C^P - Q^P\right) = 0 \tag{5.13a}$$

$$E_p \frac{\partial Q^p}{\partial T} = R_p (C^p - Q^p) + KEQ \qquad (5.13b)$$

with the boundary conditions

$$C^p(0,T) = 0 \qquad \text{no product in feed} \qquad (5.13c)$$

$$C^p(z,0) = 0 \qquad \text{reactor initially empty of product} \qquad (5.13d)$$

$$Q^p(z,0) = 0 \qquad (5.13e)$$

The algebra of the Laplace transform is tedious, but in compact form the solution to eqn. 5.13 is

$$C^p = P(e^{-Hz} - e^{-Gz})$$

where
$$P = (1 + a_1 s + a_2 s^2)^{-1}$$
$$a_1 = (E - E_p)/(KE) + K a_2$$
$$a_2 = E_p (R_p^{-1} - R^{-1})/K$$
$$H = s + E_p R_p \Lambda s / (s E_p + R_p)$$
$$G = s + E R \Lambda (s + K) / (s E + R + KE)$$

The moments for the product are listed in Table XV. Since the moments for particular components beyond the zeroth cannot be observed, these moments are used to compute the combination of the reactant and product (or total) moments. The results are

$$m_0^T = 1 \qquad (5.14a)$$

$$m_1^T = a_1 m_0^P + 1 + E_p \Delta \qquad (5.14b)$$

$$m_2^T = \frac{2\Lambda E_p^2}{R_p} + a_1^2 (1 + m_0)(1 - m_0) + 2a_1 (E_p - E\eta_g^2) m_0 - 2a_2 m_0^P \qquad (5.14c)$$

where $m_0^P = 1 - m_0$

TABLE XV.

MOMENTS OF THE FILM MODEL

	Reactant	Product	Total
Zeroth Moment	$m_0 = e^{-\tau}$	$m_0^P = 1 - e^{-\tau}$	$m_0^T = 1$
First absolute moment (normalized)	$m_1 = 1 + E\Lambda\eta_q^2$	$m_1^P = a_1 - \frac{m_0 m_1}{m_0^P} + \frac{b_1}{m_0^P}$	$m_1^T = b_1 + a_1 m_0^P$
Second central moment (normalized	$m_2 = \frac{2E^2\Lambda\eta_q^3}{R}$	$m_2^P = a_1^2 - 2a_2 - \frac{m_0 m_2}{m_0^P} - 2\left(\frac{m_0}{m_0^P}\right)^2 m_1 b_1 - \frac{m_0}{(m_0^P)^2}(m_1 + b_1)^2$	$m_2^T = \frac{2E_P^2\Lambda}{R_P} + a_1^2(1-m_0)(1+m_0) + 2a_1\Lambda(E_P - E\eta_q^2)m_0 - 2a_2(1-m_0)$

Definitions:

$$\tau = KE\Lambda\eta_q$$

$$\eta_q = \left(1 + \frac{KE}{R}\right)^{-1}$$

$$a_1 = \frac{E - E_P}{KE} + Ka_2$$

$$a_2 = \frac{E_P}{K}\left(\frac{1}{R_P} - \frac{1}{R}\right)$$

$$b_1 = 1 + E_P\Lambda$$

The zeroth moment for the total pulse is independent of the reaction rate parameter; this result is equivalent to the conservation of mass. The first moment ranges from the pure adsorption value for the reactant to the pure adsorption value of the product as the reaction rate ranges from zero to infinity. Similarly the second central moment ranges from reactant-dominated to product-dominated values with variation in the reaction rate.

To illustrate this point two sets of graphs have been prepared; these two sets illustrate low and moderate values of the transport parameters. The film model for the reaction rate approaches pure adsorption for low values of the reaction rate group, and the first and second normalized moments then are equivalent to pure adsorption. On the other hand at large values of the reaction rate parameter the zeroth moment for the reactant approaches

$$m_0 = e^{-\Lambda R}$$

which means that the probability of a molecule reacting is limited by the rate of mass transfer to the surface. This simple understanding may require revision when alternate models for transport are considered.

Figures 23-26 show the behavior of all of the moments of interest as a function of the reaction rate group K. Figure 23 shows that the maximum value of the product zeroth moment, m_0^P, is reached when K is ten or greater. Correspondingly the fraction of product remaining falls to the transport limit, $e^{-0.1} = 0.905$. The first moment for the total signal (Figure 24), m_1^T, is the sum of the unnormalized first moments of the reactant and product; the first moment is not a strong function of the extent of reaction. Consequently the first moment can be used to find an estimate of the adsorption of reactant upon the catalyst surface. The second moment about the origin (Figure 25) similarly is found to be a simple summation of the product and reactant second moments. Finally the second moment about the origin, displayed on Figure 26, shows that m_2^T makes a significant transition over a relatively narrow range of the reaction rate group. These calculations show that the second central moment can be used to obtain estimates of transport parameters under reaction conditions.

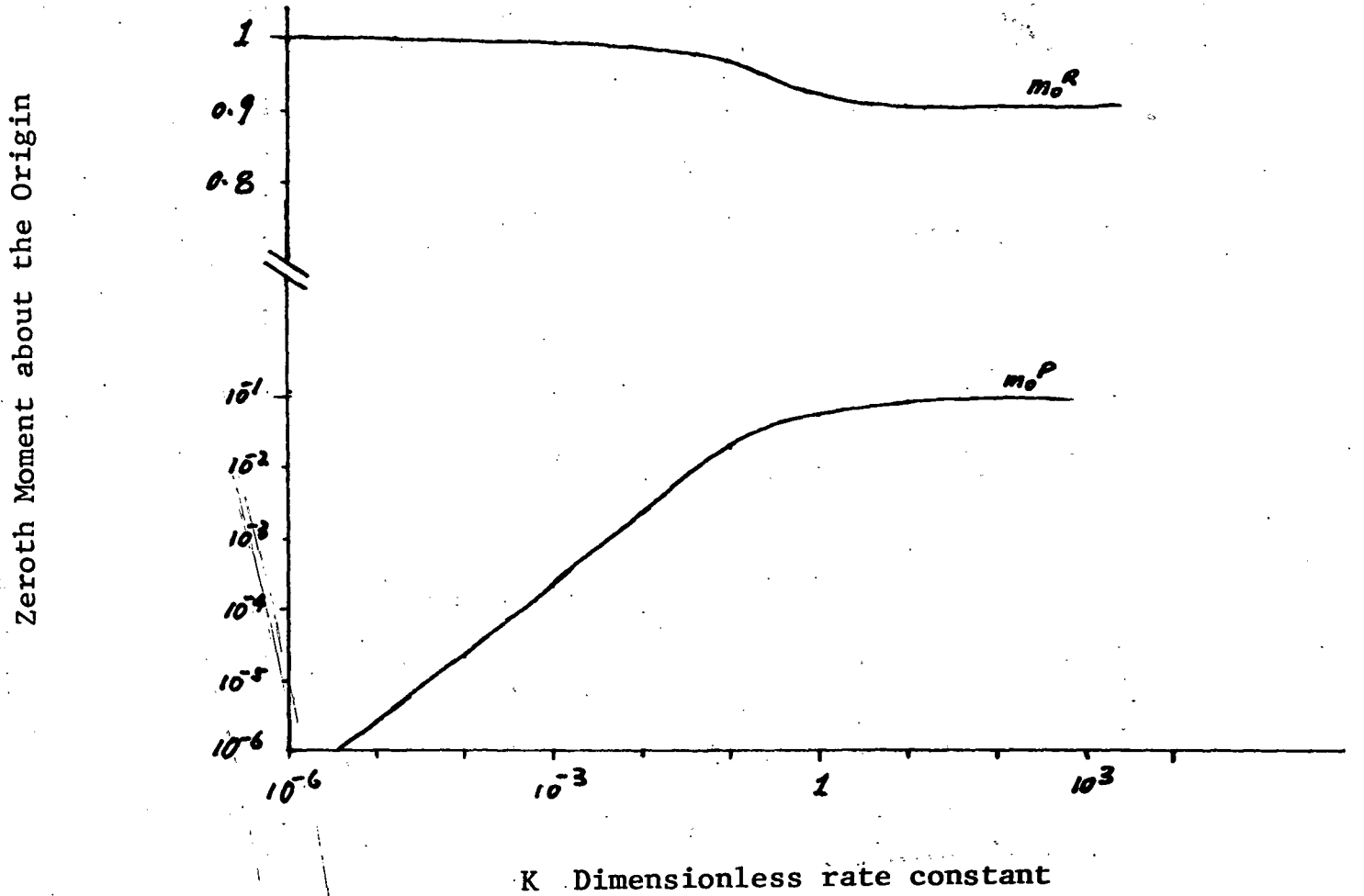

Figure 23. Zeroth Moment for a Transport-Limited Case Parameters Chosen: E =40, Ep = 20, Λ = 0.01, R = 10 = Rp, K is the independent variable.

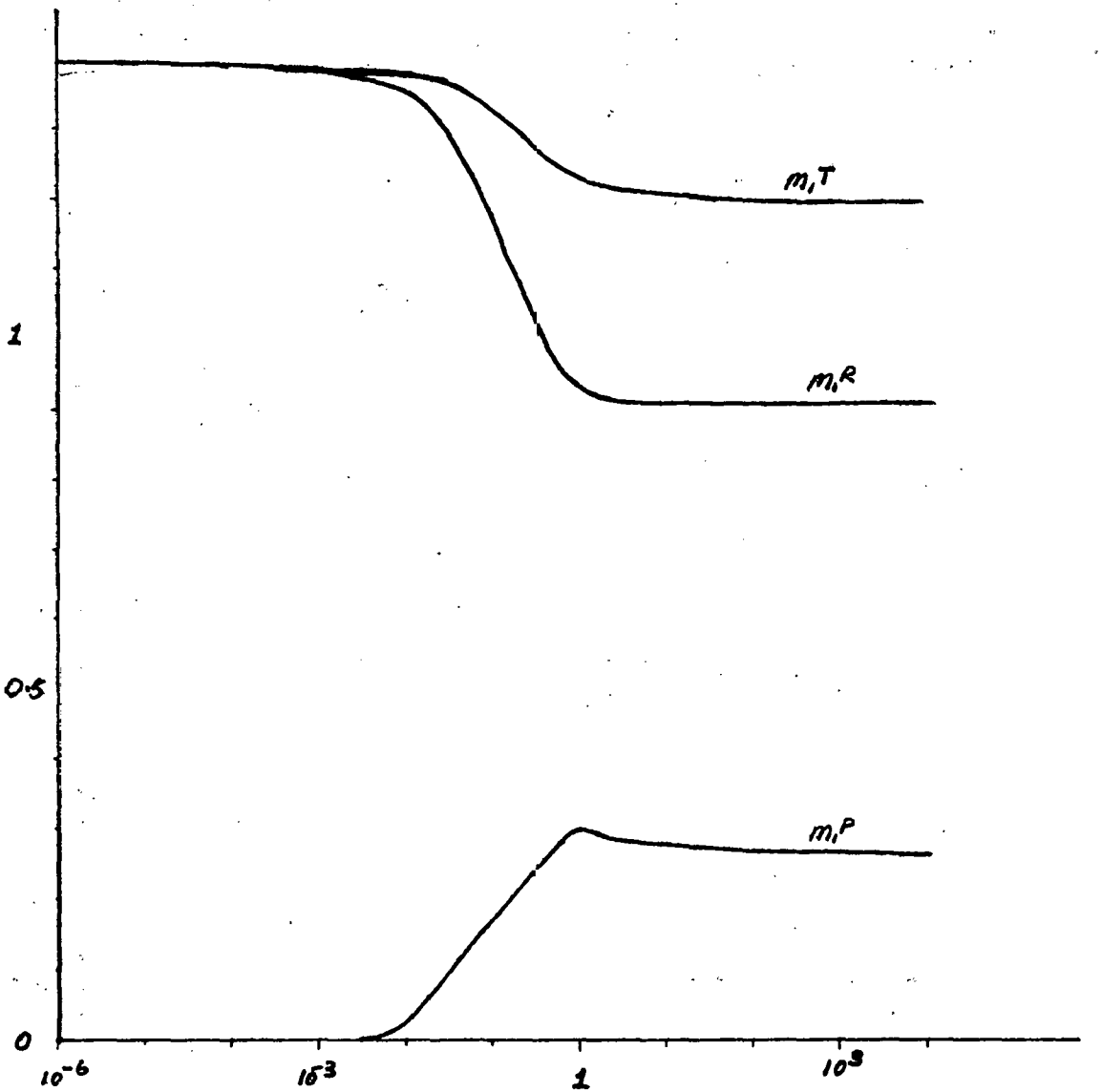

Figure 24. First Moments
Parameters Chosen: E = 40, Ep = 20, Λ = 0.01, R = 10, Rp = 10.

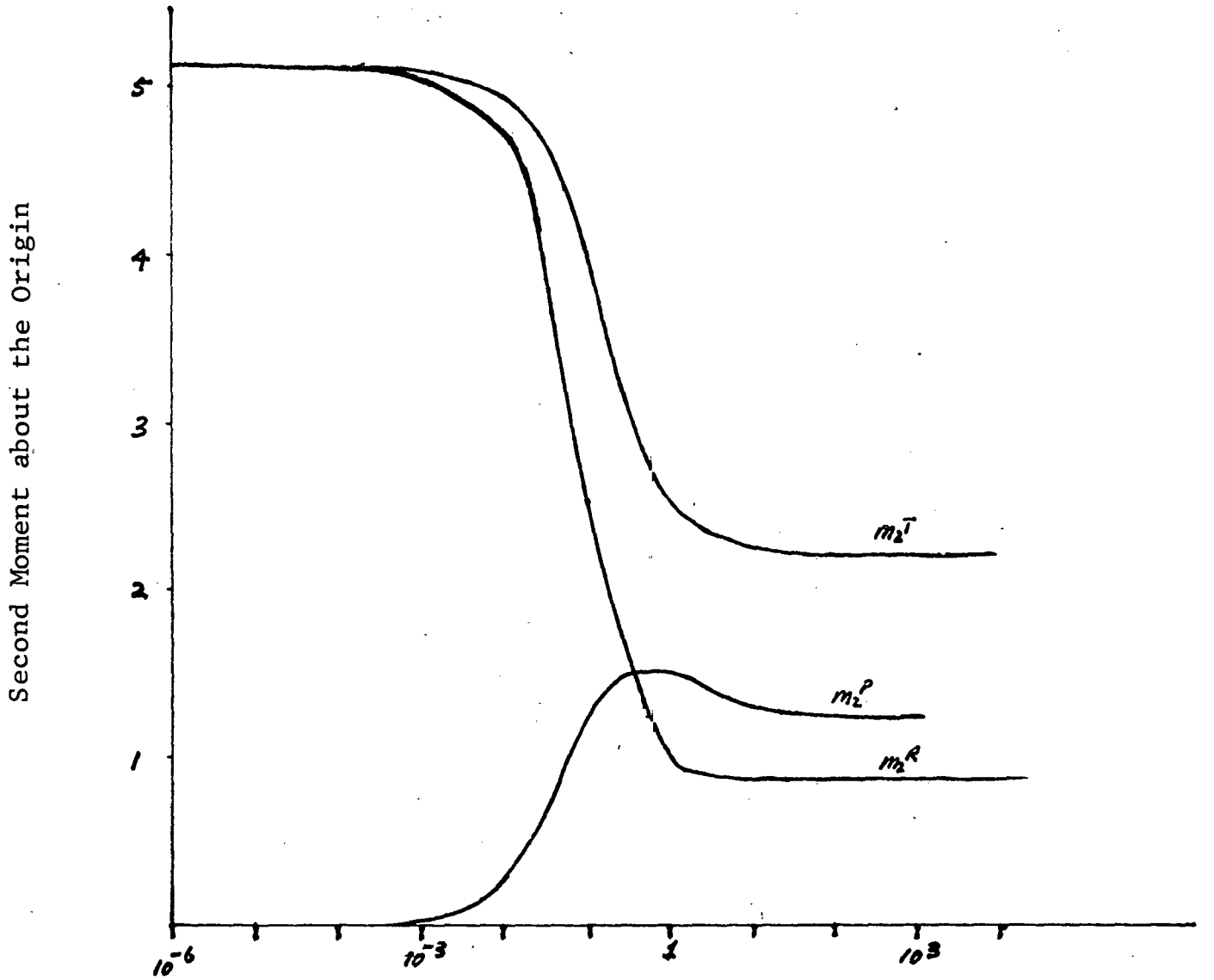

Figure 25. Second Moments about the Origin

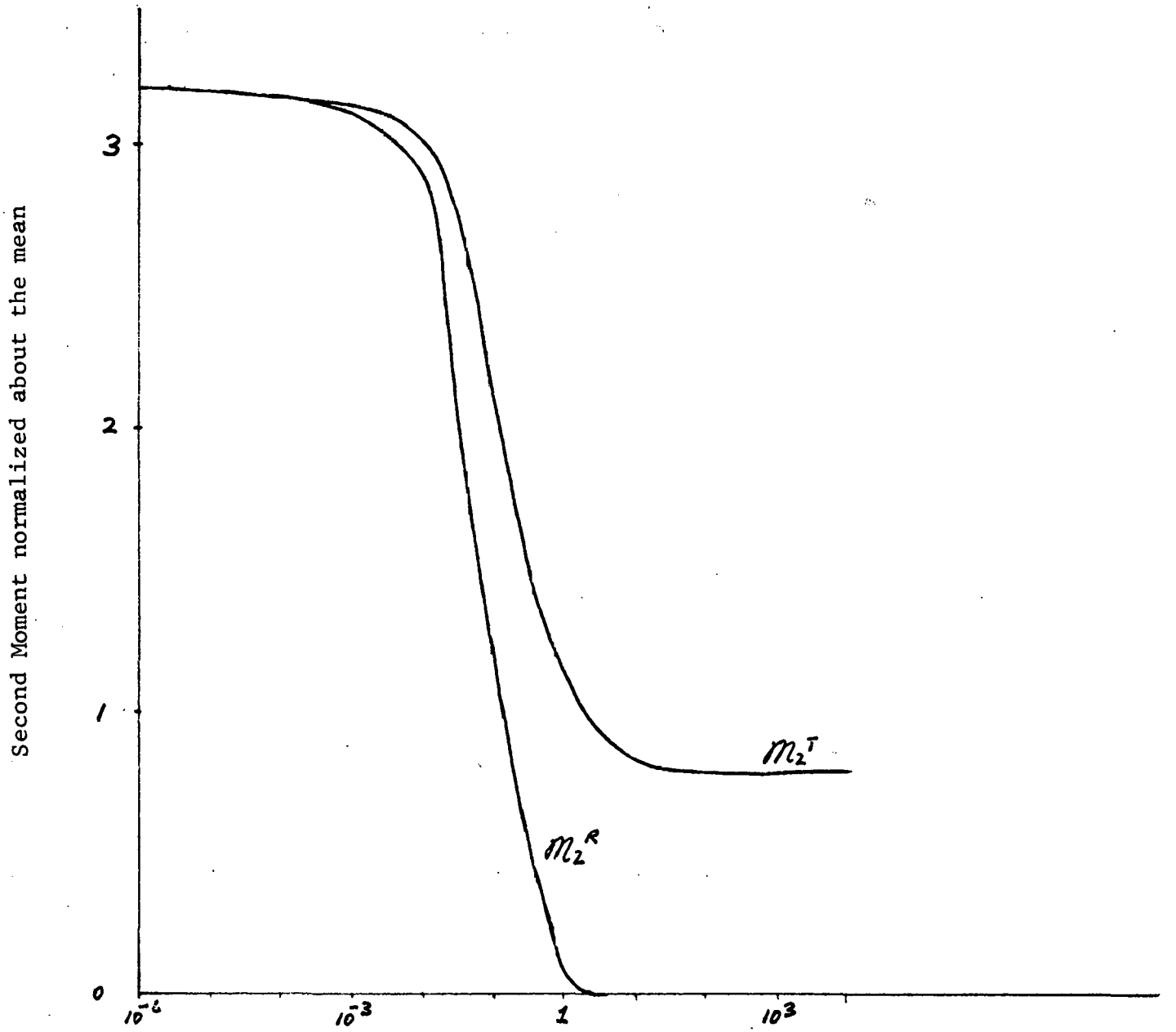

Figure 26 . Second Moments about the Mean

Similarly Figures 26-30 show the four moments for a set of parameters which yield nearly complete conversion. The shift in the total moment from reactant to product value occurs over a 2½ decade range of the reaction rate parameter K. Taken together the two sets of computations show that the conversion observed in a microreactor sometimes may be limited by transport rate but usually will follow a minor modification of the expected exponential decay for a first-order system when the fundamental kinetics are first-order.

A reaction engineering model for a microreactor just developed yields a great deal of information about the system from some routine calculations of the data used for timing the duration of the pulse in the microreactor. These results have not been available before this effort and make analysis of microreactor data possible now on a more quantitative basis.

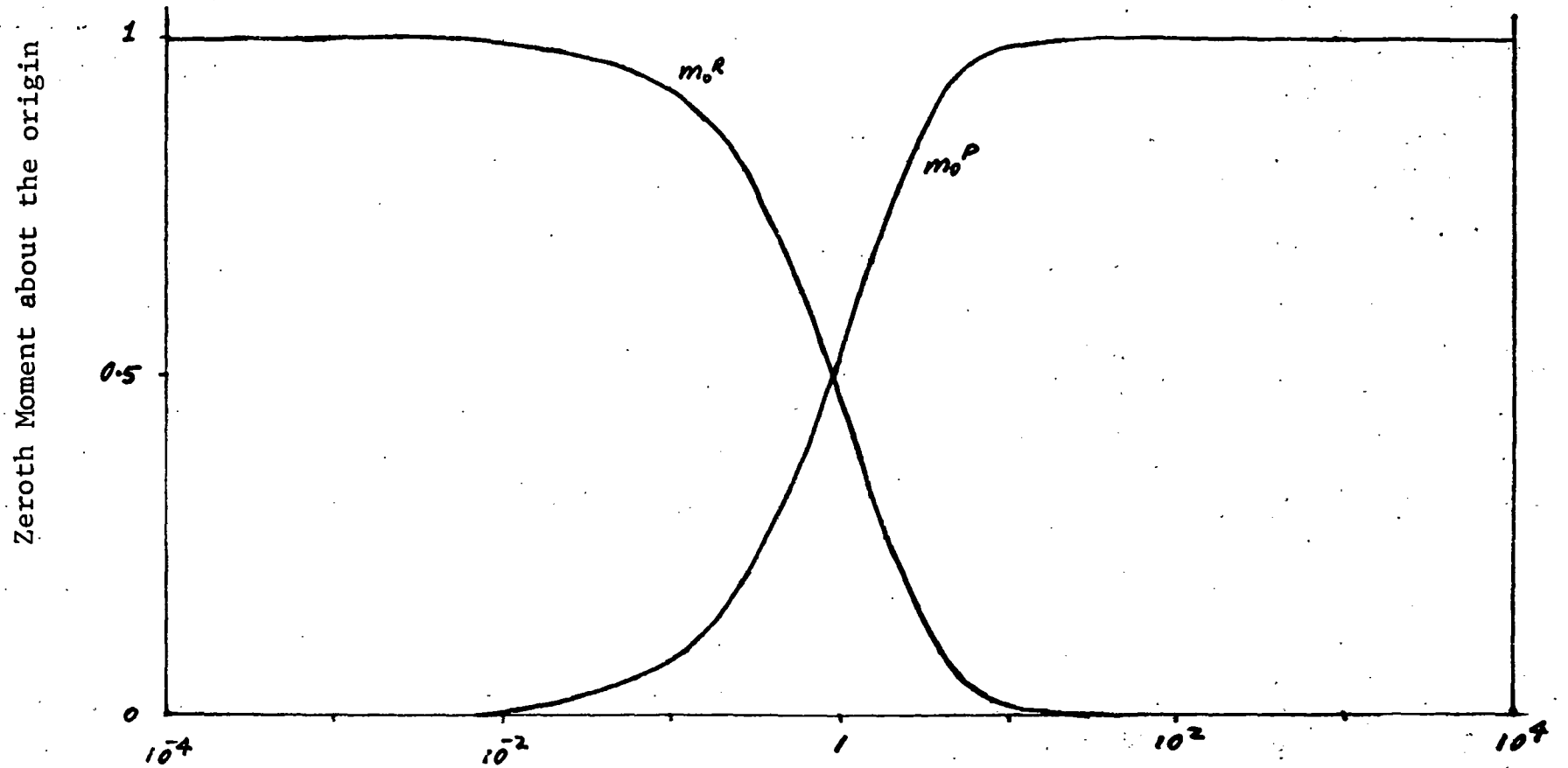

Figure 27. Zeroth Moments for a Kinetically-Controlled System
Parameters Chosen: E = 40, Ep = 20, = 0.02, F = 540, S = 70, R = 452.7, Rp = 389.7.

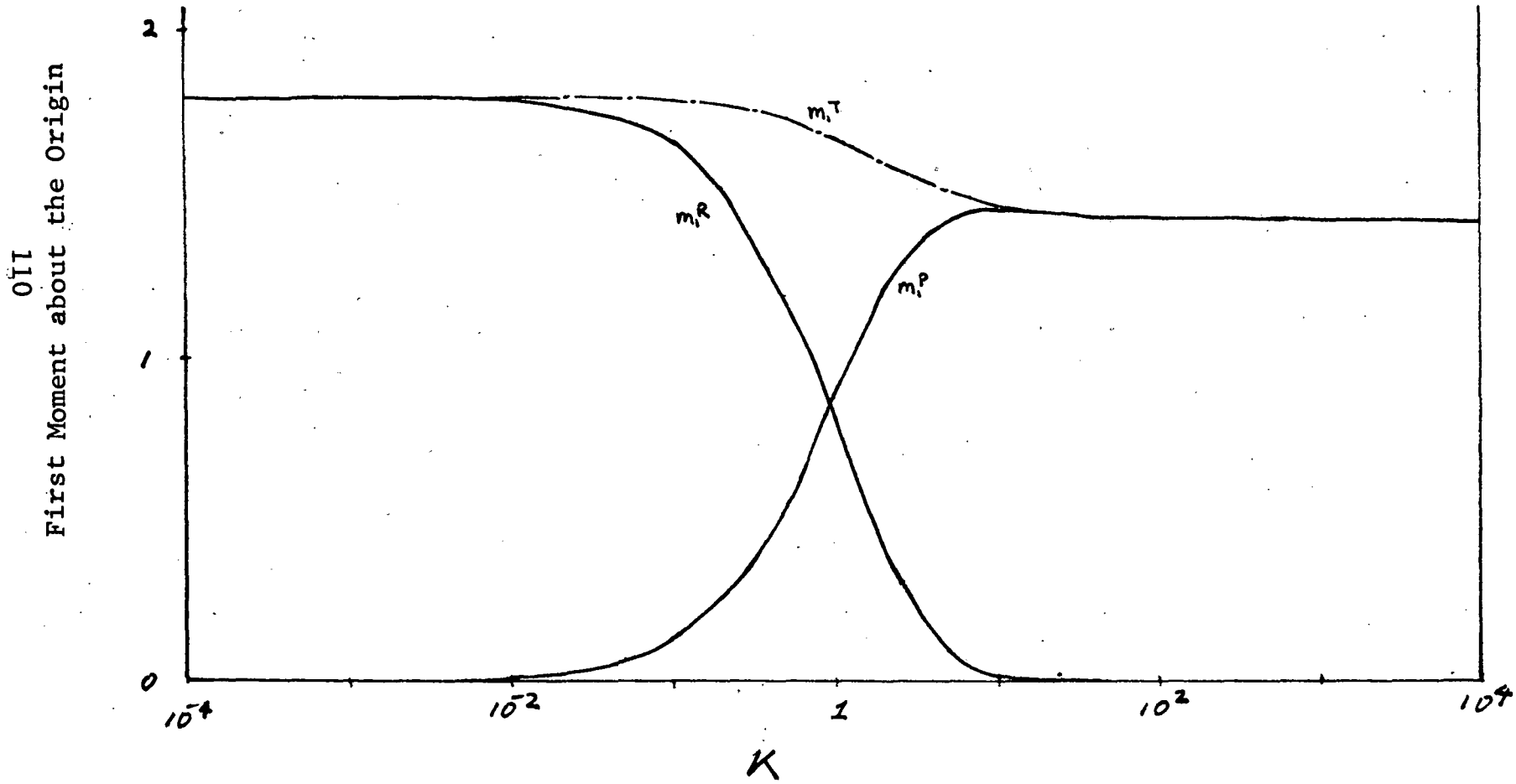

Figure 28. First Moments for a Kinetically-Limited System

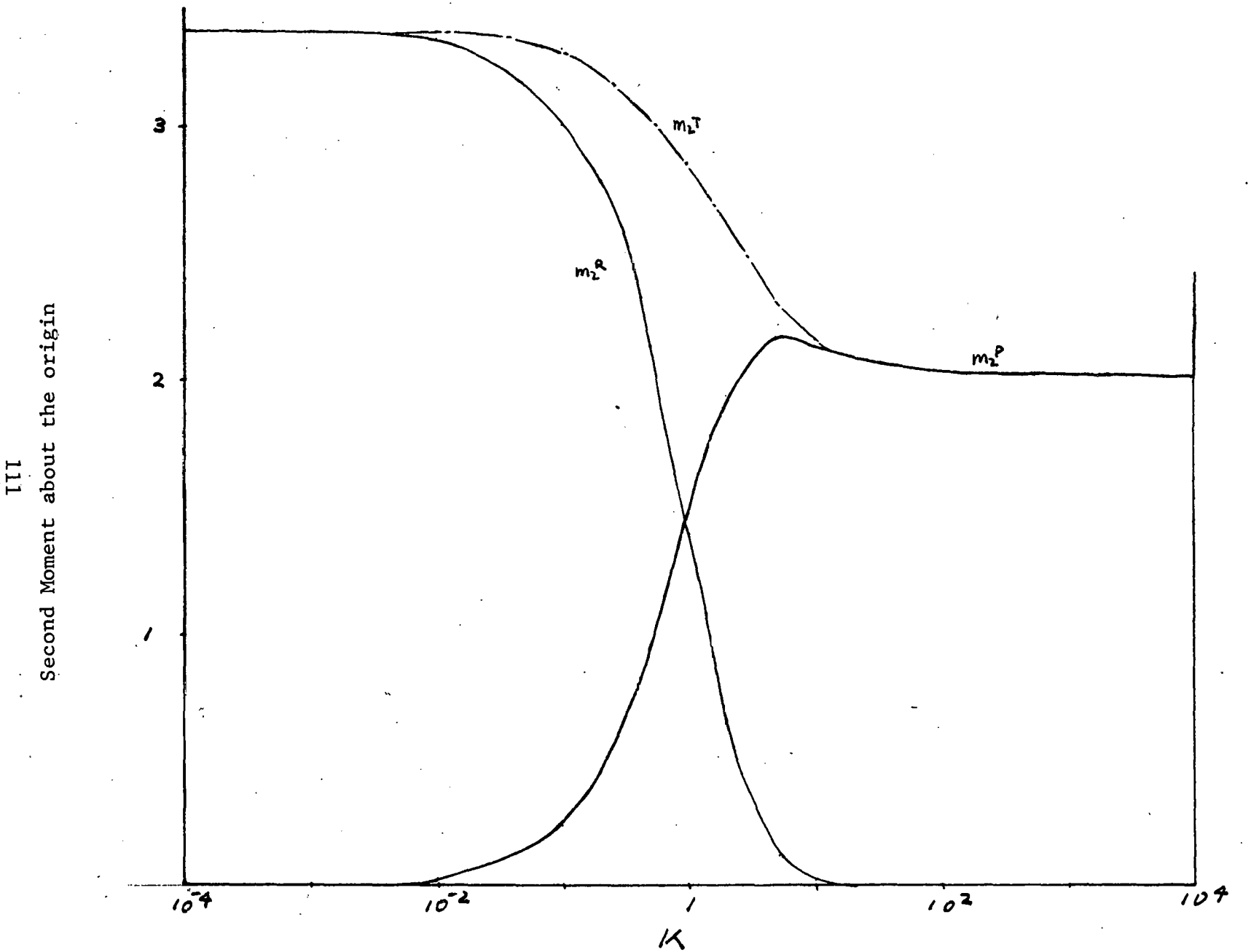

Figure 29 . Second Moments for a Kinetically-Limited System

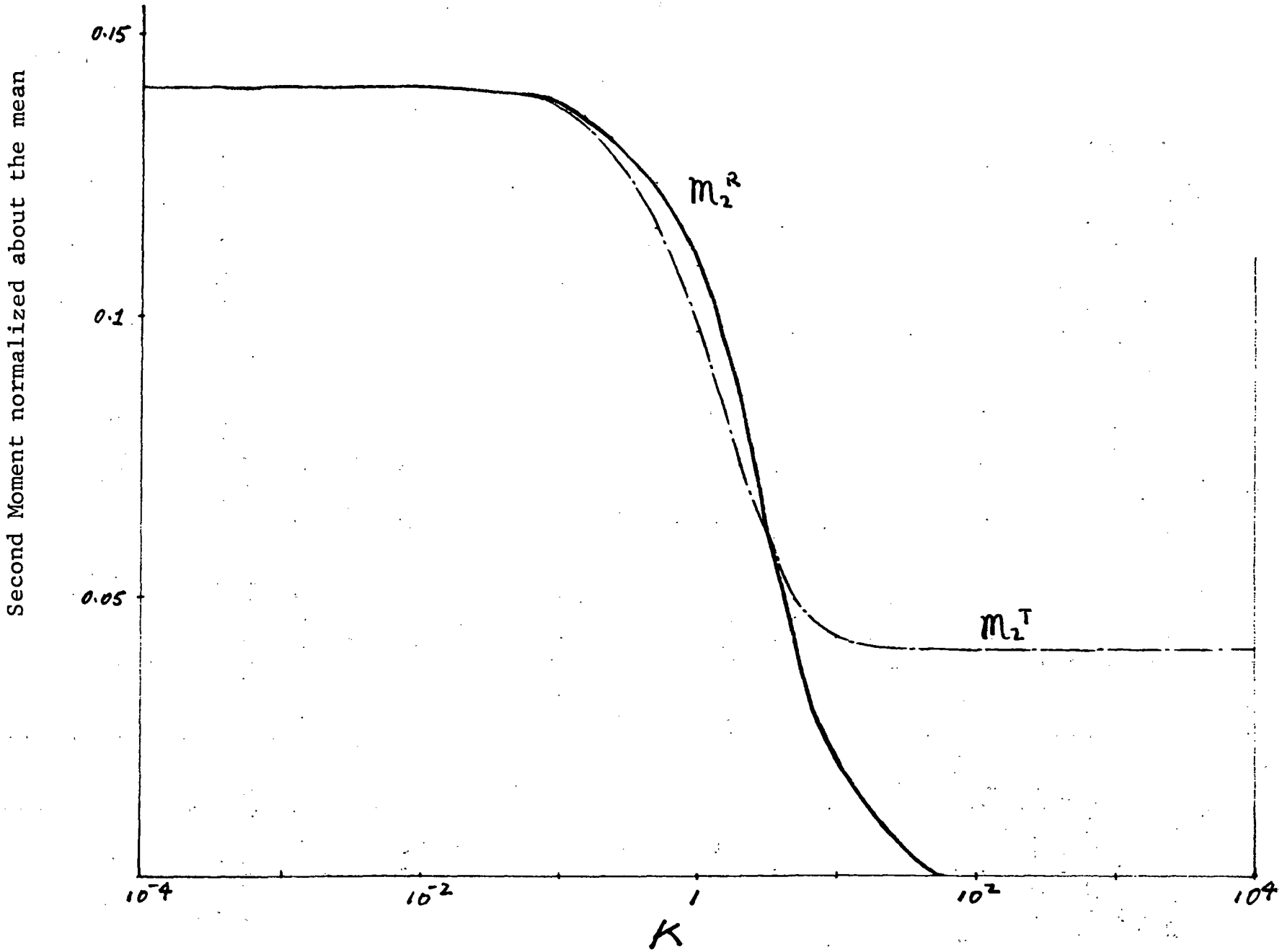

Figure 30. Second Central Normalized Moments for a Kinetically Limited System

2. Two-Phase Solid System

The catalyst particle actually is a two-phase system comprising the fluid phase and the solid phase. The adsorbed species are held on the surface of the solid phase. This two-phase system can be described in terms of a single phase system when the fluid phase in the catalyst is in equilibrium with the adsorbed species. The connection between the two viewpoints shall be made in this section.

The volumetric surface concentration, s_i, is written in terms of the surface concentration, n_i, as

$$s_i = \frac{n_i a_w \rho_p}{L} \tag{5.15}$$

where s_i = surface volumetric concentration, g mols/cm^3

n_i = surface concentration, species/cm^2

a_w = specific surface area, cm^2/g

ρ_p = apparent particle density, g/cm^3

L = Avogadro's number, species/g mol

ϵ_i = volume fraction fluid phase in the pellet

c_i = fluid phase concentration in the pellet, g mols/cm^3

$\mathcal{D}_K$ = Knudsen diffusivity, cm^2/sec

$\mathcal{D}_{eff} = \frac{\mathcal{D}_K \epsilon_i}{\gamma_i}$ effective Knudsen diffusivity, cm^2/sec

γ_i = Knudsen tortuosity factor

k_1 = first-order rate constant, sec^{-1}

The diffusion of a reactant in the pellet is coupled with adsorption and reaction is represented by the following component balance equation

$$\frac{\mathcal{D}_K \epsilon_i}{\tau} \nabla^2 c_i = \epsilon_i \frac{\partial c_i}{\partial t} + \frac{\partial s_i}{\partial t} + k_1 s_i \tag{5.16}$$

The single-phase volumetric concentration is defined as

$$q_i = \epsilon_i c_i + s_i \tag{5.17}$$

and is the concentration per unit volume in the catalyst without regard to phase. The intrinsic equilibrium between the fluid and solid phase is represented as

$$s_i = E_i c_i \tag{5.18a}$$

and therefore

$$q_i = (\epsilon_i + E_i) c_i \tag{5.18b}$$

$$q_i = (\epsilon_i / E_i + 1) s_i \tag{5.18c}$$

These two relations are introduced into the component balance equation to yield

$$\left(\frac{\mathcal{D}_K \epsilon_i}{\tau_i (\epsilon_i + E_i)}\right) \nabla^2 q_i = \frac{\partial q_i}{\partial t} + \left(\frac{E_i k_1}{E_i + \epsilon_i}\right) q_i \tag{5.19}$$

This equation demonstrates the following connection between one-phase and two-phase formulations:

One-Phase	Two-Phase
E	$E_i + \epsilon_i$
k_r	$k_1 E_i / (E_i + \epsilon_i)$
$\mathcal{D}_p$	$\mathcal{D}_K \epsilon_i / (\tau_i (E_i + \epsilon_i))$
SE	$15 \mathcal{D}_{eff} \tau / r_p^2$
KE	$k_1 \tau E_i = K_i E_i$

All the other terms in the single-phase film model are unchanged by these substitutions. Therefore the connection between a two-phase catalyst system and the single phase fluid-film model is straightforward. For example

and the remainder of the terms in the moment equations follow from the substitution of the two-phase definitions of E, k_r and Dp into the definition of the parameters.

Therefore the film model for transport in catalysts can be written in terms of fundamental catalytic parameters. For example the turnover rate is defined as the rate constant for a single site and is expected to be between 0.1 to 10 sec^{-1} for an active catalyst. For a single site mechanism the turnover for a solid-phase concentration of s_i is found as

$$\text{turnover}_{s_i} = k_1 \frac{s_{iL}}{a_w \rho_p \eta_s} \tag{5.20}$$

where η_s = number of sites per cm^2.

Similarly the turnover for complete adsorption on the surface is given as

$$\text{turnover} = k_1 \tag{5.20a}$$

The two-phase model has been developed in terms of parameters of fundamental significance to catalysis.

a. Spherical particle model

The solid film model has not been used very extensively in reaction engineering, and therefore this model is compared below to a more universally correct approach in which the reactant concentration is a function of the radial position inside the catalyst pellet. A comparison between the film model and the model considering diffusion and reaction inside a spherical particle shows that the two approaches are identical for most cases of interest in reaction engineering. This analysis shows the power of the less complex film model for representing diffusional transport in catalysts.

The approach used is similar to the development presented in the first section of this report. The component material balance for the fluid phase is matched with the component material balance equation for the solid phase. However the component material balance equation for the solid phase now is found as the solution to a partial differential equation. The remainder of the analysis is developed in a parallel (but more complex) fashion.

The fluid-phase component balance equation is written in dimensionless form as

$$\frac{\partial C}{\partial Z} + \frac{\partial C}{\partial T} + F\Lambda\left(C - C_{i,1}\right) = 0 \qquad (5.21)$$

The concentration in the interior of the pellet is found from the dimensionless form of eqn. 5.19 as

$$\nabla^2 C_i - \phi^2 C_i = \frac{E}{\theta}\,\frac{\partial C_i}{\partial T} \qquad (5.22)$$

where $\phi^2 = r_p^2 \frac{k_1}{\mathcal{D}_{eff}} E_i$ spherical Thiele modulus

$\phi^2 = r_p^2 \frac{k_{cr}}{\mathcal{D}_p}$

$\theta = \mathcal{D}_{eff}\,\tau / r_p^2$ Fourier time constant

$C_i(\rho, T)$ = interior concentration in the gas phase

ρ = dimensionless particle radius

Eqn. 5.22 is solved for the boundary conditions

$$C_i(1,T) = \text{forcing function}$$

$$C_i(0,T) = \text{finite}$$

$$C_i(\rho,0) = 0$$

via the Laplace transform to yield

$$\bar{C}_i(\rho,s) = \frac{\bar{C}_{i,1}}{\rho}\,\frac{\sinh \bar{\Phi}\rho}{\sinh \bar{\Phi}} \tag{5.23}$$

$$\bar{\Phi}^2 = \phi^2 + \frac{E}{\theta}s$$

The surface concentration $\bar{C}_{i,1}$ can be replaced by the bulk concentration by matching the external flux at the surface

$$\bar{C}_i(\rho,s) = \bar{C}\,\frac{F}{F + S_i} \tag{5.24}$$

$$S_i = \frac{3KE}{\phi^2}\left(\frac{\bar{\Phi}}{\tanh \bar{\Phi}} - 1\right)$$

The value for $\bar{C}_i(\rho,s)$ then is inserted into eqn. 5.22 to yield

$$C = \exp\left\{-(s + g_i(s))\,Z\right\} \tag{5.25}$$

where $$g_i(s) = \frac{\Lambda F S_i}{F + S_i}$$

The moments of the pellet model found by taking the derivatives with respect to s. The development is far more tedious than the film model. The results are as follows:

$$m_{0s} = \exp\left(-KE\Lambda\eta_g\right) \tag{5.26a}$$

$$m_{1s} = 1 + \frac{3E\Lambda\eta_g^2}{2\phi\,\eta_s^2} \qquad (5.26b)$$

$$m_{2s} = \frac{E\Lambda\gamma}{K} \qquad (5.26c)$$

where

$\phi = r_p\sqrt{\frac{k_1 E_i}{D_{eff}}}$ Thiele modulus

$Bi = \frac{k_g d_p}{D_{eff}}$ Biot number = $Sh\frac{D_M}{D_{eff}}$

$\eta_s = \frac{3}{\phi^2}\left(\frac{\phi}{\tanh\phi} - 1\right)$ spherical effectiveness factor

$\eta_g = \left(\eta_s^{-1} + \frac{2\phi^2}{3Bi}\right)$ global effectiveness factor

$\eta_g = \left(\eta_s^{-1} + \frac{KE}{F}\right)$

$\beta = \coth\phi - \phi\,\mathrm{csch}^2\phi$

$\gamma = 3\frac{\eta_g^2}{\eta_s^2}\beta\left(\frac{\eta_g\beta}{\eta_s Bi} + \frac{1}{4\phi}\right) - \frac{\phi^2\eta_g^2\,\mathrm{csch}^2\phi}{2\eta_s}$

Comparison of the Two Models

The film model and the spherical particle model have identical zeroth moments when the solid film parameter is defined as

$$SE = \frac{KE\,\eta_s}{1-\eta_s} \qquad (5.27a)$$

As the rate parameter k_1 approaches zero

$$SE = \frac{15 D_{eff}\,\tau}{r_p^2} \qquad (5.27b)$$

which naturally is identical to the model previously used.

A further comparison between the two formulations is found by recalling the moments for the film model

$$m_0^F = \exp\{-KE\Lambda\eta_g\}$$

$$m_1^F = 1 + E\Lambda\eta_g^2$$

$$m_2^F = \frac{2\Lambda E^2\eta_g^3}{(F^{-1} + (5E)^{-1})^{-1}}$$

The first moment is used to identify the magnitude of the equilibrium parameter, E. Therefore a critical comparison of the first moments of the two models is found as

$$e_1 = \frac{(m_1^F - 1) - (m_1^S - 1)}{(m_1^S - 1)} \tag{5.28}$$

Upon substituting the variables e_1 is found to be a function of the Thiele modulus alone

$$e_1 = \frac{2\phi\eta_s^2}{3\beta} - 1 \tag{5.29}$$

Similarly a relative error comparison of the second central moments yields

$$e_2 = \frac{m_2^F - m_2^S}{m_2^S} \tag{5.30}$$

which upon rearranging the definitions yields

$$e_2 = \frac{2}{\gamma}\left(\frac{1-\eta_s}{\eta_s} + \frac{2\phi^2}{3B_i}\right) \tag{5.31}$$

The error for the second central moment therefore is a function of the Thiele modulus and the Biot number.

Figure 31 shows e_1 as a function of ϕ. The error is unimportant until is greater than unity, and $\phi > 1$ will typically give complete reaction (99% conversion). Since complete reaction does not yield useful kinetic data operation with $\phi > 1$ is not likely to be of any interest experimentally. Therefore the film model for transport in a catalyst is an adequate representation for most experimental studies.

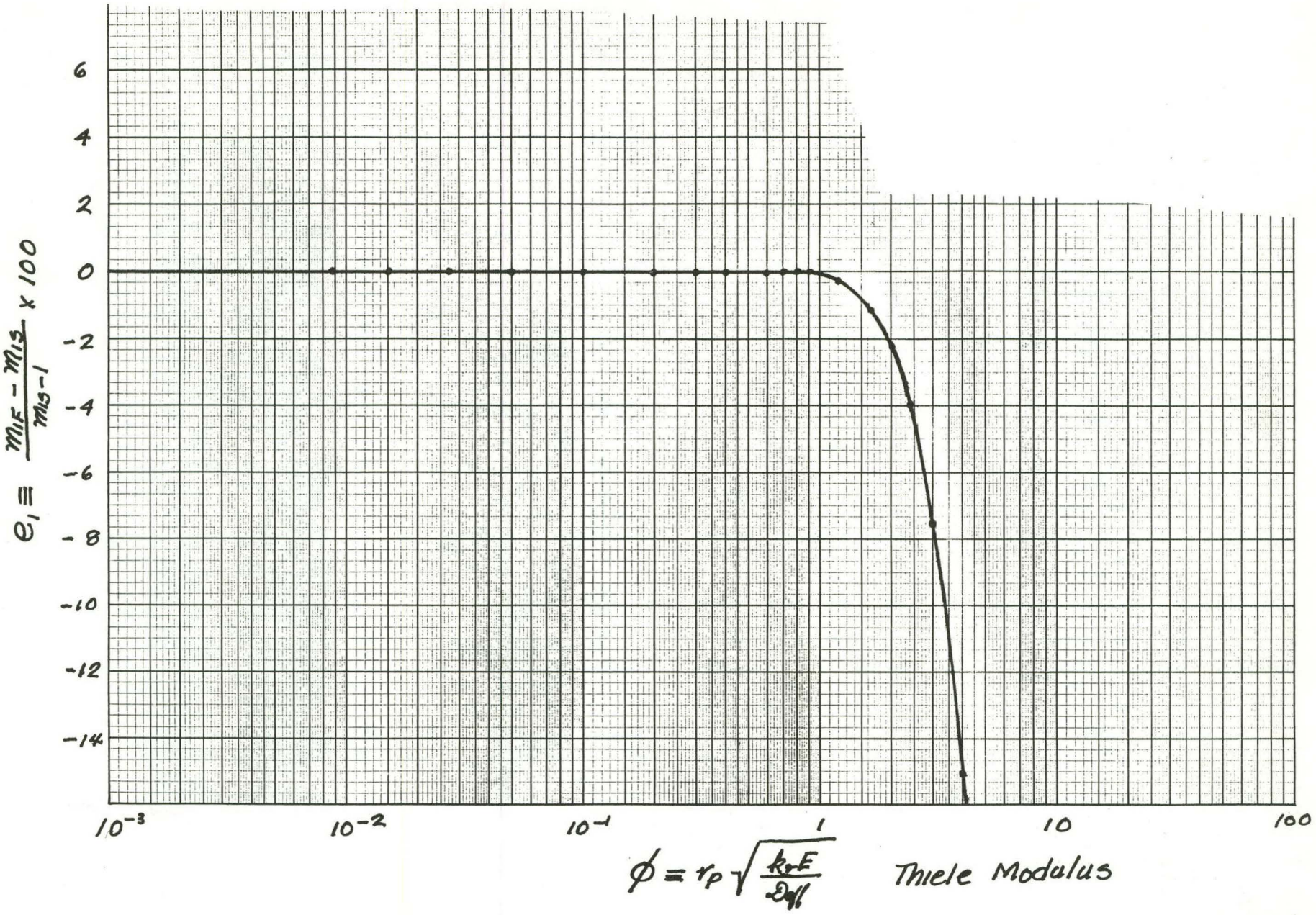

Figure 31. Relative Error in First Absolute Moment

Figure 32 shows e_2 as a function of the Thiele modulus with the Biot number as a critical parameter. The relative error is less than three percent for all reasonable values of the Biot group when the Thiele modulus is less than unity. The error of the film model is unacceptably large when the Thiele modulus is greater than two, and the figure shows an abrupt change in the magnitude of the error with increasing Thiele modulus. Under extremely reactive conditions the film model should be recast, but this mode of operation is not likely to be of kinetic interest.

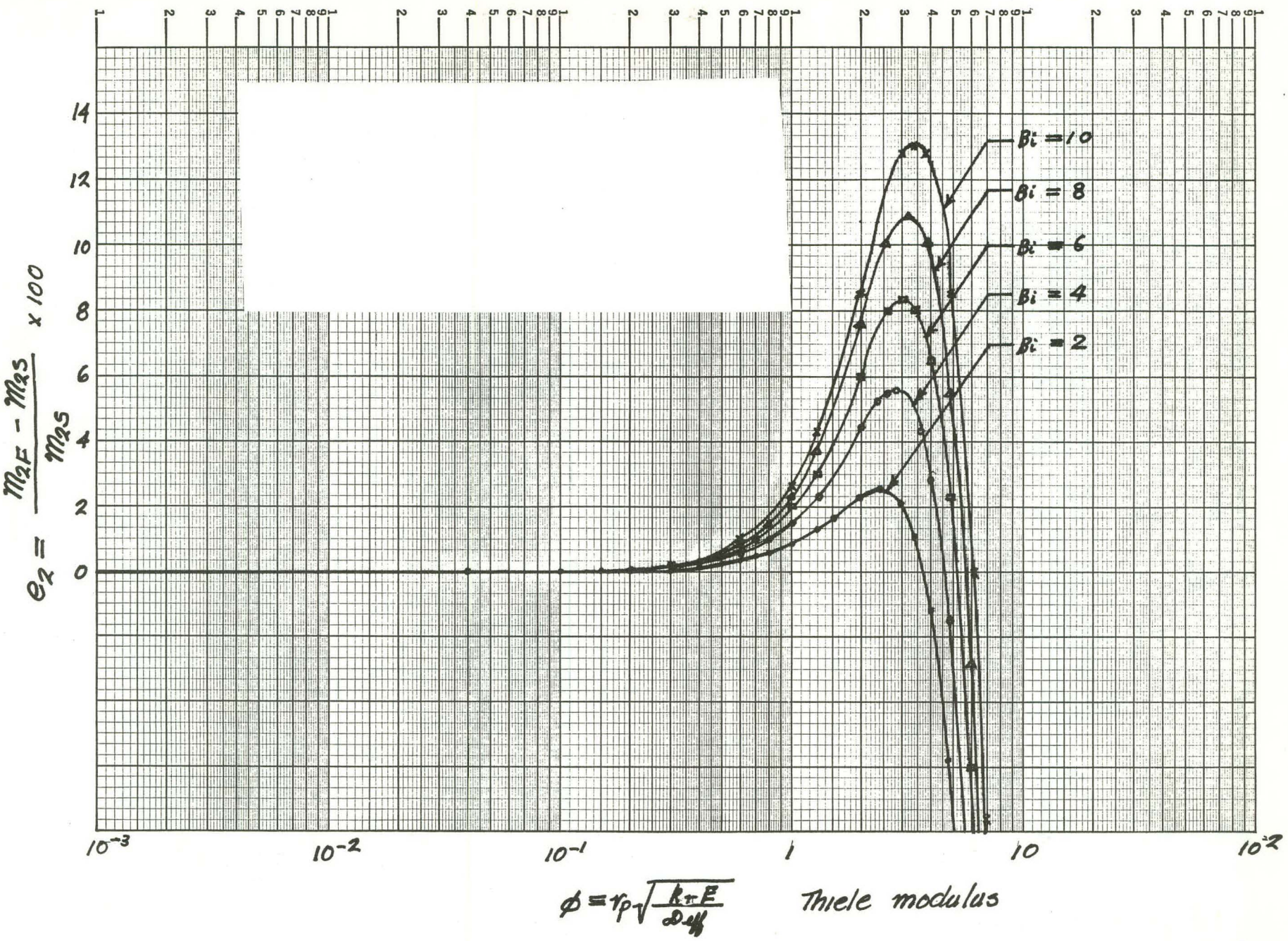

Figure 32. Relative Error in Second Central Moment

3. Pulse-Microreactor Experimental Program

Since the two liquid-phase microreactors are in constant use for Tasks 2 and 3, alternative equipment has been used to test the reaction engineering analysis. This work has been done without expenditure of ERDA Funds, but it is reported here because it establishes continuity with the ERDA supported work. The reactor was described in the First Quarterly Progress Report and is a tube filled with inert chromatographic column packing and five pellets of Harshaw 0402T catalyst. The carrier gas was H_2 in which 1.5% H_2S was added. This gas mixture serves to keep the catalyst sulfided. The pulses were produced by injection of gas or liquid samples through a heated injection port. The pulse passed first to one side of a thermal conductivity detector, then to the reactor, and back through the other side of the detector. By switching a transfer valve, the pulse was sent to an adjacent chromatograph for analysis.

This equipment was modified by the addition of a microprocessor developed by James Mankin and R. L. Pigford. The microprocessor sampled the signal from the two detectors every 10 milliseconds and stored these data for transmission to the central computer. A continuous analog of the sampled data is shown on Figure 33 ; this diagram is for a thiophene-n-pentane pulse undergoing reaction at 300°C. Although the pulses are very nearly of the skewed Gaussian form expected for simple chromatography, closer inspection shows that these pulses have small but significant tails. These tails are produced by the delay coils needed to separate the inlet and outlet pulses cleanly and by small nonlinear kinetic effects in the reaction network. These signals can be improved by design modifications.

Runs were conducted at 200, 250 and 300°C using pulses of nitrogen, n-pentane, butadiene and thiophene-n-pentane. The runs at the lower temperatures will not be discussed in this report because the thiophene reaction product recovery was not complete. The function of the different pulse materials is given in the order listed.

Table XVI gives a short summary of the data gathered. The nitrogen runs were made to establish the volume of the system which is given approzimately by the relation

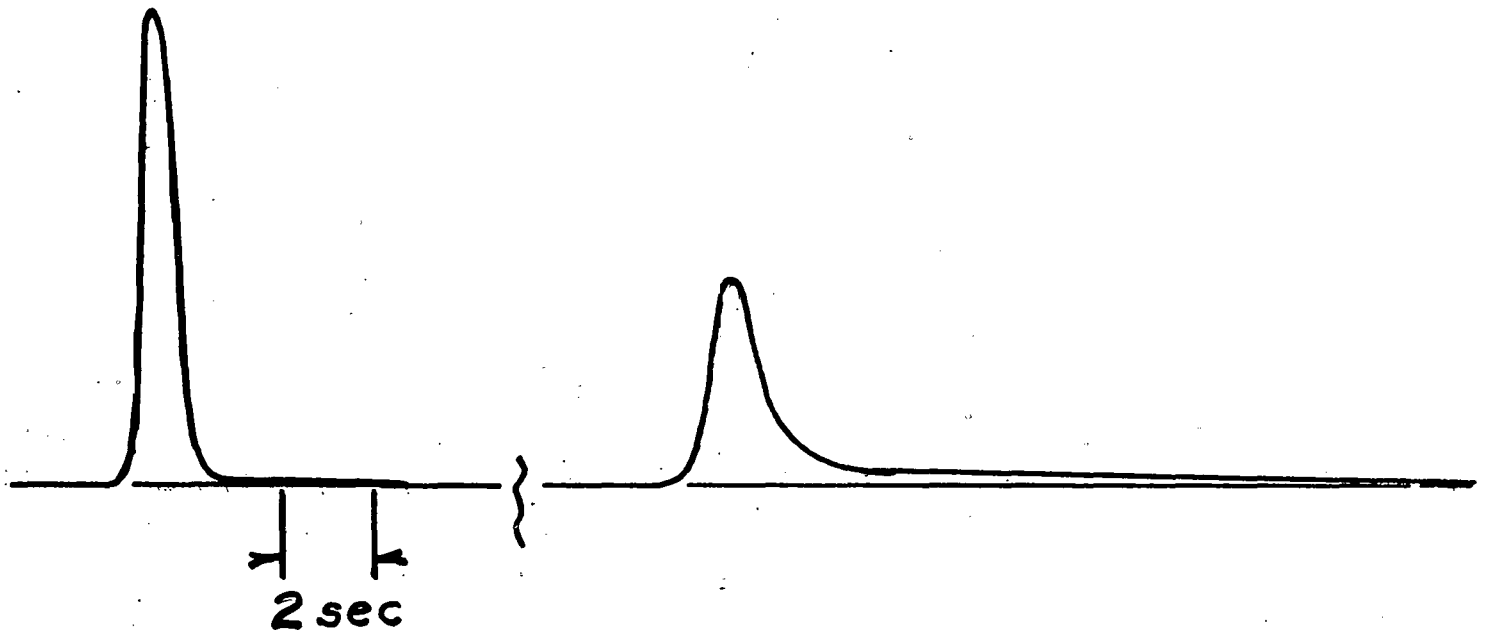

Figure 33. Pulse Output 1μℓ @ 300°C

TABLE XVI.

PULSE MICROREACTOR DATA

Pulse	Pulse Size ($\mu\ell$)	Flow Rate (ml min^{-1})	Mo out / Mo in	ΔM_1 (sec)	ΔM_2 (sec^2)	E	R	$\eta_g k_1$ (sec^{-1})
Nitrogen	40	27.4	.989	21.08	.907	0	very large	
Pentane	.1	27.4	1.00_4	22.70	11.86	4.15	8.87	
Butadiene	20	27.0	.966	25.69	52.48			
	40	27.0	1.05	25.93	75.19		79.4	
	60	27.0	1.05	26.32	87.27			
	80	27.0	1.02	26.02	87.37			
	100	27.0	1.03	25.33	56.71			
	40	13.2	1.15	56.57	630.			
	40	50.4	1.03	14.03	24.22	36.4		0.845
	40	95.5	.993	7.46	5.52			
	40	142.8	.994	5.21	2.59			
Thiophene	.5	27.0	1.04	27.44	125.3			
	1	27.0	1.09	28.99	191.7		110.	0.0965
	2	27.0	1.03	27.68	158.8	49.0±4.2		
	4	27.0	1.00	27.16	153.6			
	6	27.0	1.00	26.87	144.1			
	1.0	13.2	1.15	60.25	715.7			
	1.0	50.4	1.20	17.81	152.3			
	1.0	95.5	1.04	8.11	14.83			
	1.0	142.8	.991	5.31	5.20			

$$V_S = m_1 F^o (T/T^o) \tag{5.32}$$

where V_s is the volume of the inert system

F^o is the flow rate, cc/sec

T is the system temperature

T^o is the temperature at which the flow rate is measured.

The data given establishes that the system volume is 18.28 cm^3. This volume is contained primarily in the holdup of the transfer coils. In addition the volume fraction of catalyst, Λ, equals 6.87×10^{-3}.

These runs illustrate two other points. The ratio of the output to input zeroth moments establish that the nitrogen pulse is recovered, a condition necessary to the experiment. The small change in the second moment shows that the total axial dispersion is small, and therefore axial dispersion can be neglected in the analysis of the data. (The first order correction for axial dispersion is obtained by subtracting the axial dispersion contribution of the unadsorbed pulse from the second central moment of the other data.)

Pentane is used as a solvent and an internal standard for thiophene and therefore a series of runs were made with the solvent alone. The zeroth moment ratio shows that the pentane is recovered cleanly in the pulses; the zeroth moment ratio is near unity for all the temperatures considered. The first moment is used to obtain an estimate for the equilibrium parameter

$$E = \frac{m_1^{C5} - m_1^{N2}}{m_1^{N2} \Lambda} \tag{5.33}$$

which from the data shows that $E^{C5} = 4.15$. An Arrhenius plot of the adsorption data is given on Figure 38. The apparent heat of adsorption is -13.3 kcal/g mol; pentane is adsorbed physically on the catalyst surface.

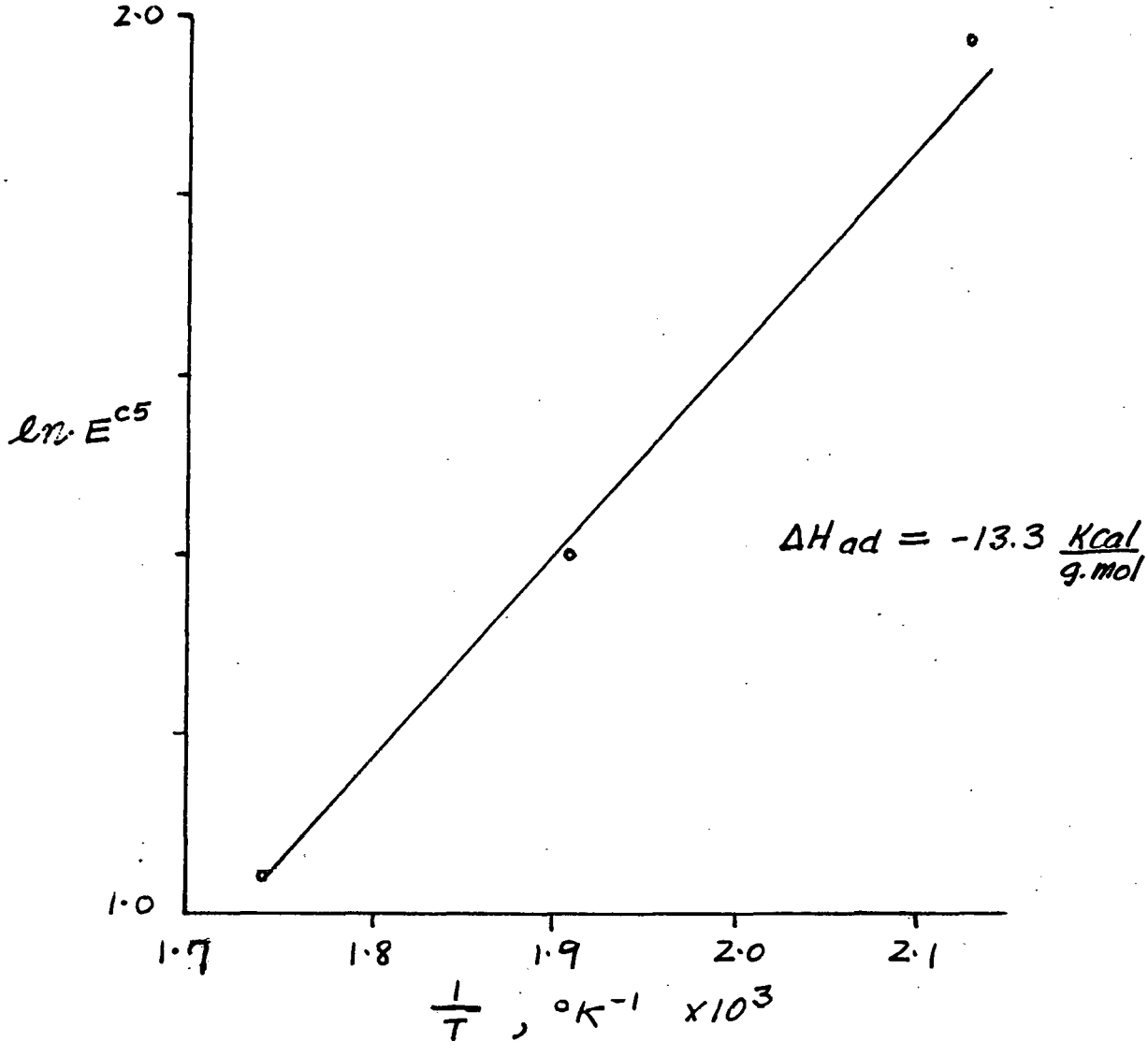

Figure 34. Pentane Adsorption

The second moment is used to estimate the effective diffusivity in the particle. The total number of transfer units is found as

$$R = \frac{2E^2\Lambda(m_1^N)^2}{m_2^{C5}} \qquad (5.34)$$

$$R = 8.87$$

and using an estimate for the gas film resistance F = 1080, the value of SE is found

$$SE = 8.95$$

The value of the effective diffusivity then is obtained

$$D_{eff} = 7.1\text{-}04 \text{ cm}^2/\text{sec}$$

The value for D_{eff} based upon Knudsen diffusion is

$$D_{eff}' = 22.\text{-}04 \text{ cm}^2/\text{sec}$$

The two results indicate a low value of the measured effective diffusivity for pentane which is not understood at this time.

A series of runs were made using butadiene as the reactant. With the large excess of hydrogen used in these experiments, the reaction network is the irreversible sequence

BDE ⟶ butenes ⟶ butane

First a series of runs were made at a fixed flow rate and variable pulse size. These runs showed that the butadiene reaction system is recovered completely independent of sample size. The analytical accuracy was best for the 40 μℓ gas sample. The consistency of the m_1 moments shows that the adsorption parameter can be determined with adequate accuracy, while the larger variance in the second moments shows the sensitivity of this parameter to pulse size.

In the next series of runs with butadiene the flow rate was varied to change the residence time in the catalyst. The data for these runs are given in Table XVIII which lists the product distribution with flow rate and estimates of the transport parameters. These estimates are made by assuming butadiene, the butenes, and butane have identical adsorption (E) values. Additional experiments are needed to confirm this assumption.

TABLE XVII.

BUTADIENE REACTION DATA

294.6°C

Product Distribution

Flow Rate, ml/min	Space Time, sec.	Butadiene	1-Butene	cis butene-2	trans butene-2	butane
13.2	43.68	0.000	0.100	0.169	0.263	0.468
27.0	21.35	0.006	0.138	0.223	0.346	0.287
50.4	11.44	0.094	0.188	0.224	0.331	0.162
95.5	6.04	0.260	0.162	0.194	0.293	0.091
142.8	4.04	0.394	0.148	0.165	0.233	0.060

Transport Parameters

Space Time, sec	E	R	SE	D_{eff}, cm^2/sec
43.68	42.6	75.7		
21.35	30.7	79.4	85.7	6.7-03
11.44	32.6	79.4		
6.04	33.9	104.0		
4.06	42.2	154.0		

$\overline{E} = 36.4$

The apparent value of the equilibrium parameter is independent of flow rate and has an average value of 36.4. The R values apparently increase with flow rate whereas the simple model suggest the opposite. The precision of the R values need to be improved to confirm this result. Nevertheless the effective diffusivity has a reasonable value (6.7-03 cm^2/sec) for the flow rate with the most precise data.

The zeroth moment data is used to find the apparent rate constant for the conversion of BDE to butenes. The fraction of the output pulse which is BDE is given as

$$C_{BDE} = e^{-EK\Lambda\eta_g} \tag{5.35}$$

The Arrhenius plot for the fraction of butadiene remaining is given on Figure 35. This plot shows that the first order reaction rate parameter is

$$\eta_g k_r = 0.845 \ sec^{-1}$$

This turnover rate establishes that the catalyst is very effective for hydrogenation.

At a lower precision the rate of hydrogenation of butenes to butane can be fit from the relation

$$C_E = \frac{1}{1-\rho}\left(C_{BDE}{}^{\rho} - C_{BDE}\right) \tag{5.36}$$

where p = the ratio of the rate constant for butene hydrogenation to the rate constant for butane hydrogenation.

= fractional concentration of butenes

Figure 36 shows a plot of the data and the trial fitting function. Although there clearly is systematic error, the data is represented approximately by the relation

* p = 0.095

Table XVII shows a comparison of the butene product distribution with other studies and the equilibrium. The data show that the fraction of butene-1 decreases with residence time on the catalyst whereas the trend in cis and trans to increase with residence time. The product distribution changes are narrow. This distribution does not agree with the data of Kolboe or Amberg. The data show an approach toward equilibrium with space time. The ratios show that butene-1 is the most favored reaction product and trans-C4 is the least favorable. These data support the reaction network proposed in the second progress report.

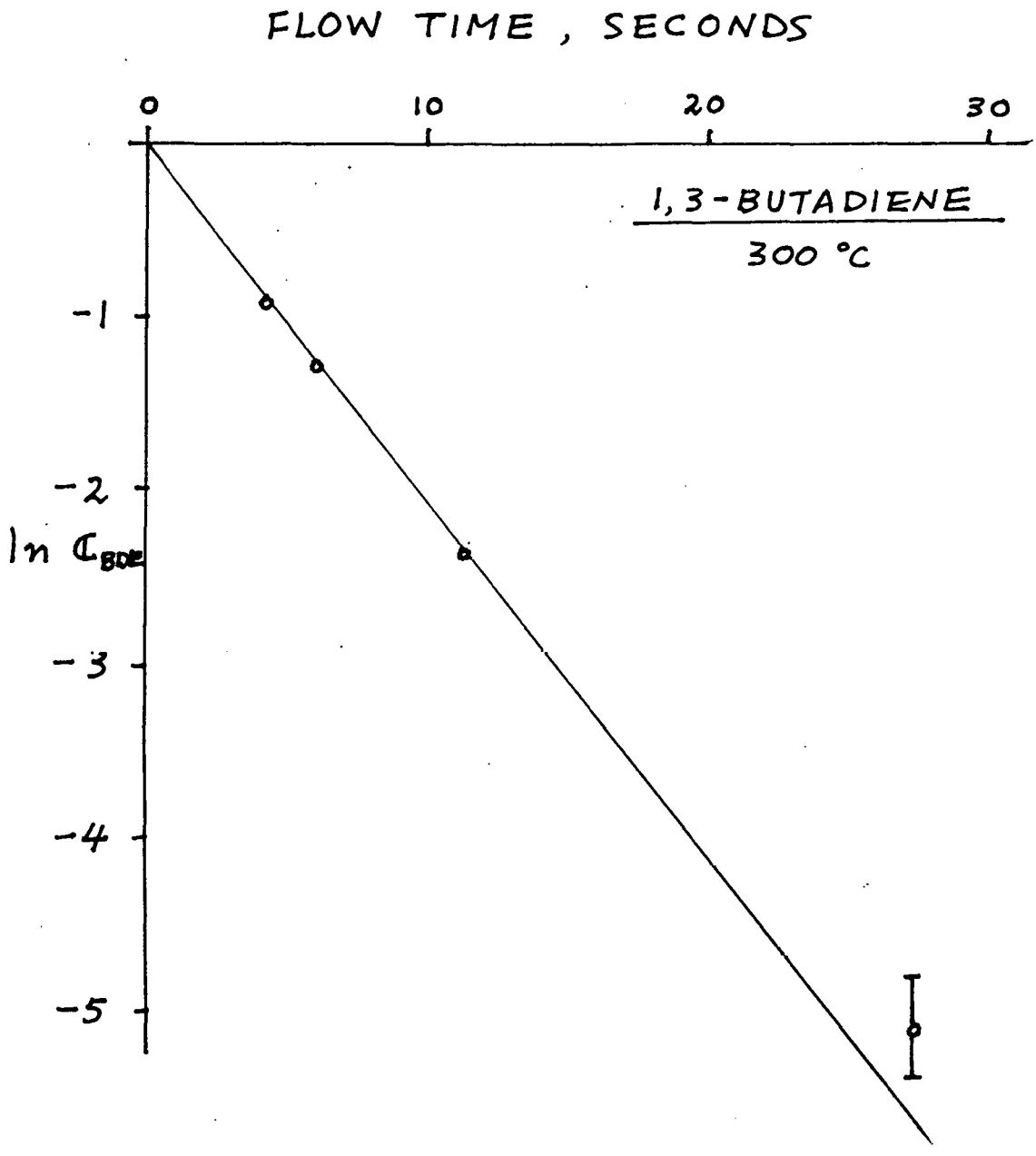

Figure 35. Butadiene Reaction Rate

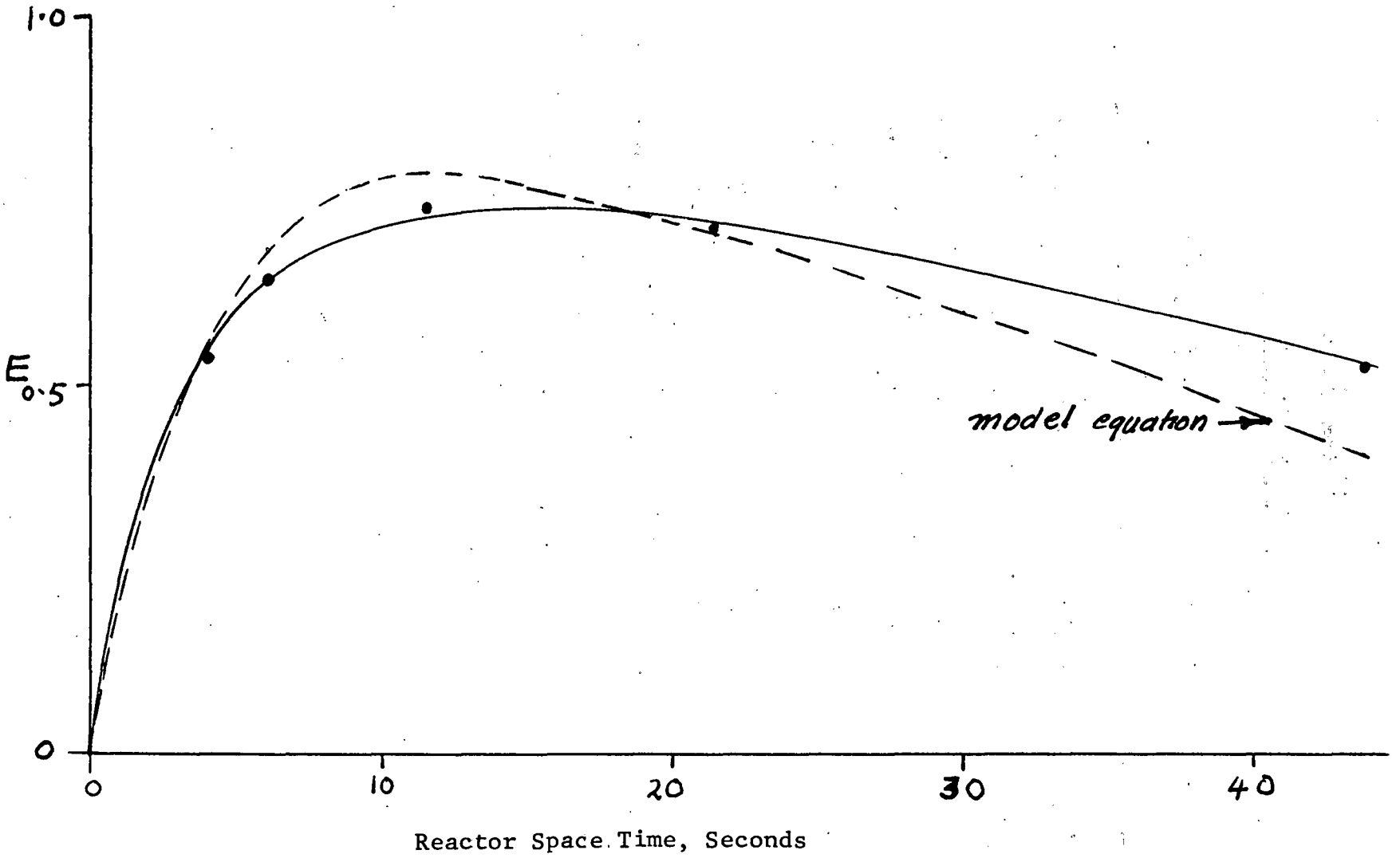

Figure 36. Butene Production Rate

TABLE XVIII.

BUTENE DISTRIBUTION

Space Time, sec	Fraction of Butenes 1-	cis-	trans-
4.04	0.271	0.302	0.427
6.04	0.250	0.299	0.451
11.44	0.253	0.301	0.446
21.35	0.195	0.315	0.490
43.65	0.188	0.318	0.494
average	0.232 ± 0.038	0.307 ± 0.008	0.461 ± 0.029
Kolboe	0.591	0.202	0.207
Owens & Amberg	0.581	0.216	0.265
equilibrium	0.144	0.318	0.538

There is evidence for a substantial contribution of internal mass transfer to the apparent kinetics. Assuming the external mass transfer is small (an assumption supported by estimation), then the value of the parameter r for the zeroth moment

$$m_0 = e^{-r} \tag{5.37a}$$

is given as

$$r = -\ln m_0 \doteq EK\Lambda\eta_s \tag{5.37b}$$

which becomes upon substitution of η_s

$$r = \frac{D_{eff}}{r_p^2}\,\tau\Lambda 3\left\{\frac{\phi}{\tanh\phi} - 1\right\} \tag{5.37c}$$

For values of ϕ greater than 20, the equation is approximately

$$r = \tau\Lambda\left\{\frac{9 D_{eff} k_r E}{r_p^2}\right\}^{1/2} \tag{5.38}$$

Using the data for τ = 6.04 sec., the fast reaction limit yields

$$k_r = 11.75 \text{ sec}^{-1}$$

$$\phi = 40.1$$

$$\eta_s = 0.073$$

These estimates are based upon D_{eff} = 6.7-03 cm^2/sec; this number needs to be confirmed with additional experimentation.

A series of runs were made with thiophene and n-pentane as a solvent and an internal standard. The first series of runs were made to establish the influence of pulse size upon the course of the reaction. The zeroth moment data showed that the pulse was completely recovered. The first moment data shows a trend for higher values of the equilibrium parameter, E, with smaller pulse size. These data suggest the adsorption of thiophene is Langmuir rather than linear. The second moment data show no obvious trend with pulse size. Therefore it is possible to estimate the effect of internal diffusion from the second moment values.

On the other hand the composition data for the thiophene runs are more complex. Figure 37A shows how the total recovery of product varies with pulse size; as the sample quantity decreases, the recovery of thiophene and reaction products improves. This result is caused by saturation of the GC with sample and also by complexities of the kinetics. Figure 37B shows that the apparent extent of reaction decreases with sample size. The extent of reaction depends upon the product, $r = \Lambda KE\eta_g$, and the trend in the data for Figure 36B match the variation in E exactly. Therefore the apparent equilibrium depends upon the previous history of the catalyst. The stabilization of the catalyst is being investigated further.

The pulse-size experiments demonstrated that the 1 $\mu\ell$ pulse gave the best G.C. analysis. This pulse size was used in a series of experiments conducted with several choices of the flow rate. Figure 37 shows the first-order kinetic plot of these data. It is apparent that there is a systematic deviation from the first-order line; however the simple first-order form represents the data provisionally. If the effectiveness factor is assumed to be unity, then the reaction rate is found as

$$\eta_s k_r = 0.0965 \text{ sec}^{-1}$$

Table XIX lists a summary of the more important parameters for thiophene. The data at constant flow show a trend for R to diminish with pulse size. This result suggests that as the pulse size increases, diffusional resistance increases by pore blockage. The total set of data then yield an estimate of the effective diffusivity

$$D_{cff} = 9.7\text{-}03 \text{ cm}^2/\text{sec}$$

and the first moment data, neglecting pentane, suggests the equilibrium is approximately

$$E = 49. \pm 4.2$$

When these values are inserted into the estimate for the effectiveness the revised rate parameter is then

$$k_r = 1.58 \text{ sec}^{-1}$$

$$\phi = 45.1$$

$$\eta_s = 0.065$$

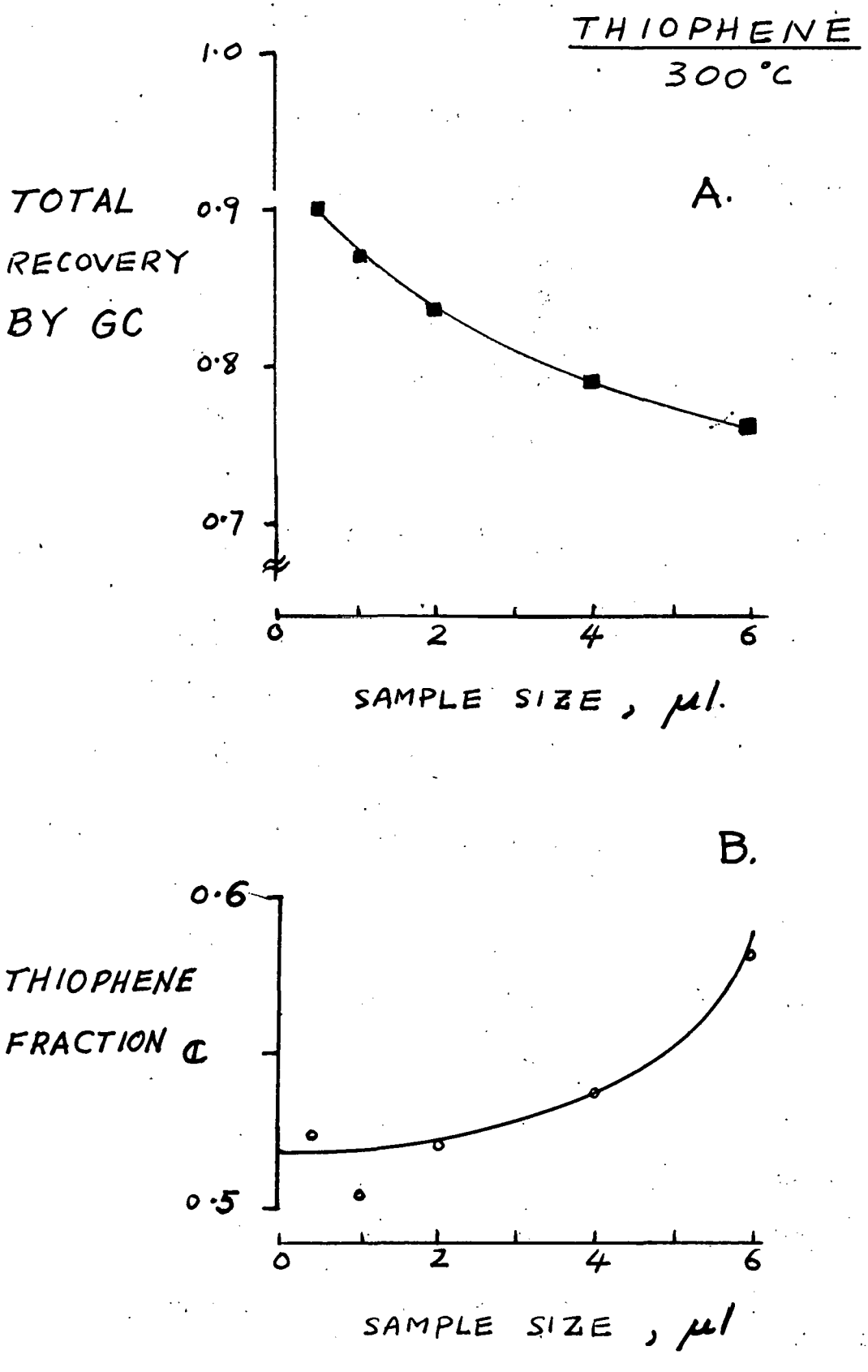

Figure 37. Effect of Pulse Size

TABLE XIX.

THIOPHENE REACTION DATA

21.4 sec space time

Pulse Size μl	C^{THIO}	C^{TOTAL}	E	$k_r \eta_g$ sec^{-1}	R
0.5	0.526	0.903	46.9	0.0931	110
1.0	0.505	0.872	57.8	0.0804	110
2.0	0.522	0.841	48.6	0.0909	94
4.0	0.537	0.791	45.6	0.0927	85
6.0	0.583	0.764	42.9	0.0855	80

Trend in data: E diminishes with pulse size

R diminishes with pulse size

recovery decreases with pulse size

Space Time sec^{-1}	C^{THIO}	C^{TOTAL}	E	R
4.04	0.857	0.956	45.8	90
6.05	0.791	0.920	49.6	83
11.46	0.671	0.943	80.6	77
21.40	0.505	0.872	45.9	110
43.77	0.353	0.820	54.8	110

$\bar{E} = 49.0 \pm 4.2$

R does not increase adequately with space time

recovery decreases with thiophene conversion

The equilibrium for thiophene on the catalyst is somewhat stronger than butadiene. The reaction rate parameter is about a decade smaller. The catalyst also is limited severely by mass transfer.

The implication of these results is simple. It is not possible to determine by direct kinetic means if butadiene is an important intermediate in the hydrodesulfurization of thiophene. The reaction rate for the conversion of butadiene to butenes is so much faster than the conversion of thiophene to products that butadiene would not be found in significant quantities even if formed.

These simple runs have illustrated some of the power of quantitative analysis of the pulses produced in operation of a microreactor. These examples also show that the experimental technique must be refined to take full advantage of the method. Once developed the method provides a rapid way for generating important quantitative information.

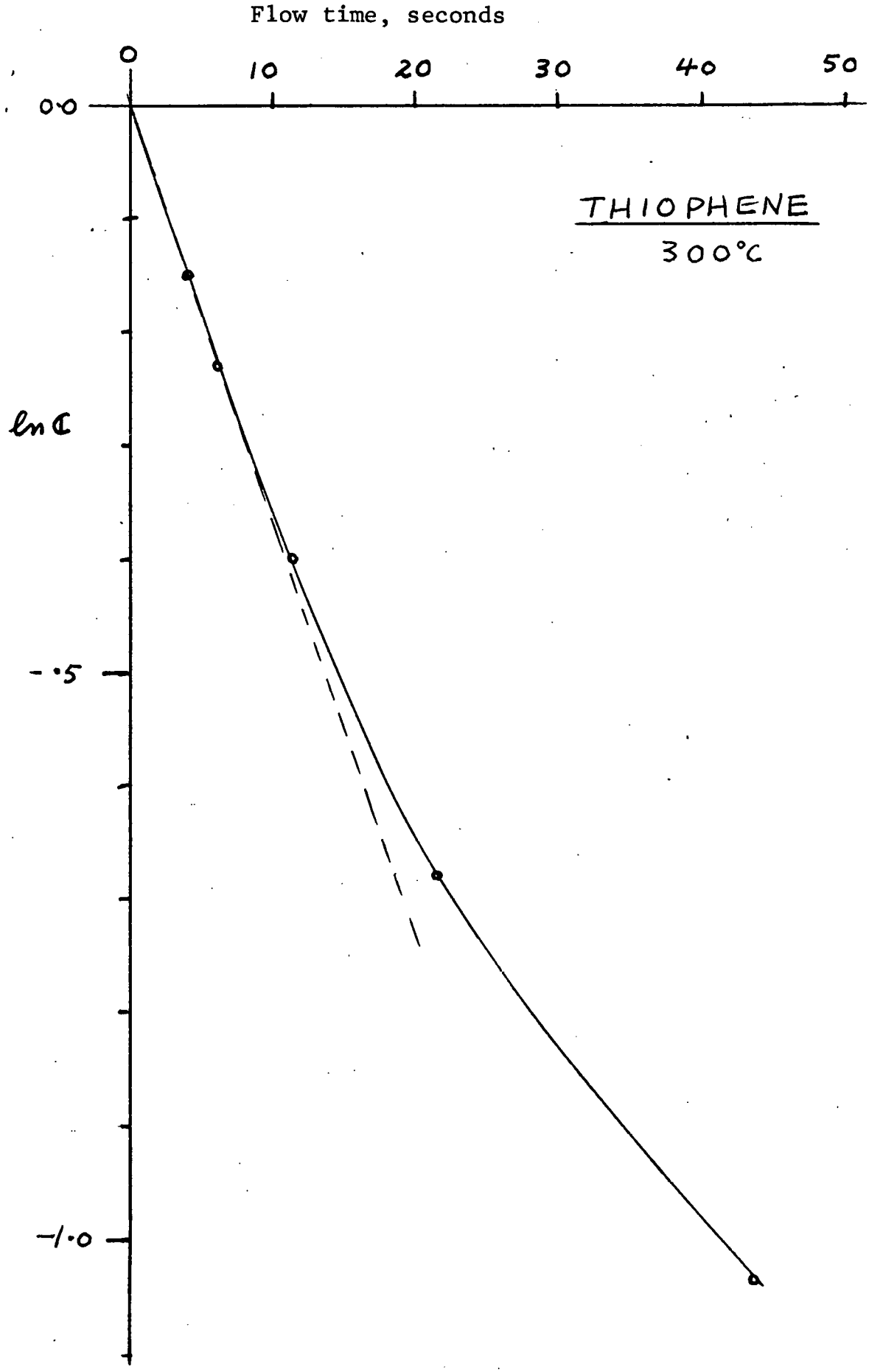

Figure 38. Thiophene Reaction Rate

Plans for Future Work

The plans for future effort during the next quarter are outlined below:

1. Model simulation of HDS and HDN reactors. The data obtained under Tasks 2 and 3 will be extended to "commercial" conditions by reactor simulation. In particular the HDS/HDN of a coal slurry in a fixed bed reactor shall be investigated.

2. Poisoning Profiles: Although the mechanisms for poisoning of the Synthoil catalyst are not yet established by these efforts, the effects of pore mouth blocking and coke laydown will be developed quantitatively.

Milestone Comments

The progress under this task can be summarized as follows:

Reaction Engineering Analysis. This task is ongoing. A series of models for pulse microreactors has been developed and is being used to test catalyst activity.

Preliminary Reactor Models. The preliminary reactor models are being developed now and will be described in the fifth progress report.

Extension of Microreactor Data. The data collected under Tasks 2 and 3 is not complete enough for the preliminary interpretation. An analysis based on the HDN of quinoline will be developed in the next quarter.

Extension of Reaction Engineering Data. A critical summary of the kinetic literature is being prepared. This review will be completed for the sixth progress report.

Nomenclature

Dimensionless Groups

$B = \mathcal{D}_{ax}/(v_i l)$	inverse Bodenstein number
$B_i = k_g d_p/\mathcal{D}_{eff}$	Biot number
$C = c/c_0$	dimensionless fluid phase concentration in bed
$C_i = c_i/c_0$	dimensionless fluid phase concentration in pellet
$E_i = s_i/c_i$	intrinsic equilibrium constant
$E = E_i + \epsilon_i$	linear equilibrium constant
$F = k_g a_s \tau$	number of gas-phase transfer units
$K = k_r \tau$	number of reaction units
$Q = q/q_\infty$	dimensionless solid phase concentration
$R = (F^{-1} + (SE)^{-1})^{-1}$	overall number of transfer units
$S = k_s a_s \tau$	number of solid phase transfer units
$T = t/\tau$	dimensionless time
$Z = z/l$	dimensionless distance parameter
$\Lambda = \epsilon_s/\epsilon_g$	volume ratio of solid phase/gas phase in bed
$\eta_g = (\eta_s^{-1} + \frac{KE}{F})^{-1}$	global efficiency of film model
$\phi = r_p \left(\frac{k_r E}{\mathcal{D}_{eff}}\right)^{1/2}$	Thiele modulus
$\rho = r/r_p$	dimensionless radius of pellet

Defining Parameters

a_s	area per unit volume of solid phase, cm^{-1}
c	concentration in vapor phase, mole cm^{-3}
c_o	arbitrary reference concentration, mole cm^{-3}
d_p	diameter of solid phase sphere, cm
$\mathcal{D}_{ax}$	axial dispersion parameter, $cm^2 sec^{-1}$
$\mathcal{D}_{eff}$	effective diffusivity in solid, $cm^2 sec^{-1}$
$\mathcal{D}_k$	Knudsen diffusivity in solid, $cm^2 sec^{-1}$
$\mathcal{D}_p$	modified diffusivity in solid film model, $cm^2 sec^{-1}$
k_i	intrinsic first-order rate constant, sec^{-1}
k_g	fluid film mass transfer conductance, cm sec^{-1}
k_r	first-order rate constant in solid film model, sec^{-1}
k_s	solid phase mass transfer parameter, $10 \cdot D_{eff}/dp$, cm sec^{-1}
ℓ	length of the system, cm
q	arbitrary reference concentration of solid phase, mole cm^{-3}
q	concentration in the solid phase, mole cm^{-3}
s	Laplace transform variable
s_i	adsorbed volumetric concentration, mol cm^{-3} (see eqn. 5.15)
t	time variable

v_i	interstitial velocity, $cmsec^{-1}$
z	length variable
ϵ	volume fraction in bed
ϵ_i	volume fraction of fluid phase in pellet
τ	time for an unadsorbed pulse to pass through the system, ℓ/v_i, sec

Subscripts

g	gas phase
p	product
s	solid phase

V. CONCLUSIONS

The first liquid-phase microreactor assembly has been modified to secure in situ sulfiding of the catalyst. A liquid-chromatography sampling valve has been installed to increase the ease of rapid sampling. The operation of the liquid-phase microreactors has met design specifications.

The liquid-phase hydrodesulfurization of dibenzothiophene demonstrates that current commercial catalysts have high (>90%) selectivity to biphenyl, the product requiring the smallest consumption of hydrogen, under conditions of adequate sulfidization of the catalyst and excess reactant hydrogen. The activity of the catalyst is very high under the clean conditions used in these experiments.

The reaction network for hydrodenitrogenation of quinoline has been established in batch autoclave experiments at commercial conditions. The network and representative first-order apparent rate constants [$(min)^{-1}$] are given below:

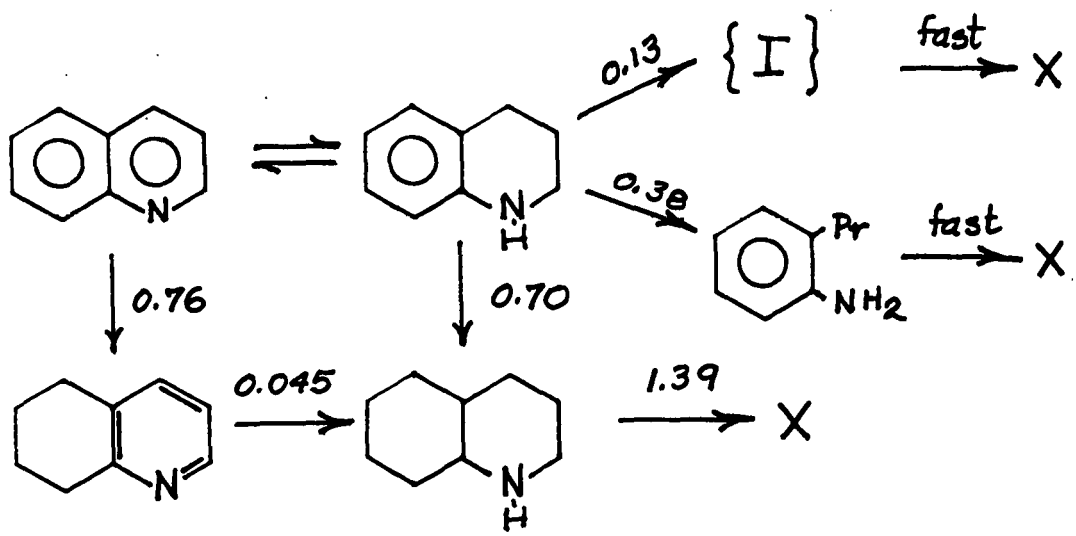

The effect of H_2 and H_2S concentration upon the reaction rates has been investigated carefully, and the contribution of catalyst type has received preliminary attention. These studies show that the reaction network can be rationalized in great part by analysis of bond reactivity. The batch experiments are being extended to acridine and carbazole. As an extension of the batch experiments quinoline is being examined in the flow icroreactor.

The deactivation of Synthoil pilot plant catalyst was investigated further during this quarter. A small sample of catalyst, removed from the front of the 1.1 in ID Synthoil pilot plant at the conclusion of Run FB-53, showed substantial cementing of coal mineral matter to the surface of the catalyst. Unlike the sample taken from the upstream region of the 5/16 in ID Synthoil reactor, the FB-53 catalyst had very little build-up of FeS_x on the external surface. The mineral matter cemented to the surface consisted primarily of clay, rutile and $CaCO_3$ reduction products.

The moment analysis of pulse microreactor data was extended to give a basis for investigation of fairly complex reaction networks. In particular the film model was extended to describe a two-phase catalyst. The transport in a spherical catalyst with reaction was compared critically to the film model. A limited range of experiments with thiophene were conducted using a microprocessor to read out the moments of the pulses. These data show the moment analysis is fairly powerful in systems of moderate complexity.

VI. LITERATURE CITED

Akhtar, S., Mazzocco, N. J., Weintraub, Murray, and Yavorsky, P. M., Energy Communications 1, 21-36 (1975).

Bartsch, R., and Tanielian, C., J. Catal. 35, 353-358 (1974).

Cecil, R. R., Mayer, F. X., and Cart, E. N., "Fuel Oil Hydrodesulfurization Studies in Pilot Plant Reactors," paper presented at Am. Inst. Chem. Engrs. Meeting, Los Angeles (1968).

Drushel, H. V., and Sommers, A. L., Anal. Chem. 39, 1819 (1967).

Drushel, H. V., preprints of Am. Chem. Soc., Atlantic City meeting, Sept. 8-13, 1967, p. 121. Division of Petroleum Chemistry, Inc. (1968).

Fieser, L. F. and Fieser, M., Introduction to Organic Chemistry, Chapter 27, D. C. Hath and Col, Boston, 1957.

Flinn, R. A., Larson, O. A., and Beuther, H., "How Easy Is Hydrodenitrogenation," Hydrocarbon Process Petroleum Refiner 42, (9), 129-132 (1963).

Frye, C. G., and Mosby, J. F., Chem. Eng. Progr. 63 (9) 66 (1967).

Hoog, H., Rec. Trav. Chim. Pays Bas 69, 1289 (1950).

Landa, S., and Mrnkova, A., Coll. Trav. Chim. Tcheques 31, 2202 (1966).

Metcalfe, T. B., "Inhibition par le sulfure d'hydrogene de la reaction l'hydrodesulfurisation des produits petroliers." Chim. Ind. Gen. Chim. 102, 1300 (1969).

Owens, J., and Amberg, C. H., Can. J. Chem. 40, 947 (1962).

Peri, J. B., J. Phys. Chem. 69, 211 (1965).

Peri, J. B., J. Phys. Chem. 69, 220 (1965).

Philipson, J. J., "Kinetics of Hydrodesulfurization of light and middle distillates," paper presented at Am. Inst. Chem. Engrs. Meeting, Houston (1971).

Rollmann, L. D., preprint San Francisco ACS meeting, August, 1976.

Satterfield, C. N., and Roberts, G. W., A.I.Ch.E. J. 14, 159 (1968).

Sūzuki, Motoyuki and Smith, J. M., Chem. Eng. Sci. 26, 221 (1971).

Urimoto, H., and Sakikawa, N., Sekiyu-Kagaku-Kyokaishi, 15, No. 11, p. 926 (1972).

VII. PERSONNEL

All of the personnel discussed in the Third Quarterly Progress Report are continuing on the sutdies; there have been no changes. Dr. Rainer Zawadski who has a B.S. degree in chemical engineering and a Ph.D. in physical organic chemistry from the University of Delaware will be joining us after three years' work as a chemical technologist in the harmaceutical industry. His coming brings a nice combination of engineering and chemical talents to the project. He will be working on the catalytic hydrodenitrogenation with Stuart Shih and will take over when Stuart leaves.

*U.S.GOVERNMNET PRINTING OFFICE:1977 - 740- 062 64